DEVELOPMENT OF A DSP-FPGA-BASED RESOLVER-TO-DIGITAL CONVERTER FOR STABILIZED GUN PLATFORMS

A THESIS SUBMITTED TO
THE GRADUATE SCHOOL OF NATURAL AND APPLIED SCIENCES
OF
MIDDLE EAST TECHNICAL UNIVERSITY

BY

YASİN ZENGİN

IN PARTIAL FULFILLMENT OF THE REQUIREMENTS
FOR
THE DEGREE OF MASTER OF SCIENCE
IN
ELECTRICAL AND ELECTRONICS ENGINEERING

MAY 2010

Approval of the thesis:

DEVELOPMENT OF A DSP-FPGA-BASED RESOLVER-TO-DIGITAL CONVERTER FOR STABILIZED GUN PLATFORMS

submitted by **YASİN ZENGİN** in partial fulfillment of the requirements for the degree of **Master of Science in Electrical and Electronics Engineering Department, Middle East Technical University** by,

Prof. Dr. Canan Özgen
Dean, Graduate School of **Natural and Applied Sciences** __________

Prof. Dr. İsmet Erkmen
Head of Department, **Electrical and Electronics Engineering** __________

Prof. Dr. İsmet Erkmen
Supervisor, **Electrical and Electronics Engineering Dept., METU** __________

Prof. Dr. Aydan M. Erkmen
Co-Supervisor, **Electrical and Electronics Engineering Dept., METU** __________

Examining Committee Members:

Prof. Dr. Kemal Leblebicioğlu
Electrical and Electronics Engineering Dept., METU __________________

Prof. Dr. İsmet Erkmen
Electrical and Electronics Engineering Dept., METU __________________

Assist. Prof. Afşar Saranlı
Electrical and Electronics Engineering Dept., METU __________________

Assist. Prof. Emre Tuna
Electrical and Electronics Engineering Dept., METU __________________

Bülent Bilgin, M.Sc.
Manager, ASELSAN __________________

Date: 31.05.2010

ABSTRACT

DEVELOPMENT OF A DSP-FPGA-BASED RESOLVER-TO-DIGITAL CONVERTER FOR STABILIZED GUN PLATFORMS

ZENGİN, Yasin
M. Sc., Department of Electrical and Electronics Engineering
Supervisor: Prof. Dr. İsmet ERKMEN
Co-Supervisor: Prof. Dr. Aydan M. ERKMEN

May 2010, 163 pages

Resolver, due to its reliability and durability, has been used for the aim of shaft position sensing of military rotary systems such as tank turrets and gun stabilization platforms for decades. Ready-to-use resolver-to-digital converter integrated circuits which convert the resolver signals into position and speed measurements are utilized in servo systems most commonly. However, the ready-to-use integrated circuits increase the dependency of the servo system to hardware components which in turn decrease the efficiency and flexibility of the servo system for changing system structures such as for changing resolver carrier frequency or changing position and speed sensors. The proposed solution to increase the efficiency and flexibility of the servo system is a software-based resolver-to-digital converter which does not require aforesaid special hardware components and presents a complete software-based solution for the conversion. The proposed software-based resolver-to-digital converter makes use of common programmable hardware components, that is, FPGA and DSP which form the heart of the servo controller technology in recent years.

The proposed structure for the conversion has three components. The first component is the signal conditioner which minimizes the disturbances coming from the resolver signals as harmonic distortions and noise. The second component, the phase-sensitive demodulator, as the name implies, is responsible for phase-sensitive demodulation of resolver signals. The third component is the estimator filter. In order to determine the optimal estimator filter, five different estimator filters with the aforesaid two components are implemented in ASELSAN’s stabilized gun system STAMP and they are compared in terms of both estimation performance and computational complexity. The implemented filters include nonlinear observer type filter which is already proposed in the literature for resolver conversion, tracking differentiator adapted to resolver conversion and kalman filters adapted to resolver conversion in different forms such as linear kalman filter, extended kalman filter and unscented kalman filter. At the end of the study, stability and sensitivity analyses are also performed for the proposed system.

Keywords: Phase-sensitive demodulation, harmonic distortions on resolver signals, software-based resolver-to-digital conversion, Kalman filtering.

ÖZ

STABİLİZE SİLAH PLATFORMLARI İÇİN DSP VE FPGA TABANLI RESOLVER-SAYISAL ÇEVİRİCİ GELİŞTİRİLMESİ

ZENGİN, Yasin
Yüksek Lisans, Elektrik ve Elektronik Mühendisliği Ana Bilim Dalı
Tez Yöneticisi: Prof. Dr. İsmet ERKMEN
Ortak Tez Yöneticisi: Prof. Dr. Aydan M. ERKMEN

Mayıs 2010, 163 sayfa

Dayanıklılığı ve güvenilirliğinden dolayı resolver, yıllardır tank tareti ve silah stabilizasyon platformu gibi askeri amaçlı döner sistemlerde kullanılmaktadır. Hali hazırda kullanıma hazır olarak sunulan ve yoğun bir şekilde servo sistemlerde kullanılmakta olan resolver-sayısal çevirici tümleşik devreleri, resolver sinyallerini kullanarak pozisyon ve hız ölçümünü gerçekleştirmektedirler. Ancak, kullanıma hazır olarak sunulan bu devreler, servo sistemin donanıma bağımlılığını artırmakta ve servo sistemin değişken resolver taşıyıcı frekanslarında resolverlerin veya değişken pozisyon ve hız sensörlerinin kullanıldığı değişken sistem yapılarına uyum sağlayabilme yetisini ve servo sistemin verimliliğini azaltmaktadır. Bu tez kapsamında soruna önerilen çözüm ise özelleşmiş donanım yapılarına ihtiyacı ortadan kaldıran ve yazılım üzerine kurulu bir yazılım-tabanlı resolver-sayısal çeviricidir. Önerilen yazılım-tabanlı resolver-sayısal çevirici, son yıllarda servo kontrolcü teknolojisinin vazgeçilmez programlanabilir donanım parçaları olan FPGA ve DSP işlemcileri kullanmaktadır.

Çevrim için önerilen yapı üç bileşenden oluşmaktadır. Birinci bileşen resolver sinyallerindeki harmonik bozulmalar ve gürültü gibi bozucu etkileri en aza indirgemek için kullanılan sinyal iyileştiricidir. İkinci bileşen, isminden de anlaşılacağı gibi, resolver sinyallerinin faza-duyarlı çözümünü gerçekleştiren faza-duyarlı çözücüdür. Sonuncu bileşen ise tahminleyici filtredir. Resolver çevrimi için kullanılabilecek en iyi tahminleyici filtreyi bulabilmek amacıyla, beş farklı tahminleyici filtre bahsi geçen diğer iki bileşen ile birlikte ASELSAN'ın stabilize silah sistemi STAMP'a uygulanmış ve bu filtreler hem tahminleme performansı hem de işlemsel karmaşıklık açılarından karşılaştırılmıştır. Uygulanan tahminleyici filtreler; literatürde resolver çevrimi için önerilmiş bulunan doğrusal-olmayan filtre, resolver çevrimine uyarlanmış takiplemeli türevleyici ve kalman filtrenin doğrusal kalman filtre, kapsamlı kalman filtre ve kokusuz kalman filtre olmak üzere resolver çevrimine uyarlanmış üç farklı formunu içermektedir. Çalışmanın sonunda önerilen sistem için kararlılık ve duyarlılık analizleri de gerçekleştirilmiştir.

Anahtar Kelimeler: Faza-duyarlı çözüm, resolver sinyallerinde harmonik bozulmalar, yazılım-tabanlı resolver-sayısal çevrim, Kalman filtreleme.

To My Family and Love

ACKNOWLEDGEMENTS

I would like to express my sincere thanks and gratitude to my supervisors Prof. Dr. İsmet ERKMEN and Prof. Dr. Aydan M. ERKMEN for their belief, encouragements, advice and criticism throughout this study.

I would like to thank ASELSAN Inc. for facilities provided for the completion of this thesis.

I would like to express my thanks to my friends and colleagues for their support and fellowship.

I would like to thank TÜBİTAK for its support on scientific and technological researches.

I would like to express my special appreciation to my family for their endless support and encouragements.

TABLE OF CONTENTS

LIST OF TABLES

LIST OF FIGURES

NOMENCLATURE

RDC	: Resolver-to-Digital Converter
IC	: Integrated Circuit
ADC	: Analog-to-Digital Converter
FPGA	: Field-Programmable Gate Array
FOC	: Field Orientated Control
PWM	: Pulse-Width-Modulation
SVPWM	: Space Vector Pulse-Width-Modulation
JONSWAP	: Joint North Sea Wave Observation Project
LKF	: Linear Kalman Filter
EKF	: Extended Kalman Filter
UKF	: Unscented Kalman Filter
DSP	: Digital Signal Processor
PLL	: Phase Locked Loop
θ	: Resolver position
w	: Resolver signals' carrier frequency

ω	: Resolver speed
FFT	: Fast Fourier Transform
ΔS	: Demodulator output percentage error for sine channel
ΔC	: Demodulator output percentage error for cosine channel
ϕ	: Estimated position
FIR	: Finite Impulse Response
IIR	: Infinite Impulse Response
T_s	: Sampling Period
K_k	: Kalman gain matrice
ε_k	: Innovation or error
θ_k^-	: Position estimate of Kalman filter
ω_k^-	: Speed estimate of Kalman filter
a_k^-	: Acceleration estimate of Kalman filter
θ_k	: Actual resolver position
$\Delta\theta$	: Resolver position estimation error
ΔT	: Torque tracking error
$\Delta\omega$	: System tracking error
ΔP	: System position tracking error

f_T	: Torque ripple frequency
$\Delta C, S$	: ΔC or ΔS

CHAPTER 1

INTRODUCTION

1.1 Motivation

Servomechanism is a device which enables automatic control means on a mechanism. The term servomechanism is only used for devices which make use of feedback signals from the mechanism that is being controlled. Using feedback signals, a servomechanism attempts to correct the performance of the mechanism according to the command set. Although any type of system using closed loop control can be classified as a servomechanism, motion control systems are the leading area of usage nowadays. In general, controlled states for such systems are position, speed, acceleration and torque.

Servomechanisms should have an input, an output, a calculator calculating the error between the input and output, an amplifier calculating the actuation and an actuator to eliminate the error. From this point of view, the first servomechanism was the sheep steering engine used on the SS Great Eastern which is launched in 1858. Thereafter, servomechanisms were used in fire-control systems and navigation systems. After a century, servomechanisms are used in many applications ranging from aeronautical to automotive [3].

Military fire-control is one of the disciplines that use servomechanisms since its invention. Fire-control concept is developed to improve hitting performance of weapon systems. These military systems are designed to improve the performance of the weapon systems in terms of rapidness of firing and hitting accuracy. A Fire-control system combines a number of components such as a fire-control computer, a servomechanism to direct the gun and a gun to fire on the target. Advanced fire-control systems have ability to interface with more components improving firing accuracy such as fire control radar, thermal and day cameras and laser range finder. Moreover, more complex fire-control systems have additional sensors. These additional sensors measure the disturbing effects deflecting the system performance from the trajectory in demand. For instance, in a stabilized gun platform, fire-control computer usually has an interface with a gyro in order to measure disturbance deflecting the gun's velocity from the velocity in demand. Using the negative feedback law, the computer continually computes the necessary correction signal for the actuators to keep the gun's velocity at desired value. This is the concept of gun stabilization. Gun stabilization is an important concept for fire-control systems. Disturbances coming from terrain will adversely affect the performance of a fire-control system without gun stabilization.

Eventually a fire-control system is a servomechanism with its ability to sense feedbacks coming from the mechanism. Servomechanisms should be able to manipulate time-based derivative of a parameter to be able to control it. For instance, a servomechanism designed to control the velocity of a robot arm should be able to change time-based derivative of velocity, that is, acceleration of the robot arm. In general, acceleration is not a direct controllable variable in servomechanisms because acceleration sensors available in the marketplace either show poor performance or are so expensive that making a cost-effective system solution very difficult. That is to say, today's systems do not allow making use of acceleration sensors to control velocity of a mechanism. Therefore, controlling velocity of a mechanism is usually realized by using torque feedback or an indirect way of sensing torque, namely by calculating torque from phase currents of servo motors. This way of speed control is a good solution when engineers care system cost, performance and reliability.

In contrast to general opinion, servomechanisms do not necessarily have a servo motor. For instance systems with closed loop temperature control are also servomechanisms although they do not have servo motors. However, motion control applications make it necessary to use servo motors in control. A motor is an electromechanical energy converter generating a force on its rotating shaft when supplied with direct current or three phase alternating current depending on the type of the motor. A servo motor is a type of motor which gives out some information related to its motion such as shaft position and speed. These may be referred as the most common feedbacks of servo motors. Processing feedback signals from servo motors and other sensors, the servo controller continually controls the voltage supplied to motor in order to correct the motion of the servomechanism. The command signal for a servo controller may be one of position, speed and torque commands.

ASELSAN is the leading company of Turkish defense industry in designing and producing stabilized fire-control systems. ASELSAN's STAMP (Figure 1-1) and STOP systems are stabilized marine gun systems equipped with advanced fire-control and servo controller units. Systems can be used with various naval guns including 12.7, 25 and 30 mm guns. They have several sensors to perform gun stabilization and target tracking on both day and night conditions. Fire on the move ability of the systems facilitates challenging military missions at sea.

The main motivation of this thesis is to improve the servo drive abilities of STAMP and STOP systems. It is intended to solve the challenging issues observed during the design stage of STAMP and STOP systems. Actually, these issues are not unique to the systems but they can be seen as general issues and they can be attributed to servo control concept.

Figure 1-1 ASELSAN’s STAMP system on a Turkish assault boat

1.2 Objectives and Contributions of the Thesis

Sensorless control of motor drives, eliminating the need for sensors in control loops, is very popular in servo controller technology recently [2]. One advantage of the sensorless control is that it reduces the cost of the controller. However, as far as the performance is considered, sensorless control algorithms have not proved reliability and quality for the high-performance servo controllers yet. Especially, in the low speed applications, the algorithms given in literature show poor performance due to the model uncertainty and noise. Therefore, system performance requirements for stabilized gun systems make it compulsory to use sensors due to poor performance of sensorless control techniques.

Resolvers are robust and reliable position sensors used in servo motors and they have been used reliably in shaft position measurement systems for decades. Ready-to-use Resolver-to-Digital Converter (RDC) integrated-circuits (ICs) are used in servo controllers most commonly to convert the modulated resolver signals into digital speed and position measurements. One disadvantage of this hardware-based conversion method is that adapting the hardware of the servo controller to the ready-to-use RDC ICs increases the cost of the servo drive considerably. Moreover, different position and speed sensors may be used to provide position and speed in a servo system. For instance, digital encoders coupled to servo motors are widely used in servo applications recently. For such a servo system structure, RDC ICs on the hardware become useless and this approach results in less cost-effective and less volume-effective servo controllers. On the other hand, hardware modifications to remove the RDC ICs will also increase the cost when one takes mass-production issues into consideration. Hardware configuration management for different system solutions will be another expensive burden of hardware modifications. Hence, if a software-based method which eliminates the need for RDC ICs to realize resolver-to-digital conversion is introduced, servo controller and servo system design and production costs will be reduced. Besides minimizing the costs, software-based RDC will enhance more flexible servo controllers since making software modifications is much more feasible and manageable than making hardware modifications.

In recent years, digital controllers have been used widely in servo applications. This trend of making use of digital controllers stem from the fact that working with digital signals by the help of computer technology is more advantageous when one takes flexibility, improvability, simplicity, cost and accuracy of control systems into consideration. Since cost effectiveness is the key point in engineering, low-cost computers are of great importance in developing hardware for digital servo controllers. Digital Signal Processor (DSP) integrated circuits with proper peripherals realize these requirements in servo controllers. Digital control of dynamical systems also necessitates utilizing Analog-to-Digital Converters (ADC) because dynamical systems may have several analog interfaces. Hence, both DSP and ADCs are widely used in servo controllers to provide cost-effective and optimal performance solutions for servo system applications. Besides DSP and ADCs, servo controllers usually have Field-Programmable Gate Array (FPGA) chips to resolve the hardware functions, for instance, to read data from digital sensors and to provide interface with digital input-output signals. Therefore, a digital control board used in a servo controller may be considered to have three fundamental components; DSP, ADCs and FPGA.

Consequently, the main goal of this thesis is to develop a software-based resolver-to-digital converter which performs the conversion by using analog-to-digital converters and common programmable hardware components; DSP and FPGA. The method will eliminate the need for RDC ICs in servo controllers and open the doors to more flexible and compact servo controller designs. It will also reduce design and production costs considerably.

The thesis proposes a software-based method for phase sensitive demodulation of resolver signals using Field-Programmable Gate Array (FPGA) and ADCs. Besides demodulation algorithm, the thesis also makes use of estimator filters to realize conversion using a Digital Signal Processor. The implemented estimator filters are Tracking Differentiator adapted to resolver conversion, Linear Kalman filter, Extended Kalman Filter, Unscented Kalman Filter and a filter proposed in the literature. The thesis compares the said estimator filters in terms of noise suppression performance, tracking performance and computational complexity in the experimental system.

Since the system is applied to a naval stabilized gun platform, bandwidth of disturbances coming from the sea is examined by the help of ocean wave spectra. To have a fair performance comparison between the estimator filters, an input set for the filters is constructed by taking system requirements, spectral analysis of ocean waves and noise characteristics of naval servo systems all into consideration.

Resolver signals are susceptible to electromagnetic contamination and harmonic distortions. Hence, the thesis focuses on understanding the noise and harmonic distortions on resolver signals and disturbing effects of them on position and speed signals. This is important to understand the acceptable error levels in the servo system resulting from the resolver. In order to minimize the disturbances coming from such resolver signal imperfections, the thesis proposes a mixed-signal signal conditioner.

At the end of the study, stability and sensitivity analyses are also performed for the proposed system.

1.3 Outline of the Thesis

In the first chapter of the thesis, the motivation, objectives and contributions of the thesis are given. In the second chapter, the literature survey conducted on the related subjects is presented. In the third chapter, proposed software-based resolver-to-digital converter is explained in details. The fourth chapter gives performance, stability and sensitivity analyses of software-based Resolver-to-Digital converter. The fifth chapter concludes the study and refers to the future works. Finally in Appendix section details related to programming and hardware are given.

CHAPTER 2

LITERATURE SURVEY

This chapter gives a background for the thesis study. More specifically, the first section of this chapter summarizes the essential components of a servo system. The first section is also important for performance and sensitivity analyses since it covers the necessary information related to servo system modeling. The second section of this chapter gives an insight into the ocean wave spectra from which we extract the bandwidth requirements for servo controllers in naval applications. The required bandwidth should be known to design a well-tuned system which operates satisfactorily in the sea environment. The third section gives some rules of thumb related to control system design such as sampling theorem and aliasing. The fourth section deals with random variables and Kalman filtering which will be necessary for designing the estimator filters. Lastly, the fifth section inspects the similar studies performed by researchers for estimation of position and speed from resolver signals.

2.1 Servo System Components

2.1.1 Servo Motors and Servo Drives

A servo motor can be classified as AC or DC according to electrical supply, brushed or brushless according to its commutation and synchronous or asynchronous according to its slip. The most commonly used servo motors in today's servomechanisms are DC brushless and AC induction motors. They are both widely used in servomechanisms with some major differences in control software and hardware. Contrary to general opinion, both DC brushless and AC induction motors are classified as AC motors and they need three phase balanced AC currents to operate. AC induction motor is an asynchronous motor while DC brushless motor is a synchronous motor.

The rotor of a DC brushless motor includes permanent magnets that generate a magnetic field passing through the stator windings. This magnetic field interacts with the magnetic field generated by the current vector flowing within the stator windings. This interaction produces a torque between rotor and stator which can be transmitted to a rotating shaft. The current waveforms of the motor should be continuously updated to keep these magnetic fields' interaction so that a smooth torque waveform is produced and the efficiency of converting electrical energy to mechanical energy is maximized.

The induction machine has no magnets in the rotor side. It has stacked steel laminations forming a structure like a cage whose end points are shorted. Current vector in the stator windings creates a rotating magnetic field inside the motor and this magnetic field enters the rotor side inducing a voltage in the shorted cage proportional to motor's slip rate. This induced voltage results in a current in the rotor which consequently generates another rotating magnetic field. Two magnetic fields interact with each other to produce torque between the stator and the rotor.

Driving a DC brushless motor make it necessary to use an absolute position sensor whereas driving an AC induction machine requires a speed sensor. Furthermore, AC induction machine may be operated with sensorless algorithms. Running an AC induction machine without speed sensor using Kalman Filter is given in [1]. Thus, using an AC induction motor for a servo application may be cost-effective. However, using a DC brushless motor may be more convenient when efficiency, sensitivity and reliability issues are taken into consideration.

A fair comparison between AC induction motors and DC brushless motors is made in [4]. The paper can be summarized as following. DC brushless motors can be operated with almost unity power factor while the peak power factor value for an AC induction machine may be 85%. Moreover, DC brushless motors are more suitable for the applications where sensitive control of position and speed is required. The disadvantage of DC brushless motors is that copper, eddy and hysteresis losses become comparable to output power when driving the motor in low torque-low speed demands. This is due to the fact that DC brushless motor has a constant direct magnetic field density generated by the permanent magnets. This prevents optimizing the magnetic field density so as to minimize copper, eddy and hysteresis losses. On the contrary, direct axis magnetic field density can be adjusted by the voltage to frequency ratio in an AC induction motor. Therefore, using AC induction motor may be more efficient in terms of copper, eddy and hysteresis losses. Although having these advantages, all in all, DC brushless motor will be more efficient. Moreover, AC induction motors are not suitable when the aim is sensitive position and speed control of a servomechanism.

In conclusion, when efficiency, sensitivity and reliability considerations are taken into account, using DC brushless motors will be more effective in a stabilized gun application since there are limited power source and high sensitivity requirements.

A servo drive controller corrects the performance of a servo motor by using command and feedback signals. It is responsible for managing a servo motor to be able to ensure position and speed of a servomechanism. It attempts to eliminate the error between the command and feedback by providing servo motors with three phase balanced currents.

A servo drive controller is composed of hardware components, software components, interfaces with command and feedback signals and power elements transferring power to servo motor. In general, a processor board, a gate driver circuitry and sensors constitute the hardware components. Processor board is programmed using embedded software developing tools. Interfaces with command and feedback signals are provided by either analog or digital channels. Power MOSFETs and IGBTs are used as power elements in servo drives.

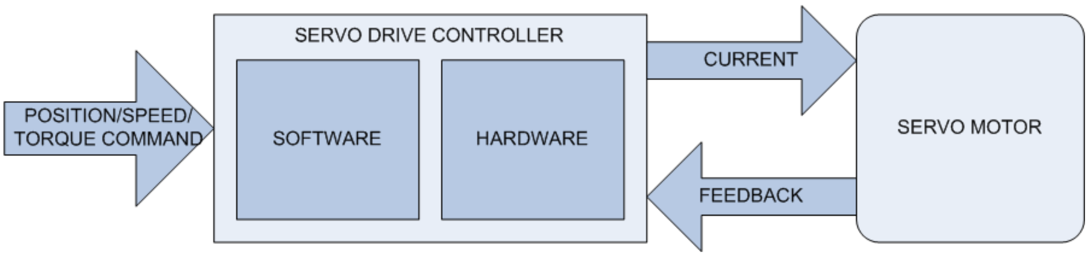

Figure 2-1 Generalized structure of a servo drive controller

In a position controlled servo drive, three control loops are used to increase the performance and accuracy. The main and innermost loop is reserved for torque control. In general, torque control is achieved using Field Orientated Control (FOC) technique with Space Vector Pulse-Width-Modulation (SVPWM). FOC uses current feedbacks and motor position to apply the right current vector so that the servo motor can produce torque. The loop over the torque loop is the speed loop. Taking command and feedback signals, speed loop regulates the speed of the motor by actuating the torque loop. The outermost loop in a position controlled servo drive is the position loop. To keep position in control, position loop induces the speed loop. This is the cascade control of position. Cascade control improves the performance of a servo system considerably [2].

If the aim is tracking a target, as in the case of naval stabilized gun platform, a position error controlled servo drive should be implemented. This is due to the fact that the target pointer in a fire-control system usually gives relative position of the target with respect to the gun. In other words, a servo drive controller used in a fire-control system usually takes the position error between the target and the gun. In order to eliminate this error, it is enough that servo drive controller has the ability to change the speed of the gun. Since the command is already the same with the position error itself, there is no need for an additional position sensor.

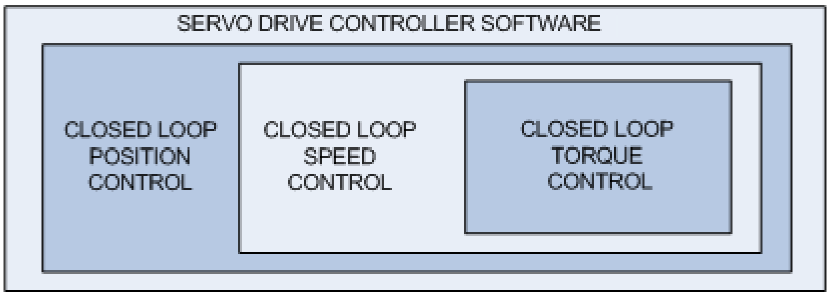
SERVO DRIVE CONTROLLER SOFTWARE
CLOSED LOOP POSITION CONTROL
CLOSED LOOP SPEED CONTROL
CLOSED LOOP TORQUE CONTROL

Figure 2-2 Position controlled servo drive controller’s nested control loops

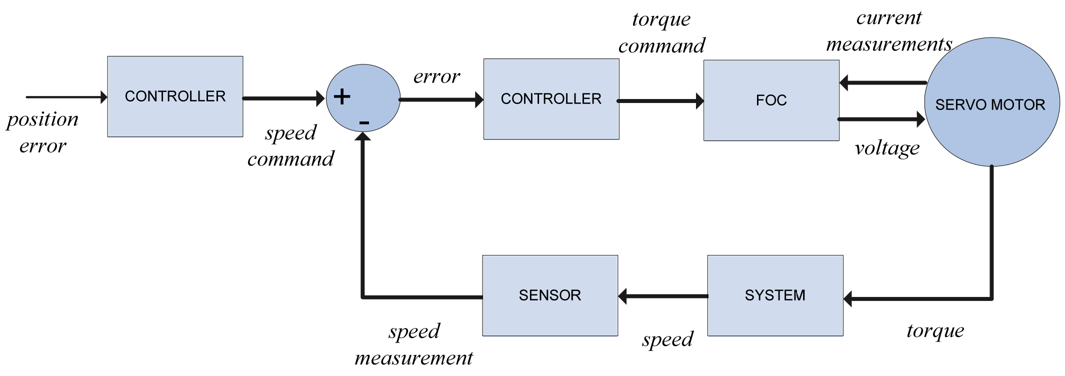

Figure 2-3 Position error controlled servo drive controller’s structure

Speed feedback is usually obtained from a gyro in a stabilized gun system as it produces an absolute speed feedback. That is to say, a gyro gives out the velocity of the gun with respect to earth. This makes stabilization possible even if there are disturbing effects coming from terrain. Velocity feedback can also be acquired from a resolver sensor which is widely used in servo motors. In fact, resolver sensors are used for commutation of servo motors and they originally give out position of the motor. Resolver position signal can be differentiated to form up a speed signal. Nevertheless, this speed signal will become a relative speed of motor rotation with respect to motor body. As a result, speed information obtained from resolver is not used in stabilization process.

2.1.2 Field Orientated Control of Torque

Most of servo drive controllers designed today implement Field Orientated Control technique to manage torque of servo motors. Field Orientated Control eliminates disadvantages of classical torque control techniques by using projections which transfers a three phase time dependent system into a two phase time independent system. The disadvantages of classical control techniques are summarized in [5].

- Classical torque control techniques does not have three phase imbalance management,
- Classical torque control techniques enforce operating with sinusoidal references which is so difficult,
- Classical torque control techniques cannot prevent motor from uncontrollable high peak and transient currents.

Field Orientated Control uses some projections transferring three phase time and speed dependent system into a two co-ordinate time independent system (rotor reference frame, *dq* frame). By implementing two transformations called Clarke transformation and Park transformation, the stator currents may be handled as if they are time and speed independent variables.

2.1.2.1 Mathematical Model of a Permanent Magnet Synchronous Motor

Before giving Park and Clarke transformations, it will be useful to examine motor model in rotor reference frame. An AC brushless motor can be modeled as a Permanent Magnet Synchronous Machine with sinusoidal flux distribution. The motor electrical model can be summarized by the following equation sets in rotor reference frame (*dq* frame) [6].

Equation in *d* axis:

$$V_d = Ri_d + L_d \frac{di_d}{dt} + L_q p\omega i_q \tag{2.1}$$

Equation in *q* axis:

$$V_q = Ri_q + L_q \frac{di_q}{dt} + L_d p\omega i_d + \lambda p\omega \tag{2.2}$$

Torque equation:

$$T = 1.5p(\lambda i_q + (L_d - L_q)i_d i_q) \tag{2.3}$$

where V_d and V_q are *d* and *q* axes voltages, R is the resistance of stator windings, i_d and i_q are *d* and *q* axes currents, L_d and L_q are *d* and *q* axes inductances, ω is the speed of the rotor, p is the number of pole pairs and lastly λ is the amplitude of the flux generated by rotor's permanent magnets in stator windings.

The back-EMF term, $\lambda p\omega$, affects the *q* axis equation only. As the motor speed increases, V_q should also be increased to keep i_q constant at steady state. Both axes have speed and current dependent parasitic terms. Since L_d and L_q values are usually very similar, torque term can be simplified as:

$$T \approx (1.5p\lambda i_q) \tag{2.4}$$

In conclusion, a torque control scheme should regulate i_d and i_q to have a smooth torque signal. The control signals are V_d and V_q to achieve this aim.

2.1.2.2 Current Transformations

[7] Clarke transformation transfers this three phase system into a two-coordinate orthogonal, time varying system, namely alfa and beta axes.

$$i_{alfa} = i_a$$
$$i_{beta} = \frac{1}{\sqrt{3}} i_a + \frac{2}{\sqrt{3}} i_b \qquad (2.5)$$

Park transformation transfers two coordinate time varying system into a time invariant system, namely direct and quadrature axes.

$$\begin{aligned} i_d &= i_{alfa} \cos\theta + i_{beta} \sin\theta \\ i_q &= -i_{alfa} \sin\theta + i_{beta} \cos\theta \end{aligned} \qquad (2.6)$$

Direct axis is aligned to rotor flux while quadrature axis is orthogonal to rotor flux. Therefore, *d* component is called the flux component, while *q* component is called the torque component. What we want to control are two orthogonal, time independent current variables, i_d and i_q, which are responsible for producing flux and torque respectively. The flux component of the current vector should be regulated at zero when a permanent magnet motor is used. Therefore, closed loop control of i_d and i_q is required. Widely, a proportional-integral-derivative controller is used as controller due to its simplicity and reliability.

Inverse Park Transformation takes voltages V_q and V_d in rotating reference frame, and gives orthogonal components V_{alfa} and V_{beta}, the voltage vectors in rotating reference frame. Following equations describe the Inverse Park Transformation:

$$\begin{aligned} V_{alfa} &= V_d \cos\theta - V_q \sin\theta \\ V_{beta} &= V_d \sin\theta + V_q \cos\theta \end{aligned} \qquad (2.7)$$

2.1.2.3 Space Vector Pulse Width Modulation

Motor terminal voltages, V_q and V_d are realized by help of Space Vector Pulse-Width-Modulation (SVPWM) and a PWM inverter. SVPWM calculates necessary duty-cycles to generate gate switching signals for power elements in the inverter structure. The inverter transfers power from bus bar to servo motor by switching in accordance with these gate switching signals. SVPWM technique minimizes harmonic contents of sinusoidal phase voltages applied to servo motor [8]. Minimum-harmonic-content sinusoidal phase voltages also minimize copper, eddy and hysteresis losses of servo motor. Implementation of SVPWM with a software switched pattern is explained in a detailed way in [9].

2.2 Ocean Wave Spectra and Servo Drive Bandwidth Requirements

In a servo drive application, bandwidth of speed and torque loops should be adjusted such that it covers the frequency spectrum of whole disturbing effects coming from terrain and servomechanism itself. For a naval system, frequency spectrum of external disturbances can be explained using ocean wave spectra. This is due to the fact that external disturbances in a naval system are dominantly originated from sea surface waves. Since the main goal of a naval stabilized gun system is to stabilize its gun at sea, the bandwidth of the servo drive system should be fixed by taking sea wave spectrum into consideration. There are also some internal disturbances caused by several effects within the system. Internal disturbances generally affect the torque loop performance. Hence these effects will not be handled in the thesis.

Surveying ocean wave spectrum is a way to describe the external disturbances in a naval stabilized gun system. Using an idealized spectrum, required bandwidth of speed loop can be found so that servo drive can compensate for disturbances coming from sea. One of these idealized spectrums is the Pierson & Moskowitz Spectrum proposed in 1964. [10]

Firstly, a definition of fully developed sea should be made. Surface waves stem from the wind. When the wind blows for a long time over a sea which is deep and large enough, surface waves start to move in accordance with the wind. If a sea satisfies these criteria, it is called as a fully developed sea. Pierson & Moskowitz Spectrum is defined for a fully developed sea. Another concept is the developing sea concept. A sea which has not yet reached steady state with the wind is called a developing sea. Searching for Joint North Sea Wave Observation Project (JONSWAP), Hasselman *et al.*, (1973), claimed that wave spectrum is never fully developed and changes continuously with time and distance. Then a new spectrum, JONSWAP spectrum is formed. Although proposal of Hasselman disproves the Pierson-Moskowitz Spectrum of a fully developed sea, two spectrums are very similar except for the fact that for JONSWAP spectrum the wave energy increases with time and distance from a lee shore (called *fetch* in mathematical derivations of the JONSWAP spectrum) [10].

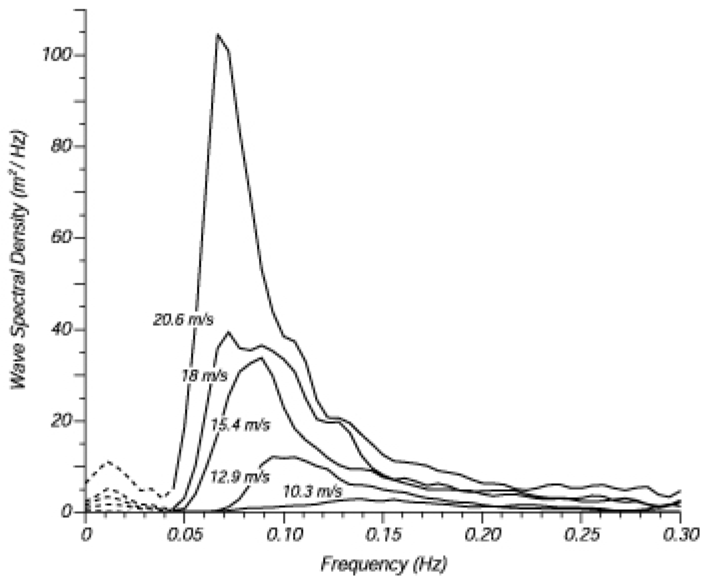

Figure 2-4 Pierson-Moskowitz sea spectrum with respect to wind speed [10]

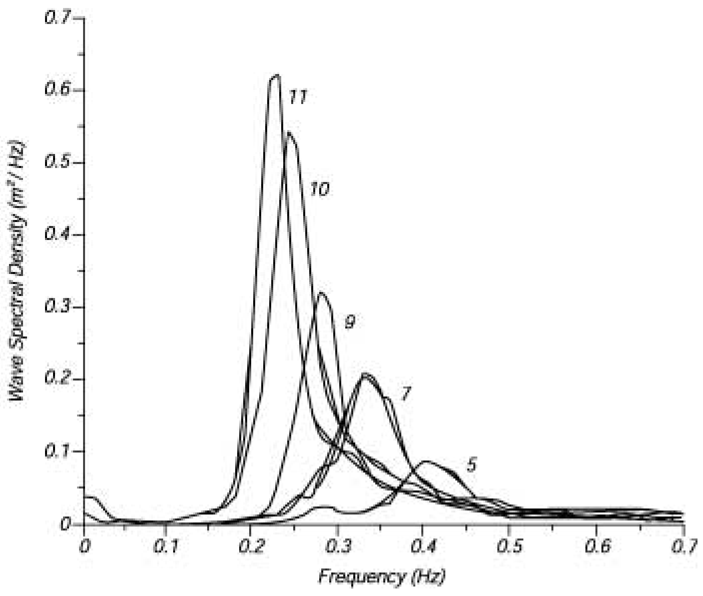

Figure 2-5 JONSWAP sea spectrum with respect to fetch when a constant speed wind is present [10]

The theory also explains how ocean waves are generated by the wind. A summary can be found in [10].

The bandwidth of ocean waves can be located from Pierson & Moskowitz sea spectrum. It is obvious that disturbances coming from sea will be at frequencies lower than 0.5 Hz. Nevertheless, it does not mean that the bandwidth of the speed loop should be 0.5 Hz. That is to say, servo drive should be able to reject speed disturbances coming with a frequency of 0.5 Hz without showing excessive phase shift. Otherwise, excessive delay in servo loop will decrease the performance. Besides, servo loop approaches to instability as the delay increases. Hence, for a stable and reliable control, each constituent of the servo loop should show a minimum delay within the sea spectrum.

2.3 Sampling Theorem and Aliasing

A control system designer should always be aware of the sampling theorem. The sampling theorem implies that sampling frequency of an analog signal should be chosen as $W_s > 2W_{max}$, also known as Nyquist criterion, where W_{max} is the highest-frequency component present in continuous time signal. However, practical considerations on the closed loop system generally make it necessary to sample at a frequency much higher than $2W_{max}$. Usually, W_s is chosen to be $10W_{max}$ to $20W_{max}$ [11].

Low sampling frequency results in the folding effect (aliasing) in frequency spectra. The folding effect is defined as the overlap in the frequency spectra if the sampled analog signal has components whose frequency is higher than $W_s /2$. If the sampling frequency is not twice the full bandwidth of the continuous time signal, a folding error is present in the discrete time signal. The periodicity of the sampled signal may be represented by the formula:

$$X^*(s) = X^*(s \pm jW_s k), \quad \text{k=1,2,3..} \qquad (2.8)$$

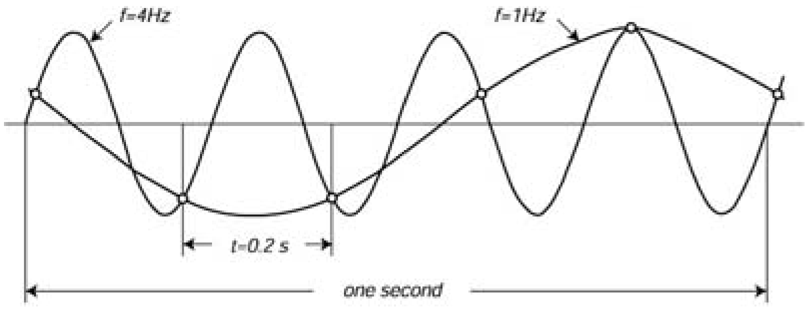

Figure 2-6 Aliasing in sampling [10]

In general, signals in control systems have high-frequency components. For instance, in a servomechanism, high-frequency noise on analog channels will always exist. As a result, a folding error will appear in the frequency spectra of discrete time signal unless the analog signal is sampled at twice the bandwidth of noise.

In order to avoid aliasing, we must either choose the sampling frequency high enough or use an anti-aliasing filter to filter out the high-frequency components of the continuous time signal [11]. Since it is not applicable to increase the sampling frequency, using an anti-aliasing filter may be a more applicable solution to aliasing problem. An analog low pass filter can be used as an anti-aliasing filter.

In practice, continuous-time to discrete-time conversion of a signal is realized using Analog-to-Digital converters (ADCs). When an analog signal is digitalized via an ADC, some other concepts should also be considered such as resolution, accuracy, quantization error, nonlinearity and aperture error.

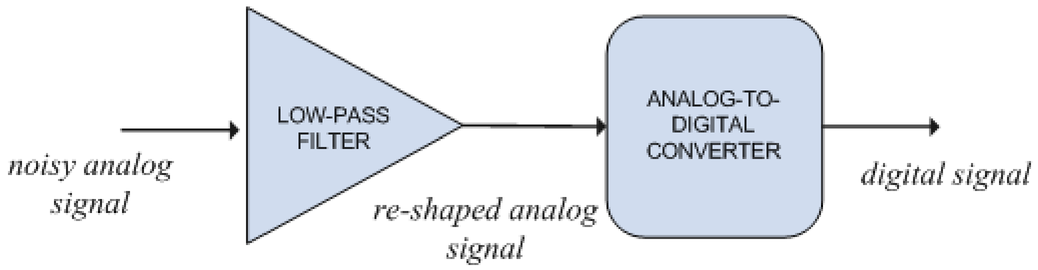

Figure 2-7 Anti-aliasing filtering and analog-to-digital conversion

2.4 Estimation and Kalman Filtering

Estimation is the calculated approximation of a signal when it is not precisely known or it is incomplete or uncertain. In engineering applications, for instance obtaining time derivative of a noisy signal, estimation is of great importance because it removes the necessity of direct differentiation which is noise amplification in other saying. Kalman filter with its various forms is an indispensable estimation tool widely used in engineering applications.

In this section, firstly, noise characteristics of a random variable will be studied and the borders between white noise and colored noise will be drawn. Then, discrete time Kalman filter approach will be studied for linear systems. Finally, Extended Kalman filter and Unscented Kalman filter approaches for nonlinear systems will be investigated.

2.4.1 Characteristics of Random Variables

A random variable is a variable whose value is not exactly known before the process actually runs. For instance, noise on the analog channel of a system is a random variable whose value cannot be known exactly but can be expressed with a mean and variance by help of statistical data. Hence, random variables can be expressed by some probability laws. Moreover, some probability density and distribution functions can be written based on the statistical data collected for them. The most common probability distribution function seen in nature is the Gaussian distribution. A random variable is called as Gaussian if it has a probability density function expressed by the formula:

$$pdf(x) = \frac{1}{\sigma\sqrt{2\pi}} \exp\left(\frac{-(x-\mu)^2}{2\sigma^2} \right) \tag{2.9}$$

In this formula, μ is the mean and σ^2 is the variance. A Gaussian distribution with zero mean will have a peak at zero point in its probability density plot. This shows that, the expected value of this random variable is zero. Variance of a Gaussian distribution, which is square of standard deviation, informs us about the possible deviations of the random variable from its mean.

When a random variable, for instance process noise or measurement noise in a dynamical system, is independent of its past and future values for all time, this random variable is named as white noise. If a random variable does not satisfy above condition, it is a colored noise. The power spectrum of a random variable which is defined as the Fourier transform of the autocorrelation determines the color content of the random variable. The Wiener-Khintchine equations show the relation between the Fourier transform and the autocorrelation function for a continuous time system.

$$S(w) = \int_{-\infty}^{\infty} R(\tau)e^{-jw\tau}d\tau$$
$$R(\tau) = \frac{1}{2\pi}\int_{-\infty}^{\infty} S(w)e^{jw\tau}dw \qquad (2.10)$$

For the discrete domain these equations may be stated as follows:

$$S(w) = \sum_{k=-\infty}^{\infty} R(k)e^{-jwk}, w \in [-\pi, \pi]$$
$$R(k) = \frac{1}{2\pi}\int_{-\infty}^{\infty} S(w)e^{jwk}dw \qquad (2.11)$$

Mathematically speaking, a white noise will have equal power at all frequencies in both continuous time and discrete time domains. A continuous time white noise will have an autocorrelation function given by the expression:

$$R(\tau) = R(0)\delta(\tau) \qquad (2.12)$$

In this expression, $\delta(\tau)$ is the continuous-time impulse function. Similarly, a discrete time white noise will have an autocorrelation function given by the expression:

$$R(k) = \begin{cases} \sigma^2 & k = 0 \\ 0 & k \neq 0 \end{cases} \qquad (2.13)$$

Therefore, power spectrum expression for a continuous time white noise process will be:

$$S(w) = R(0) \text{ for all w} \qquad (2.14)$$

For a discrete time white noise process it will be:

$$S(w) = R(0) = \sigma^2,\ w \in [-\pi, \pi] \qquad (2.15)$$

This implies that a white noise will have constant power at all frequencies. Another concept is uncorrelated noise. An uncorrelated noise vector implies that the elements of the vector are uncorrelated with each other resulting in a diagonal covariance matrice of the form

$$\begin{pmatrix} \sigma_1^2 & 0 & . & . & 0 \\ 0 & \sigma_2^2 & . & . & 0 \\ . & . & . & . & . \\ . & . & . & . & . \\ 0 & 0 & . & . & \sigma_n^2 \end{pmatrix} \tag{2.16}$$

This section gives some introductory information about a Gaussian, white and uncorrelated random variable. This is important to understand the conditions under which the Kalman filter shows its optimal performance. More information about random variables is revealed in a great detail in [12].

2.4.2 Kalman Filtering

Estimating state of a linear system is a common problem for most of engineering disciplines. Kalman filter is a tool that solves this problem optimally for linear systems. Any linear system can be expressed by the equations:

$$\begin{aligned} x_k &= F_k x_{k-1} + G_{k-1} u_{k-1} + w_{k-1} \\ y_k &= H_k x_k + v_k \end{aligned} \tag{2.17}$$

In these representations of dynamical system, x is the state of the system, u is the input to the system, y is the output of the system, w is the process noise and v is the measurement noise. Since process noise and measurement noise are random variables, the estimate of the state will also be a random variable. Hence, error between the estimate and the actual state is also a random variable. What Kalman filter does is to minimize expected value of this random variable while estimating the state at each time when a new output data of the system is available.

When process noise and measurement noise are both Gaussian, zero-mean, white, and uncorrelated, Kalman filter is the best linear estimator for the estimation problem. Although there is an open door of designing nonlinear filters showing better performance, the best linear solution of the estimation problem is the Kalman filtering. For the cases when process noise and measurement noise are not Gaussian, Kalman filter still gives out the optimal linear solution even though some nonlinear ways of getting better performance may still exist [12].

2.4.2.1 Discrete Time Kalman Filter

The discrete time Kalman filter has two update processes for each time step called *time update* and *measurement update*. In the time update step, a priori estimate of the state is made based on the system dynamics already known without using the measurement at that time step. After calculating priori state estimate, time update step for calculation of priori estimation error covariance is applied. In the measurement update process, measurement is taken into account to form up posteriori state estimate and estimation error covariance. Measurement update process makes it necessary to calculate a gain matrice called Kalman filter gain. Kalman filter gain is calculated to correct the priori state estimate and estimation error covariance taking the measurement into account.

Any system can be formulated in state-space form using state and output update equations and noise processes:

$$\begin{aligned}
&x_k = F_k x_{k-1} + G_{k-1} u_{k-1} + w_{k-1} \\
&y_k = H_k x_k + v_k \\
&E\{w_k w_j^T\} = Q_k \delta_{kj} \\
&E\{v_k v_j^T\} = R_k \delta_{kj} \\
&E\{w_k v_j^T\} = 0
\end{aligned} \tag{2.18}$$

In the above formulation, w is process noise and v is measurement noise. δ is Kronecker delta function. Noise processes are white, zero-mean, uncorrelated processes and their covariance matrices Q_k and R_k are known. Then the algorithm [12] may be summarized as follows:

1. The first step is the initialization of the Kalman filter. x_0 is the best estimate of initial state of system. P_0^+ is the uncertainty in estimating the initial state of the system.

$$\begin{aligned} x_0^+ &= E(x_0) \\ P_0^+ &= E\{(x_0 - x_0^+)(x_0 - x_0^+)^T\} \end{aligned} \tag{2.19}$$

2. The following equations should be evaluated at each time step when a new output data of the system is available.

   - Priori estimation error covariance:

$$P_k^- = F_{k-1}P_{k-1}^+F_{k-1}^T + Q_{k-1} \tag{2.20}$$

   - Kalman filter gain:

$$K_k = P_k^- H_k^T (H_k P_k^- H_k^T + R_k)^{-1} \tag{2.21}$$

   - Priori state estimate:

$$x_k^- = F_{k-1}x_{k-1}^+ + G_{k-1}u_{k-1} \tag{2.22}$$

   - Posteriori state estimate:

$$x_k^+ = x_k^- + K_k(y_k - H_k x_k^-) \tag{2.23}$$

   - For posteriori estimation error covariance, there are three different expressions defined in literature two of which are given here:

$$
\begin{aligned}
P_k^+ &= (I - K_k H_k) P_k^- (I - K_k H_k)^T + K_k R_k K_k^T \\
P_k^+ &= (I - K_k H_k) P_k^-
\end{aligned}
\tag{2.24}
$$

There are two types of covariance measurement update equations. The first type Joseph stabilized covariance measurement update equation which guarantees P_k^+ to be symmetric positive definite as long as the initial covariance is symmetric positive definite. Although the second form is the simplest in terms of computational burden, it does not guarantee symmetry and positive definiteness [12].

In real time applications, Kalman filter gain can be calculated offline to save computational effort due to the fact that Kalman gain is not dependent on measurements and system dynamics does not change with time for a linear time-invariant system. As a result, Kalman gain can be calculated using only system parameters (F, G, H, R, Q) which are known before the system actually runs [12].

Although Kalman filter is derived for linear systems, it can be expanded to nonlinear systems. This will be very useful because most real systems show nonlinear dynamics. Using first order Taylor series expansion for linearization, Extended Kalman filter is a way of estimation in nonlinear systems. However, it is not the only way. Another way of estimation in nonlinear systems is Unscented Kalman filter which uses Unscented Transforms to transfer Gaussians through nonlinear system dynamics.

2.4.2.2 Extended Kalman Filter

Most of real systems have nonlinear dynamics. To be able to estimate the states of a nonlinear system using a discrete time Kalman filter, we should first discretize the system dynamics.

Any nonlinear system can be formulated by the following system equations:

$$\begin{aligned} x_k &= f_{k-1}(x_{k-1}, u_{k-1}, w_{k-1}) \\ y_k &= h_{k-1}(x_k, v_k) \end{aligned} \tag{2.25}$$

In (2.25), w is process noise and v is measurement noise. Noise processes are white, zero-mean, uncorrelated processes and their covariance matrices Q_k and R_k are known. Then the discrete time extended Kalman filter algorithm can be summarized [12] by the following equations:

1. The first step is the initialization of the Kalman filter. x_0 is the best estimate of initial state of system. P_0^+ is the uncertainty in estimating the initial state of the system.

$$\begin{aligned} x_0^+ &= E(x_0) \\ P_0^+ &= E\{(x_0 - x_0^+)(x_0 - x_0^+)^T\} \end{aligned} \tag{2.26}$$

2. The following equations should be evaluated at each time step when a new output data of the system is available.

   - Partial derivatives of f_{k-1} with respect to state and process noise are evaluated around posteriori estimate of state.

$$\begin{aligned} F_{k-1} &= \frac{\partial f_{k-1}}{\partial x}(x = x_{k-1}^+) \\ L_{k-1} &= \frac{\partial f_{k-1}}{\partial w}(x = x_{k-1}^+) \end{aligned} \tag{2.27}$$

   - Time update of the state estimate and estimation error covariance is carried out.

$$\begin{aligned} P_k^- &= F_{k-1}P_{k-1}^+F_{k-1}^T + L_{k-1}Q_{k-1}L_{k-1}^T \\ x_k^- &= f_{k-1}(x_{k-1}^+, u_{k-1,} 0) \end{aligned} \tag{2.28}$$

- Partial derivatives of h_k with respect to state and measurement noise are evaluated around priori estimate of state.

$$\begin{aligned} H_k &= \frac{\partial h_k}{\partial x}(x = x_k^-) \\ M_k &= \frac{\partial h_k}{\partial v}(x = x_k^-) \end{aligned} \tag{2.29}$$

- Measurement update of the state estimate and estimation error covariance is carried out.

$$\begin{aligned} K_k &= P_k^- H_k^T (H_k P_k^- H_k^T + M_k R_k M_k^T)^{-1} \\ x_k^+ &= x_k^- + K_k [y_k - h_k(x_k^-, 0)] \\ P_k^+ &= (I - K_k H_k) P_k^- \end{aligned} \tag{2.30}$$

Extended Kalman filter gain cannot be calculated offline due to the fact that Kalman gain is dependent on partial differentiations at each mean point. Therefore, Extended Kalman filter seems to need more computational effort while running in real-time.

2.4.2.3 Unscented Kalman Filter

Extended Kalman Filter approximates nonlinear system functions using Taylor series expansion for transformation of Gaussian signals. However, Taylor series expansion is not the only way to perform this transformation through the nonlinear system dynamics. There is one more way which may give better results. It is the Unscented Transform. In this section of the thesis, a summary of the Unscented Kalman filter from [13] will be given.

Unscented Kalman Filter makes use of Unscented Transform to linearize nonlinear system functions. Let us assume we have a nonlinear function called f. The first step of linearization is to extract sigma points from the Gaussian signal and calculate the weights corresponding to these sigma points. For an n-dimensional Gaussian signal, there will be 2n+1 sigma points which are located at mean and two points symmetrically chosen with respect to the mean.

The equations to choose sigma points for a Gaussian $N(\mu,\Sigma)$ are given as:

$$\begin{aligned} X^0 &= \mu \\ X^i &= \mu + (\sqrt{(n+\lambda)\Sigma}), \quad \text{for i=1,..,n} \\ X^i &= \mu - (\sqrt{(n+\lambda)\Sigma}), \quad \text{for i=n+1,..,2n} \end{aligned} \tag{2.31}$$

In (2.31), $\lambda = \alpha^2(n+\kappa) - n$ and parameters α and κ determine the locations of the symmetrical sigma points. For each sigma point, there exist two weights which are calculated according to the following rules:

$$\begin{aligned} w_m^0 &= \frac{\lambda}{n+\lambda} \\ w_c^0 &= \frac{\lambda}{n+\lambda} + (1-\alpha^2+\beta) \\ w_m^i &= w_c^i = \frac{1}{2(n+\lambda)}, \quad \text{for i=1,..,2n} \end{aligned} \tag{2.32}$$

The parameter β is optimally 2 when the distribution is an exact Gaussian. In the second step, sigma points should be passed through nonlinear function *f*.

$$Y^i = f(X^i) \tag{2.33}$$

The third and final step of the unscented transform is to calculate new mean and covariance parameters of resulting Gaussian. The parameters can be calculated from the equations:

$$\begin{aligned} \mu' &= \sum_{i=0}^{2n} w_m^i Y^i \\ \Sigma' &= \sum_{i=0}^{2n} w_c^i (Y^i - \mu')(Y^i - \mu')^T \end{aligned} \tag{2.34}$$

The system equations of a nonlinear system can be expressed as follows:

$$\begin{aligned} x(k+1) &= g(x(k),u(k),k)+w(k) \\ y(k) &= h(x(k),k)+v(k) \end{aligned} \tag{2.35}$$

In the above given expression, w is the process noise and v is the measurement noise. Noise is white, zero mean and uncorrelated. A summary of the Unscented Kalman Filter algorithm is given below.

- The inputs for the algorithm are μ_{t-1}, Σ_{t-1}, u_t and z_t. In the first step, sigma points are extracted from the previous estimate and estimation error covariance.

$$X_{t-1} = (\mu_{t-1} \quad \mu_{t-1}+\gamma\sqrt{\Sigma_{t-1}} \quad \mu_{t-1}-\gamma\sqrt{\Sigma_{t-1}}) \tag{2.36}$$

- Calculated sigma points are passed through the nonlinear function *g* with the input u_t.

$$X_t^* = g(u_t, X_{t-1}) \tag{2.37}$$

- Mean and variance parameters are calculated from the sigma points.

$$\begin{aligned} \mu_t^* &= \sum_{i=0}^{2n} w_m^i X_t^{*i} \\ \Sigma_t^* &= \sum_{i=0}^{2n} w_c^i (X_t^{*i}-\mu_t^*)(X_t^{*i}-\mu_t^*)^T + Q \end{aligned} \tag{2.38}$$

- A new set of sigma points are extracted and passed through the nonlinear function *h*.

$$\begin{aligned} X_t &= (\mu_t^* \quad \mu_t^*+\gamma\sqrt{\Sigma_t^*} \quad \mu_t^*-\gamma\sqrt{\Sigma_t^*}) \\ Z_t &= h(X_t) \end{aligned} \tag{2.39}$$

- Using these new sigma points, prediction z_t^* and uncertainty S_t is calculated.

$$z_t^* = \sum_{i=0}^{2n} w_m^i Z_t^i$$
$$S_t = \sum_{i=0}^{2n} w_c^i (Z_t^i - z_t^*)(Z_t^i - z_t^*)^T + R \tag{2.40}$$

- Cross covariance between state and observation is calculated.

$$\Sigma_t^{x,z} = \sum_{i=0}^{2n} w_c^i (X_t^i - \mu_t^*)(Z_t^i - z_t^*)^T \tag{2.41}$$

- The Kalman gain is calculated using cross covariance matrix.

$$K_t = \Sigma_t^{x,z} S_t^{-1} \tag{2.42}$$

- Finally, estimation update is completed by calculating the parameters μ_t and Σ_t. The outputs of the algorithm are the parameters μ_t and Σ_t.

$$\mu_t = \mu_t^* + K_t(z_t - z_t^*)$$
$$\Sigma_t = \Sigma_t^* - K_t S_t K_t^T \tag{2.43}$$

Unscented Kalman Filter makes use of Unscented Transform to transform Gaussian signals through the nonlinear functions. The algorithm is more complex compared to the Extended Kalman Filter which uses only the first order term of Taylor series expansion. Although, asymptotic complexity seems to be the same when UKF and EKF are compared, in fact, the EKF is faster in practical applications. Although estimation performance of UKF is better than that of EKF generally, in most practical applications EKF and UKF show very similar performance [13]. However, if the system has intensive nonlinearities, EKF may generate unreliable estimates [25]. In that case, using UKF will upgrade the estimation performance considerably. One more advantage of UKF is that, it does not require differentiation of nonlinear functions. It is a differentiation-free nonlinear estimator [12].

2.5 Resolvers and Resolver-to-Digital Conversion

Resolvers have been used to sense angular position in industrial and military applications for nearly 50 years. It is a cost-effective and robust position sensor which can be used in challenging environments due to its simplicity, durability and reliability. A resolver is simply a rotating transformer. When excited with an AC signal through the reference inputs, it gives out two outputs called sine output and cosine output. They are named with these names because amplitudes of them are proportional to sine of rotor position and cosine of rotor position respectively. These two signals together are named as resolver format voltages [14]. The signals can be expressed mathematically as:

- Reference input: $A \sin wt$
- Sine Output: $AB \sin\theta \sin wt$
- Cosine Output: $AB \cos\theta \sin wt$

θ is angular position of the motor, w is the excitation frequency, A is the excitation amplitude and B is the transformation ratio of the resolver.

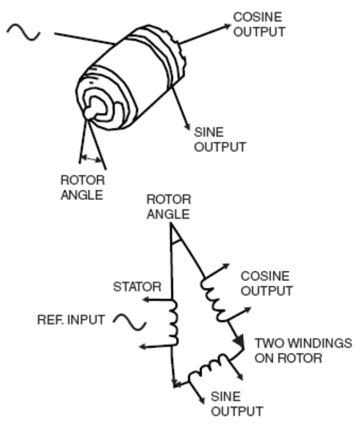

Figure 2-8 Resolver and resolver signals

Resolvers make interface electronics necessary to get a digital angular position measurement. This interface electronics converting resolver format voltages into meaningful digital data is called as Resolver-to-Digital converter. There are different types of Resolver-to-Digital converters available in the market. However, the most effective types are tracking type Resolver-to-Digital converters [14]. The advantages of the tracking type converters over other type converters are:

- Ratio metric Operation
- Noise Immunity
- Instant Digital Data
- Velocity voltage outputs.

Besides the advantages of tracking type Resolver-to-Digital converters, there are still some problems with this type of converters. These problems [14] are summarized as follows:

- Digital output lags actual position during acceleration.
- Flickering exists when the digital data is not an exact representation of the input angle.
- Common and differential phase shifts and distortions on the resolver format voltages may affect the performance of the conversion badly and result in noisy speed and position signals.
- Speed voltages exist on the resolver format voltages which deteriorate the conversion performance.

To eliminate these disadvantages, many methods are described in the literature. The inspected methods are handled in the next section.

2.5.1 Resolver-to-Digital Conversion Methods Proposed in the Literature

Acquiring velocity information from noisy position data is a known problem on which researchers have been studying consistently for decades. Therefore, literature includes so many investigations dealing with this problem. The main idea behind these investigations is the same and can be summarized by the expression that engineers designing servomechanisms want to know time based derivative of a system parameter. This is unavoidable especially in the cases when derivative of a system parameter is also another system parameter to be controlled.

Resolver is an indispensable position sensor for servo applications due to its simplicity, robustness and reliability. Resolver gives out position information by amplifying an AC input signal so that it generates two amplitude modulated AC signals as outputs which are named as resolver format voltages. The first amplitude modulated signal carries the information of cosine of the angular position while the second one carries the information of sine of the angular position. Therefore, what the engineers should do is to extract position information and estimate velocity information from resolver format signals.

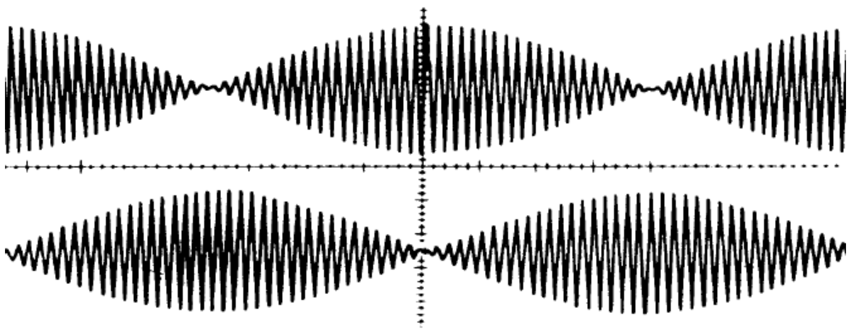
Figure 2-9 Resolver format signals as motor rotates

Literature survey performed on resolver-to-digital conversion give rise to a useful knowledge about the conversion process. A summary of literature survey performed on resolver conversion is given in this section.

Sarma, Agrawal and Udupa have developed a software based Resolver-to-Digital converter using a DSP based reference generator [15]. Since the reference frequency changes from resolver to resolver, software based reference generator implies a more flexible Resolver-to-Digital converter which can be used with any resolver. Demodulation of resolver format voltages is made using synchronous amplitude demodulation technique. They sampled resolver format voltages at the peaks of reference signal. After demodulation, they used a look-up-table including arctangent values for a complete 360° rotation in order to get the position information from sine and cosine envelops. Although results show a good performance in position estimation, velocity estimation problem is not dealt in the paper. Hence, the method can be seen as a trigonometric calculator rather than an estimator. Similar solutions are given in [16, 17, 18].

Harnefors [2] used a Linear Kalman Filter structure to estimate position and speed from noisy resolver format voltages. He used *dq* transformation matrice to have a steady-state Discrete Time Algebraic Riccati equation so that Kalman filter gain matrice could be calculated offline before the system actually runs. This results in a reduction in computational burden. Furthermore, in the study, he has formed up the system model in such a way that the acceleration error present in a tracking resolver conversion process is eliminated.

Bellini and Bifaretti [19] used a Discrete Time Kalman filter with a Phase Locked Loop based filter to estimate position and speed of a resolver. Since a PLL structure is implemented, using a Steady State Linear Kalman filter becomes sufficient for estimation. Furthermore, this model of system was formed up so that the filter can also perform an estimation of the acceleration. Therefore, the outputs of the filter do not lag the actual state even if acceleration is present in the motion. Moreover, it is stated that by the help of the filter, noise on the speed output is reduced compared to other methods.

Kaewjinda and Konghirun [20] implemented digital version of a classical tracking type Resolver-to-Digital converter using a Digital Signal Processor. The algorithm is confirmed in a vector controlled drive system of a Permanent Magnet Synchronous Machine. Moreover, offset calibration of resolver is made to eliminate offset errors in angle sensing. They also introduced a digital tracking type Resolver-to-Digital converter with a hardware error calculation algorithm [34]. Both structures they introduced are very similar to tracking type resolver-to-Digital converters except for the fact that the algorithms are implemented in a Digital Signal Processor.

Harnefors and Nee [21] designed a nonlinear observer for resolver-to-digital conversion process. Actually, the observer is a generic type observer that can be adapted to several processes. For instance, the observer can be used for estimating speed and position of a PMSM using fundamental excitation. The same algorithm may also be used for saliency and signal injection to estimate position of a PMSM with different d and q axes' inductances. Lastly, the algorithm can also be employed for resolver position and speed estimation process. The algorithm makes use of a nonlinear observer whose structure can be configured according to one of the above described processes. The study also includes stability and noise analyses of the proposed filter. The analyses are very useful from the view of practical implementations.

Lastly, Murray and Li designed a digital tracking resolver-to-digital converter in [22]. The converter makes use of a hardware error calculation scheme and a DSP IC, namely, TMS320C14. The converter is simply a digitized version of the classical tracking type RDC. The proposed method utilizes a hardware component to realize the error calculation and a DSP to implement the tracking loop.

2.5.2 Tracking Differentiators

Pure differentiation is known as to amplify the noise level on a discrete time signal. Another way of obtaining time-based derivative of a signal without amplifying the noise is the tracking differentiation. Not originally proposed for resolver-to-digital conversion, when adapted to this process, the tracking differentiator may perform a good performance. Hence, the filter is adapted to the resolver conversion process in Chapter 3 and some introductory information about the method is given in this section.

Gao inspected discrete time differentiators in terms of tracking performance [23]. The inspected differentiators include linearized approximations of pure differentiation as first order approximation and second order approximation;

$$\frac{s}{(\tau s+1)^m} \text{ , } m=1,2,.. \tag{2.44}$$

$$\frac{1}{\tau_2-\tau_1}\left(\frac{1}{\tau_1 s+1}-\frac{1}{\tau_2 s+1}\right) \tag{2.45}$$

Gao also inspected tracking differentiator in the form;

$$\begin{aligned}\frac{dx_1}{dt} &= x_2 \\ \frac{dx_2}{dt} &= -R\,\mathrm{sgn}\left(x_1 - v(t) + \frac{x_2\left|x_2\right|}{2R}\right)\end{aligned} \tag{2.46}$$

In above given representations of Tracking Differentiator, v is the input, x_1 and x_2 are the filter states and R is the filtering parameter of the tracking differentiator. This is a simplified form of tracking differentiator. Gao also examined Robust Exact Differentiator (RED) introduced in [24]. The paper includes the comparison test of the above mentioned differentiation methods. The performances of four different differentiators are compared to true derivative which is set as step response of a second order system. It is underlined that a white noise of 10% is added to signal before differentiation. The performances of the differentiators with respect to the true derivative are shown in Figure 2.12.

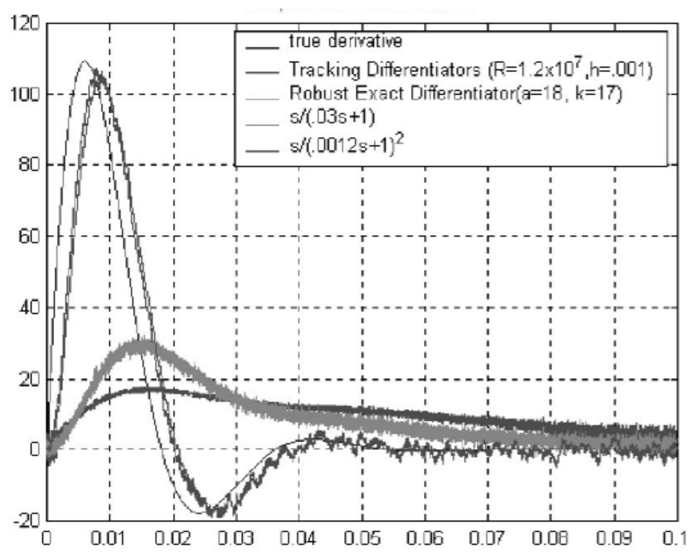

Figure 2-10 Comparative test results for implemented differentiators in [23]

Gao concluded that Tracking Differentiator has the best performance. Second order approximation's performance is also good while first order approximation and Robust Exact Differentiator performed poorly.

Consequently, the Tracking Differentiator is a successful means of differentiation in discrete domain. Since it uses a simple nonlinear function, it is practical in terms of computational complexity. It needs neither the system model nor the noise model. The tracking differentiation is described in details in [25] and [26].

2.6 Conclusion of the Literature Survey

In order to help the reader to have an insight into the proposed system and performed performance, stability and sensitivity analyses, a comprehensive literature survey covering all related subjects is given in this chapter. In this section, a conclusion made on the resolver-to-digital conversion methods proposed in the literature will be given rather than a conclusion covering the entire chapter.

The methods proposed in [15], [16], [17] and [18] are trigonometry-based methods. Hence, they perform the conversion by using various trigonometric functions in an open-loop structure which yield more noisy resolver position signals compared to the closed-loop structures. What is more is that since they use open-loop structures, they cannot produce speed signals, which is a serious drawback of them.

The method proposed in [2] makes use of a linear Kalman filter by linearizing the resolver conversion process by the help of *dq* transformation matrices. This method has some advantages such as giving out speed estimate and having zero acceleration error. Actually, the filter proposed in [19] is very similar to the filter proposed in [2] from practical point of view. A similar method is also designed and implemented in the thesis study by making use of "one step Kalman filter equations".

Methods proposed in [20] and [22] are similar methods both of whom implement a digital version of type 2 tracking resolver-to-digital converter. This converter structure possesses a drawback which is lagging under acceleration.

The filter proposed in [21] makes use of a structure in the form of a nonlinear observer and this structure is already realized as a part of the thesis and its performance is compared to other implemented filters.

The aforesaid studies in the literature solve the problem of designing a software-based resolver-to-digital conversion partially since the proposed filters make use of demodulated resolver signals. That is to say, the studies in the literature propose methods for neither demodulating resolver signals nor minimizing the resolver signal imperfections. Hence, intended to eliminate this deficiency of the literature, the thesis forms a complete solution for the problem of software-based resolver-to-digital conversion. For this purpose, besides the estimation algorithms, the proposed system has a software-based demodulator to realize the demodulation of resolver signals and a signal conditioner to minimize the disturbances coming from resolver signal imperfections. Moreover, the thesis introduces novel methods for estimation of position and speed from demodulated resolver signals such as Extended Kalman filter, Unscented Kalman filter and Tracking Differentiator approaches.

CHAPTER 3

DEVELOPMENT OF A DSP-FPGA-BASED RESOLVER-TO-DIGITAL CONVERTER

3.1 Proposed Resolver-to-Digital Converter

Resolvers have been used to sense angular position in industrial and military applications for nearly 50 years. It is a cost-effective and robust position sensor which can be used in challenging environments due to its simplicity, durability and reliability. Resolvers require an electronics interface which is named as resolver-to-digital converter for converting resolver signals into digital position and speed measurements. Since the proper current vector applied to a servo motor is calculated using motor shaft position, resolver-to-digital converter is the heart of a servo controller when servo motors coupled to resolver sensors are present in the servo system.

A resolver sensor is simply a rotating transformer. Excited by a high frequency reference signal, the resolver sensor gives out two signals which are named as resolver format signals. Resolver format signals carry the shaft position information through differential channels and at the end of these channels a resolver-to-digital converter waits to convert resolver format signals into digital angular position and angular velocity signals.

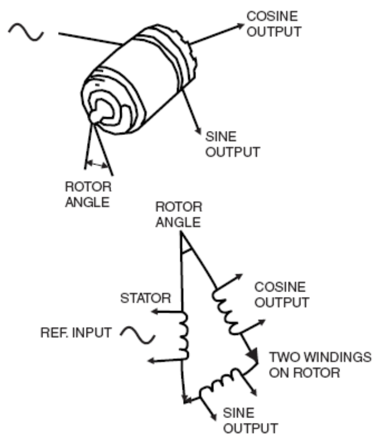

Figure 3-1 Resolver and resolver signals

The reference input of the resolver is excited by an AC voltage whose fundamental frequency is w rad/s;

- Reference input: $\sin wt$

Then, the rotor windings will modulate the reference voltage as sine and cosine functions of resolver position;

- Sine Output: $\sin\theta \sin wt$
- Cosine Output: $\cos\theta \sin wt$

where θ is angular position of the resolver rotor with respect to resolver stator and w is the reference signal's frequency (carrier frequency of resolver signals) in rad/s. Utilizing the resolver signals, a resolver-to-digital converter (RDC) estimates resolver position (θ) and resolver speed $\left(d\theta / dt \right)$.

The block diagram of the software-based resolver-to-digital converter proposed in the thesis is shown in Figure 3-3. The important parameters related to the converter such as sampling rate and signal frequencies are also given in Figure 3-3. The proposed RDC is implemented in the stabilized gun platform system seen in Figure 3-2.

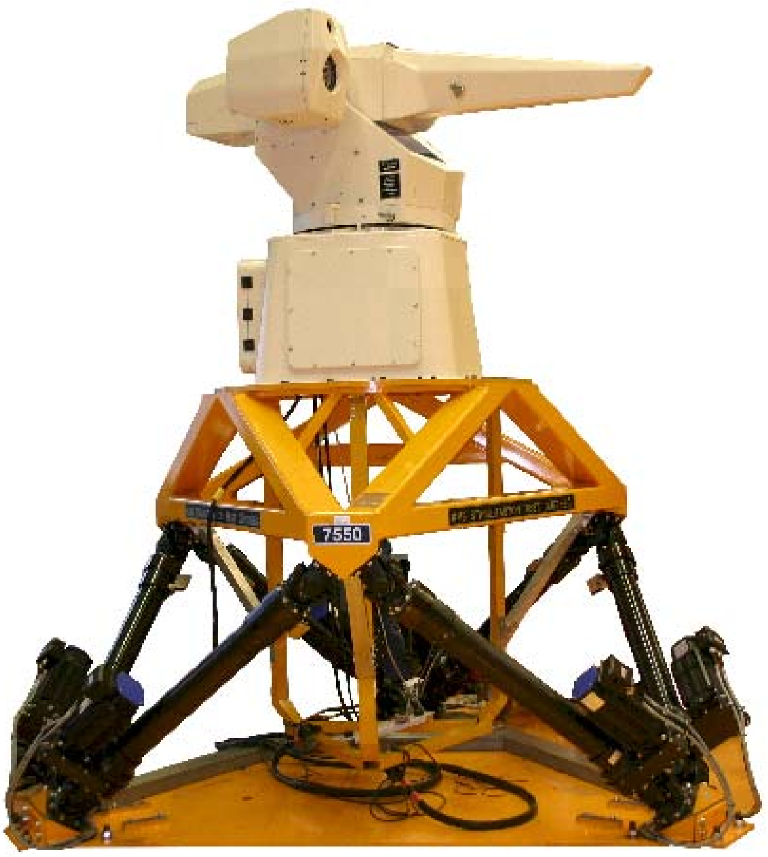

Figure 3-2 ASELSAN’s stabilized gun system STAMP on a STEWARD platform

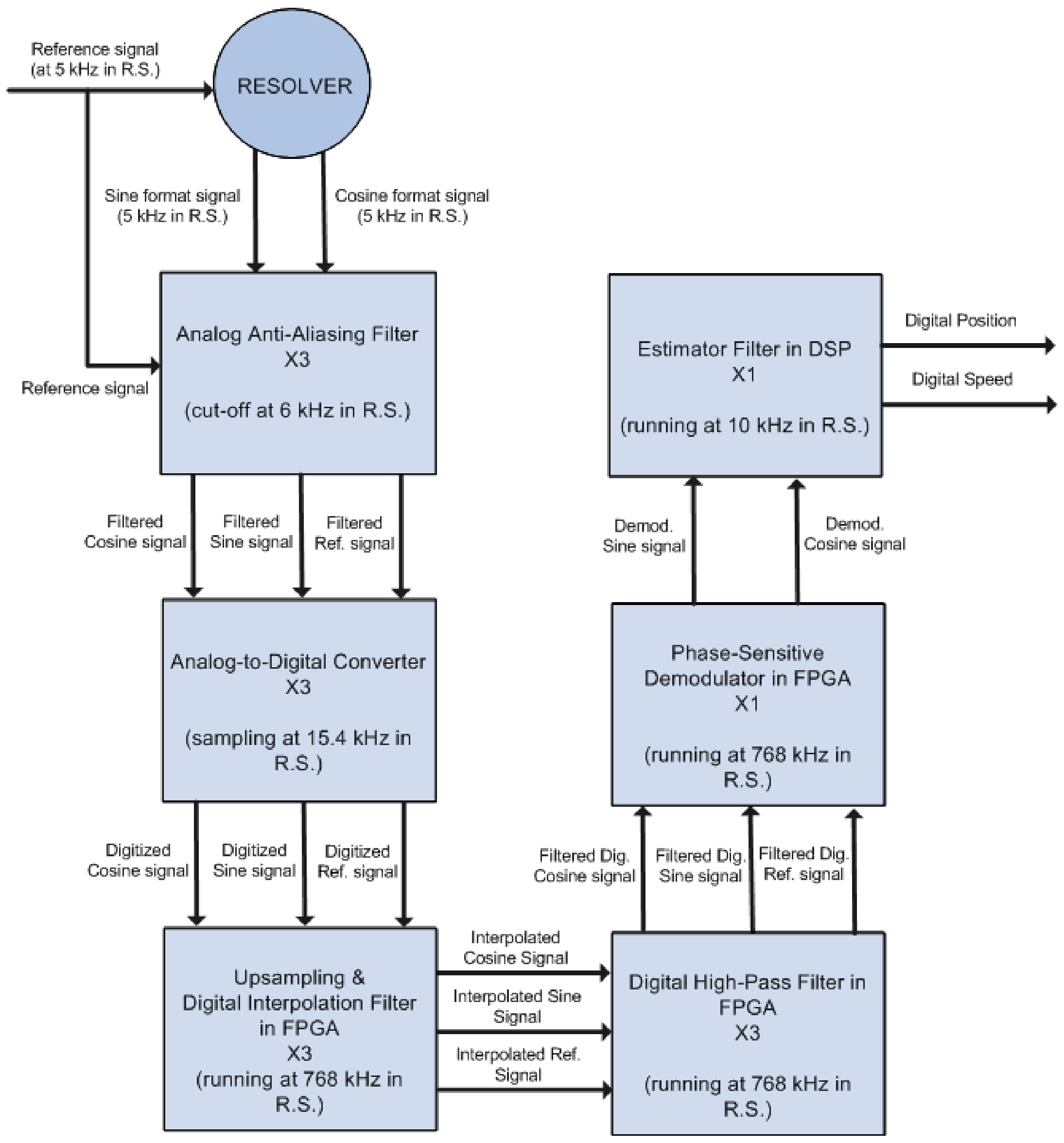
Reference signal (at 5 kHz in R.S.)
RESOLVER
Sine format signal (5 kHz in R.S.)
Cosine format signal (5 kHz in R.S.)
Reference signal
Analog Anti-Aliasing Filter X3 (cut-off at 6 kHz in R.S.)
Filtered Cosine signal
Filtered Sine signal
Filtered Ref. signal
Analog-to-Digital Converter X3 (sampling at 15.4 kHz in R.S.)
Digitized Cosine signal
Digitized Sine signal
Digitized Ref. signal
Upsampling & Digital Interpolation Filter in FPGA X3 (running at 768 kHz in R.S.)
Interpolated Cosine Signal
Interpolated Sine Signal
Interpolated Ref. Signal
Digital High-Pass Filter in FPGA X3 (running at 768 kHz in R.S.)
Filtered Dig. Cosine signal
Filtered Dig. Sine signal
Filtered Dig. Ref. signal
Phase-Sensitive Demodulator in FPGA X1 (running at 768 kHz in R.S.)
Demod. Sine signal
Demod. Cosine signal
Estimator Filter in DSP X1 (running at 10 kHz in R.S.)
Digital Position
Digital Speed

Figure 3-3 Proposed RDC and details related to implementation of it in real-time (R.S. in the block diagram stands for "Realized System")

3.1.1 Components of the Proposed RDC

Resolver signals may be contaminated by high-frequency noise and distorted due to disturbances coming from both transmission channels and resolver sensor itself (section 3.2). In order to minimize and/or eliminate the deteriorating effects of resolver signal imperfections on RDC's performance, analog anti-aliasing filters and digital filters are utilized in the proposed structure.

The proposed system has three analog-to-digital converters (ADCs) to digitize three resolver signals (section 3.2.3.2). Before the digitization, three anti-aliasing filters are used to minimize the high-frequency distortions and noise present in resolver signals (section 3.2.3.1). After sampling, digital interpolation filters, implemented in the Field-Programmable Gate Array (FPGA), reconstruct the resolver signals from sampled signals (section 3.2.3.2). In order to eliminate the low-frequency harmonic distortions and DC offset present in the reconstructed resolver signals, digital high-pass filters are also implemented in the FPGA (section 3.2.3.3).

The core of the proposed RDC is the estimator filter that estimates the resolver position (θ) and speed $\left({}^{d\theta}\!/_{dt}\right)$ from the demodulated resolver signals, namely $\sin\theta$ and $\cos\theta$ signals (section 3.4). Hence, to provide the estimator filter with $\sin\theta$ and $\cos\theta$ signals, the proposed RDC also has a phase-sensitive demodulator implemented in FPGA (section 3.3).

3.1.2 Forming the System Structure for the Proposed RDC

DSP and FPGA, both having advantages and disadvantages, actually they are not competitors but they may be complementary parts of an efficient system. Floating-point tasks with lower sampling rates and increased arithmetic complexity suit the DSP more whereas fixed-point arithmetic tasks with higher sampling rates and repetitive behavior suit the FPGA more. For instance, realizing a floating-point multiplier in FPGA is unreasonable since it will cover much area (logic gates) in FPGA while DSP's Central Processing Unit (CPU) with its highly-developed arithmetic sub-units will realize the operation with a little effort. On the other hand, FPGA can handle high-frequency data streams easily where DSP cannot handle them efficiently. As a result, in the proposed system, software components that require higher sampling rates are embedded into the FPGA whereas software components that have higher arithmetic complexity are embedded into the DSP. Table 3-1 shows the assignments of the components.

Table 3-1 Forming system structure

Component	Sampling Frequency	Arithmetic Complexity	Destination
Interpolation Filter	768 kHz	Low	FPGA
High-Pass filter	768 kHz	Low	FPGA
Demodulator	768 kHz	Low	FPGA
Estimator filter	10 kHz	High	DSP

3.2 Resolver Signal Imperfections and Filtering Resolver Signals to Improve Resolver-to-Digital Conversion Accuracy

In this section, resolver signal imperfections are investigated and their disturbing effects on the performance of the software-based RDC are analyzed both mathematically and numerically. Then, the signal conditioner designed to minimize these disturbing effects are explained in details. The improvement made in resolver conversion performance is also presented with test results.

3.2.1 Resolver Signal Imperfections - Low and High Frequency Harmonic Distortions in Resolver Signals

The Fast Fourier Transform (FFT) analysis performed on pure resolver signals has shown that resolver signals have harmonic distortion components within a wide frequency spectrum. Comparing the harmonic components' frequencies with the Nyquist frequency of the system, we can divide resolver signal imperfections into two main groups. Low-frequency harmonic components whose frequency spectrum is below the Nyquist frequency form up the first constituent of the imperfections in resolver signals. These components can be eliminated in digital domain since they do not result in misinformation by aliasing. High-frequency harmonic components and very-high-frequency noise whose frequency spectrum lies above the Nyquist frequency are the second constituents of resolver signal imperfections. It is concluded that this type of components should be eliminated using analog pre-filters in front of digitization in order not to result in misinformation by aliasing.

From the sampling theorem, we know that the frequency components exceeding the Nyquist frequency will be folded in the digitized signal and they will be seen as lower frequency signals. FFT analysis of resolver signals shows that there is also substantial amount of low-frequency distortions and DC offset in resolver signals. Figure 3-4 shows the result of the FFT analysis of the resolver sine signal when the resolver rotor position is 90° (i.e. FFT analysis of $\sin\theta \sin wt$ where $\theta = \pi/2$).

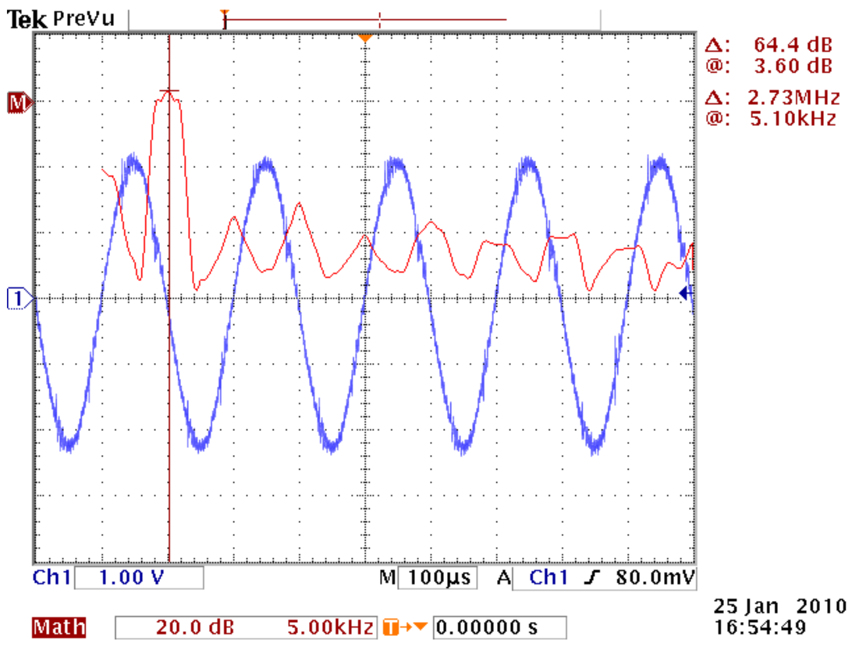

Figure 3-4 Pure resolver signal $\sin(\pi/2)\sin wt$ (blue signal) and its FFT (red signal)

When Figure 3-4 is examined closely, it is observed that pure resolver signals have harmonic distortion components at frequencies kw where $k = 0, 2, 3, 4, 5$ and w is the fundamental frequency (w=2πf and f=5000 Hz in the experimental system). The amplitudes of the harmonic distortion components in the realized system are measured as given in Table 3-2.

Table 3-2 Distortion levels in pure resolver signals normalized to fundamental component

Component Type	Frequency	Magnitude	
		dB	**%**
Low-frequency Distortion	DC offset	-23.6	6.66
Fundamental Component	5 kHz	0	100
High-frequency Distortions	10 kHz	-38	1.26
	15 kHz	-33.6	2.09
	20 kHz	-43.6	0.66
	25 kHz	-39.6	1.05
High-frequency Noise	>>25 kHz	<<-40	<<1

3.2.2 Disturbing Effects of Resolver Signal Imperfections on Software-Based Conversion Performance

The misinformation in frequency spectrum due to aliasing will deteriorate the conversion performance and cause an error in position estimation which is called as position estimation error. Furthermore, not only aliasing components but also low-frequency harmonics and DC offset will cause error in position estimation.

From the sampling theorem, we know that the frequency component at $f = nf_s \pm f'$, where f_s is the sampling frequency and *n* is an integer, will appear in the sampled signal as if there is a frequency component at $f = f'$. An example from the experimental system may be that the frequency component at 10 kHz will appear as a frequency component at 5.4 kHz after sampling process since the sampling rate is 15.4 kHz. Table 3-3 shows the aliases of the frequency components present in resolver signals in the experimental system.

Table 3-3 Aliases of the resolver signals' components in the experimental system where the Nyquist frequency is 7.7 kHz

Aliasing	**Actual Frequency**	**Seen as**
No aliasing since f<7.7 kHz	DC	DC
	5 kHz	5 kHz
Aliasing occurs since f>7.7 kHz	10 kHz	5.4 kHz
	15 kHz	400 Hz
	20 kHz	4.6 kHz
	25 kHz	9.6 kHz

The following analysis proves the disturbing effects of harmonic distortions on the software-based conversion performance. We can start the analysis by modeling a resolver signal with harmonic distortion components. The distorted sine signal will be

$$\sin\theta\left(\sin wt + \sum_{k=2}^{k=N} C_k \sin(kwt + \xi_k) + D\right) \tag{3.1}$$

The term $\sin\theta\sin wt$ in (3.1) stands for the actual resolver sine signal. Hence, θ is the resolver position and w is the fundamental frequency in rad/s ($w = 2\pi f$ and f=5 kHz). The term $\sin\theta\sum_{k=2}^{k=N} C_k \sin(kwt + \xi_k)$ represents the high-frequency harmonic distortions where C_k represents amplitudes of the harmonics and ξ_k represents phase angles of them. Lastly, the term $D\sin\theta$ is for the low-frequency harmonics which are modeled using a DC offset neglecting other components.

The discrete model of the resolver signal when aliasing is taken into account will be

$$\sin\theta\sin(wnT_s) + \sum_{k=0}^{\infty} C_k^* \sin(w_k^* nT_s + \xi_k^*) + D\sin\theta \tag{3.2}$$

where T_s is the sampling period and nT_s represents the sampling instants on time axis. C_k^* , ξ_k^* and w_k^* are magnitudes, phase angles and frequencies of the aliases respectively.

The sampled signal will be demodulated by phase-sensitive demodulator which can be modeled as a half-period integrator from *0* to *1/2f.* Hence, the demodulator output for sine channel can be derived by the following operations;

$$\pi f \int_0^{1/2f} \left(\sin\theta \sin(wnT_s) + \sum_{k=0}^{\infty} C_k^* \sin(w_k^* nT_s + \xi_k^*) + D\sin\theta \right) dt \tag{3.3}$$

$$= \pi f \int_0^{1/2f} \sin\theta \sin(wnT_s) dt + \int_0^{1/2f} \sum_{k=0}^{\infty} C_k^* \sin(w_k^* nT_s + \xi_k^*) dt + \sin\theta \int_0^{1/2f} D dt \tag{3.4}$$

$$= \sin\theta + \pi f \sum_{k=0}^{\infty} C_k^* \int_0^{1/2f} \sin(w_k^* nT_s + \xi_k^*) dt + \sin\theta \frac{\pi D}{2} \tag{3.5}$$

The first term in (3.5) represents the demanded output of the demodulator for sine channel. However, since half-period integration of the aliasing components and DC component, represented by the second term and the third term in (3.5) respectively, will be nonzero, the demodulator output will deviate from the demanded output $\sin\theta$. Similarly, demodulator output for cosine channel will also deviate from the demanded output $\cos\theta$ because of the same reason.

By the help of a reasonable assumption that half-period integration of aliasing components will be proportional to the amplitude of the resolver signal ($\sin\theta$ or $\cos\theta$), the misinforming demodulator outputs for sine and cosine channels can be modeled as $\sin\theta + \Delta S \sin\theta$ and $\cos\theta + \Delta C \cos\theta$ respectively.

The estimator filter in the proposed system runs to eliminate the error between the actual position (θ) and the estimated position (ϕ) by using the error signal calculator expressed by the equation set (3.6).

$$\sin\theta\cos\phi - \cos\theta\sin\phi = \sin(\theta-\phi) \tag{3.6}$$

We can assume that the estimator filter tracks the position information carried by the demodulator outputs with zero error.

$$\sin\theta\cos\phi - \cos\theta\sin\phi = \sin(\theta-\phi) = 0 \tag{3.7}$$

However, when the demodulator output is misinforming as in the case of software-based demodulator, although the estimator filter tracks the demodulator outputs with zero error, it will track the actual position with a nonzero error. If we write the misinforming demodulator outputs into (3.7), the tracking error $\Delta\theta$ will be found as

$$(\sin\theta + \Delta S\sin\theta)\cos\phi - (\cos\theta + \Delta C\cos\theta)\sin\phi = 0 \tag{3.8}$$

$$\sin(\theta-\phi) + \Delta S\sin\theta\cos\phi - \Delta C\cos\theta\sin\phi = 0 \tag{3.9}$$

$$\sin(\theta-\phi) \approx \theta-\phi = \Delta\theta = \Delta C\cos\theta\sin\phi - \Delta S\sin\theta\cos\phi \tag{3.10}$$

Hence, the analysis proves that resolver signal imperfections degrade the conversion accuracy and induce a nonzero position estimation error. Moreover, the analysis shows that the estimation error is dependent on the actual position (θ), estimated position (ϕ) and demodulator output deviations (ΔS and ΔC).

3.2.3 Position Estimation Error due to Resolver Signal Imperfections and Resultant Disturbances on Torque and Speed of the Motor

Since there are many aliases in the digitized resolver signals and their frequencies, amplitudes and phases are not exactly known, it seems challenging to calculate an approximate value for the position estimation error due to aliasing components. However, an upper limit can be calculated using the information given in Table 3-2 and Table 3-3 with the assumption that amplitudes of the aliases cannot exceed the amplitudes of the original signals. On the other hand, it seems possible to calculate an approximate value for the position estimation error due to low-frequency harmonic components and DC offset since they appear in the digital signal without encountering any transformation.

Table 3-4 Calculated maximum percentage errors at the demodulator outputs due to low-frequency harmonics (ΔD) and high-frequency harmonics (ΔE)

Actual Frequency	**Frequency in Digital Domain**	**Max imum Amplitude of the Distortion**	**Phase of the Alise when max. error exist**	**Error at the Dem. Output**	ΔD	ΔE
DC	DC	6.66%	-	10.35%	10.35%	-
10 kHz	5.4 kHz	1.26%	0°	1.25%	-	
15 kHz	400 Hz	2.09%	~75°	3.19%	-	
20 kHz	4.6 kHz	0.66%	0°	0.43%	-	
25 khz	9.6 kHz	1.05%	0°	0	-	
Noise	Noise	Neglected		0	-	<4.89%

Table 3-4 gives the calculated maximum errors at the demodulator output due to both aliasing (ΔE) and non-aliasing components (ΔD). Then the upper limit for the total demodulator output error can be calculated by summing up ΔE and ΔD as

$$\Delta S = \Delta C = \Delta D + \Delta E = 15.24\% \qquad (3.11)$$

Using ΔS and ΔC values, the position estimation error can be calculated using (3.10). In order to avoid iterations in solving (3.10), it is assumed that ϕ is equal to θ in calculation of the multiplicative terms $\cos\theta\sin\phi$ and $\sin\theta\cos\phi$. In the calculations, the resolver rotor is assumed to be rotating with a speed of 2π rad/s and ΔS and ΔC are assumed to be normally distributed with mean zero and variance 0.4% (corresponding to a maximum error of 15% approximately). Figure 3-5 shows the variation of the calculated position estimation error.

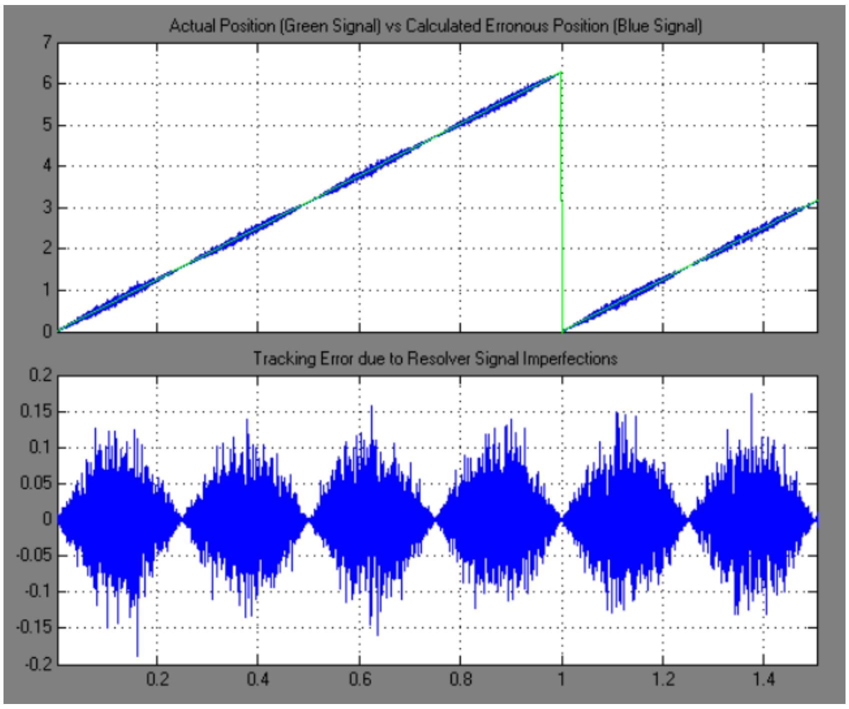

Figure 3-5 Actual position, estimated erroneous position and position estimation error with respect to time (s)

The experimental system without eliminating resolver signal imperfections will have a maximum position estimation error of 0.1 rad (5.73 deg) as seen in Figure 3-5. Moreover, erroneous position information will also cause erroneous torque feedback and degrade the torque loop performance. In the experimental system, since the torque feedback is not a measurable variable, it is calculated using motor phase currents and rotor position to be able to form up a torque control loop. The calculation of the torque is made by the help of a special transformation which shows the relation between the torque feedback and resolver shaft position θ as

$$T = i_a\left(-\sin\theta + {}^{1}\!/\!{}_{\sqrt{3}}\cos\theta\right) + {}^{2}\!/\!{}_{\sqrt{3}}\, i_b\cos\theta \qquad (3.12)$$

where signals i_a and i_b stand for the motor phase currents. To observe the effect of the position estimation error on torque loop performance, a simulation is performed using (3.10) and (3.12). In the simulation model, a one pole pair synchronous motor with a resolver sensor rotating with a speed of 2π rad/s is simulated. The model has Inverse Park and Inverse Clarke transforms in order to simulate the motor phase currents i_a and i_b. The true torque is calculated by using the correct position signal whereas the erroneous torque is calculated by using the position signal with the estimation error. In the simulation, ΔS and ΔC are assumed to be normally distributed with mean zero and variance 0.4% (corresponding to a maximum error of 15%). The correct and erroneous signals for position and torque are shown in Figure 3-6.

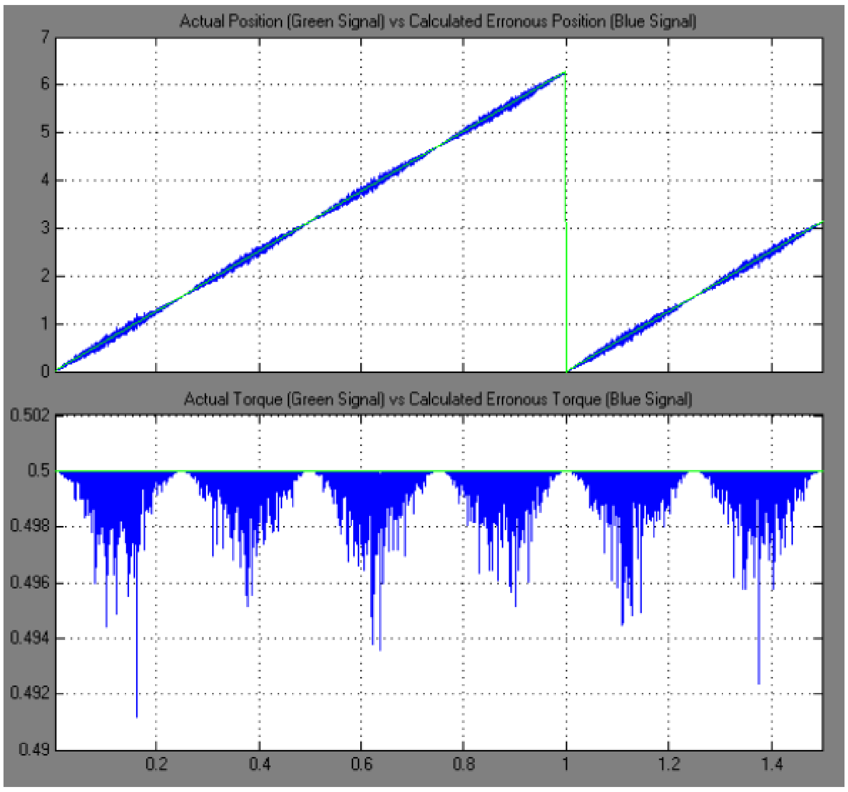

Figure 3-6 Effect of misinforming position signal on torque feedback signal (horizontal axis is time axis in seconds)

It is concluded that the maximum error in torque estimation due to position estimation error will be 1% of the demanded torque. Since a closed loop torque control technique (Field Orientated Control) is implemented in the experimental system, misinforming torque estimation will result in undesirable oscillations in motor torque. Depending on the inertia and the frictional forces of the motor and the experimental system that is actuated by the motor, these undesirable oscillations may create unrecoverable disturbing effects on the speed loop of the system. For instance, Figure 3-7 shows how the same amount of ripple in motor torque (1% of maximum achievable torque) disturbs the speed of the experimental system. It is observed that speed of the system incurs an oscillation with peak-to-peak amplitude of 2°/sec. This amount of uncontrollable oscillation in speed of the system will degrade target tracking performance of the stabilized gun platform.

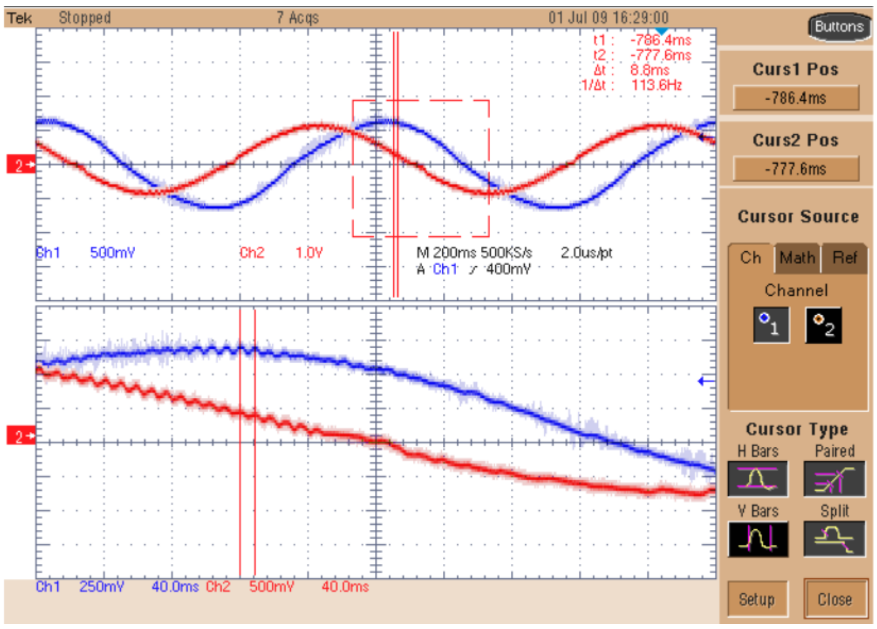

Figure 3-7 Oscilloscope screen showing torque signal (red signal where 10V means maximum torque) with 1% torque ripple and ripple's disturbing effect on speed of the experimental system (blue signal where 10V corresponds to 100°/sec)

The disturbing effect originating from resolver signal imperfections in the proposed software-based RDC will degrade the performance of the gun stabilization system and the experimental system will face up with oscillations in motor torque and speed. Therefore, minimization of this disturbance is of great importance to minimize oscillations in system and to maintain high-performance target tracking with high-performance gun stabilization. The proposed method to eliminate/minimize resolver signal imperfections is a mixed-signal signal conditioner which uses analog and digital filters as seen in Figure 3-8.

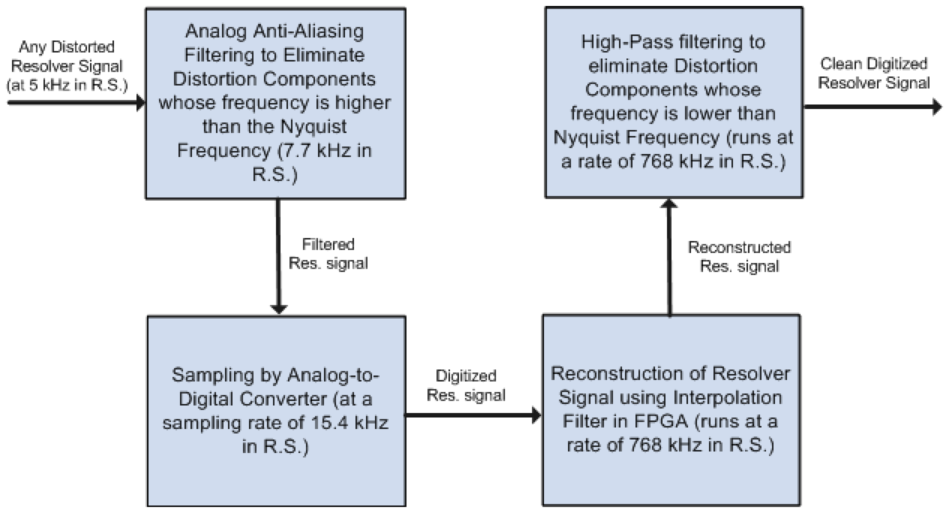
Any Distorted Resolver Signal (at 5 kHz in R.S.)
Analog Anti-Aliasing Filtering to Eliminate Distortion Components whose frequency is higher than the Nyquist Frequency (7.7 kHz in R.S.)
Filtered Res. signal
Sampling by Analog-to-Digital Converter (at a sampling rate of 15.4 kHz in R.S.)
Digitized Res. signal
Reconstruction of Resolver Signal using Interpolation Filter in FPGA (runs at a rate of 768 kHz in R.S.)
Reconstructed Res. signal
High-Pass filtering to eliminate Distortion Components whose frequency is lower than Nyquist Frequency (runs at a rate of 768 kHz in R.S.)
Clean Digitized Resolver Signal

Figure 3-8 Proposed mixed-signal signal conditioner to obtain distortion-free and noise-free digital resolver signals (R.S. stands for “Realized System”)

3.2.3.1 Minimization of High-Frequency Harmonic Distortions and Noise (“Aliasing Components”) in Resolver Signals Using Analog Anti-Aliasing Filters

In order to prevent aliasing, we should use pre-filters, named as anti-aliasing filters in front of the source signals to reshape the frequency spectrum by suppressing the frequency components beyond the Nyquist frequency [27]. Filter parameters such as bandwidth and filtering order should be assigned based on the system parameters such as resolver carrier frequency, sampling frequency and maximum speed that the resolver rotor may reach in the experimental system.

Since the Nyquist frequency (7.7 kHz) is close to resolver signal carrier frequency (5 kHz) in the experimental system, higher order filters would be better in suppression of the undesirable high-frequency components because higher order filters have sharper magnitude plots beyond the cut-off frequency. On the other hand, it is a known fact that as the filter order increases phase contribution of the filter also increases. More phase contribution means more delay in measurements and increasing estimation error. Furthermore, implementation cost of the filter also increases as the filter order increases. Considering above mentioned factors, a table examining cost, performance and delay of different order filters is formed. To prevent suppression of the fundamental component at 5 kHz which carries the actual position data θ, the filters' cut-off frequencies are set to 6 kHz which is close to the midpoint between 5 kHz and 7.7 kHz. Table 3-5 gives position estimation errors due to delays that anti-aliasing filters introduce to resolver signals in the experimental system. The measurements are made when the resolver rotates with a speed of 4800 deg/sec. This speed value is close to the maximum speed of the experimental system. Therefore, the error values given in Table 3-5 can be regarded as the maximum error values due to anti-aliasing filtering delays in the experimental system.

Table 3-5 Position estimation error due to delay introduced by the different order anti-aliasing filters in the experimental system

	Order 1 Filter	Order 2 Filter	Order 3 Filter
Phase at 5 kHz	-39.8 deg	-76.7 deg	-111.8 deg
Suppression at 7.7 kHz	-4.4 dB	-5.7 dB	-7.4 dB
Op-amps for realization	1	1	2
Position tracking error when res. rotor speed is 4800 deg/s	0.1061 deg	0.2045 deg	0.2981 deg

The analysis shows that position estimation error due to anti-aliasing filtering will be much smaller than the error due to resolver signal imperfections which has been calculated as 5.73 deg in the previous section. Hence, high-frequency suppression ability and cost of the filter becomes more important in choosing the right order anti-aliasing filter. Examining Table 3-4, it is concluded that the second order filter is the most practicable filter for the experimental system. The filter suppresses high-frequency harmonic components substantially (Figure 3-9) and it can be realized using only one operational-amplifier.

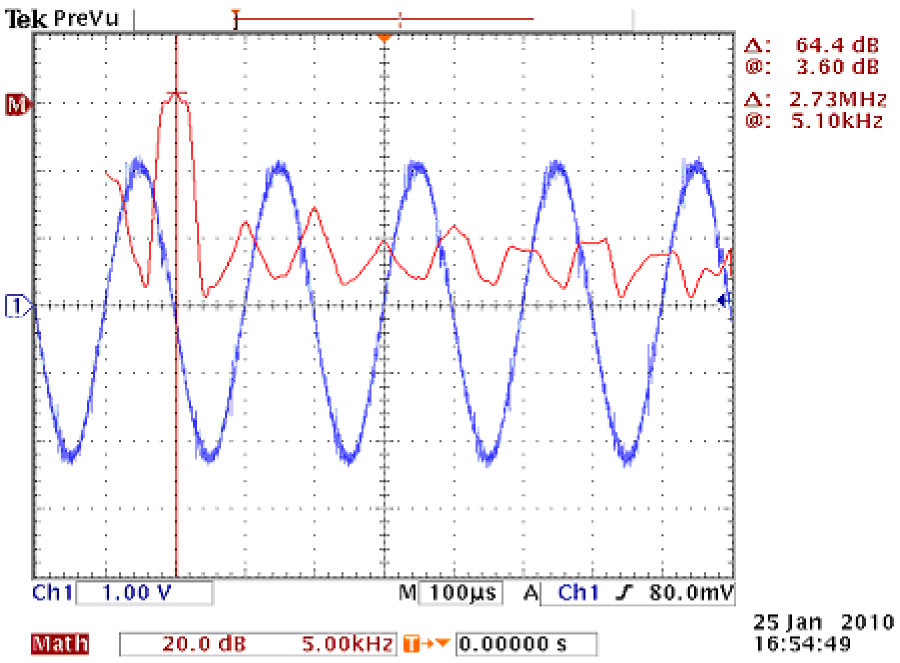

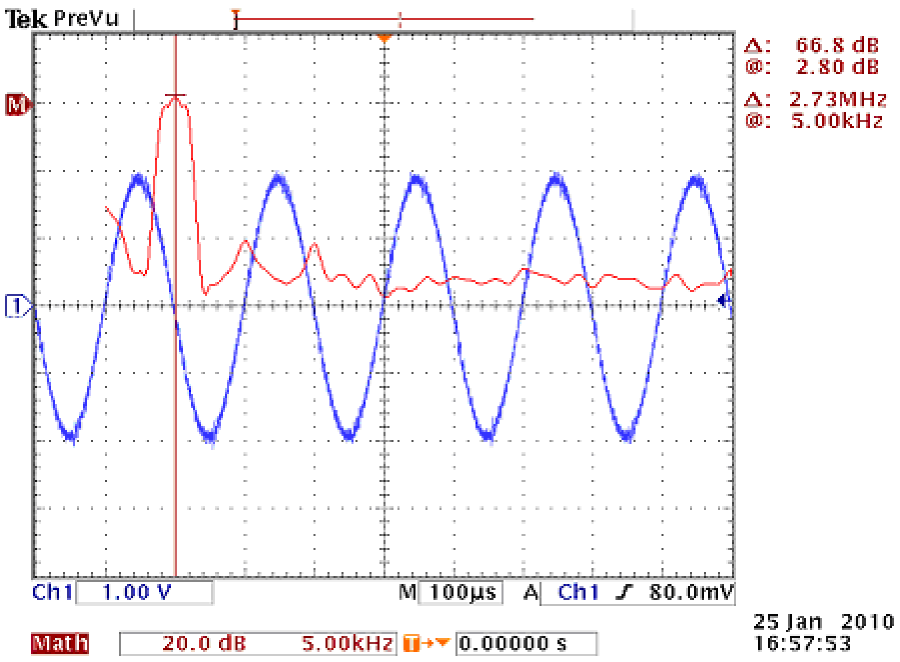

Figure 3-9 Pure resolver sine signal and its FFT (red signal) on the above scope screen and resolver sine signal after filtered by the anti-aliasing filter and its FFT (red signal) on the below scope screen

The filter improves the accuracy of the demodulated data by 62.37%. The details related to the filter's performance are given in Table 3-6.

Table 3-6 Anti-aliasing filter's performance

Before Anti-aliasing Filtering				
Frequency	Amplitude of Harmonic Dist. dB	Amplitude of Harmonic Dist. %	Error at demodulator output	ΔE
10 kHz	-38	1.26	1.25%	
15 kHz	-33.6	2.09	3.19%	
20 kHz	-43.6	0.66	0.43%	
25 kHz	-39.6	1.05	0%	<4.89 %
After Anti-aliasing Filtering				
Frequency	Amplitude of Harmonic Dist. dB	Amplitude of Harmonic Dist. %	Error at demodulator output	ΔE
10 kHz	-42.8	0.72	0.71%	
15 kHz	-43.6	0.66	1.00%	
20 kHz	<-52.8	<0.2	<0.13%	
25 kHz	<-52.8	<0.2	0%	<1.84%
Suppression of High-frequency Harmonic Distortions at Demodulator Output	62.37%			

3.2.3.2 Digitization and Reconstruction of Filtered Resolver Signals in FPGA

Analog-to-digital conversion rate should satisfy the Nyquist criterion for the fundamental component to guarantee the feasibility of the software-based resolver-to-digital converter. ADCs used in the experimental system have a sampling rate of 15.4 kHz and they satisfy the Nyquist criterion for the fundamental frequency 5 kHz. Their conversion resolution is 16 bit in signed fixed-point arithmetic (two's complement form).

From the sampling theorem we know that if the sampling frequency is sufficiently high compared to the bandwidth of the continuous-time signal ($w_s > 2Bandwidth$), the original signal can be reconstructed from the sampled signal using an ideal sinc filter. Since an ideal sinc filter is non-causal and has an infinite delay, it is not physically realizable [28]. Hence, a windowed digital low-pass filter to reconstruct the resolver signals in discrete-domain is used instead.

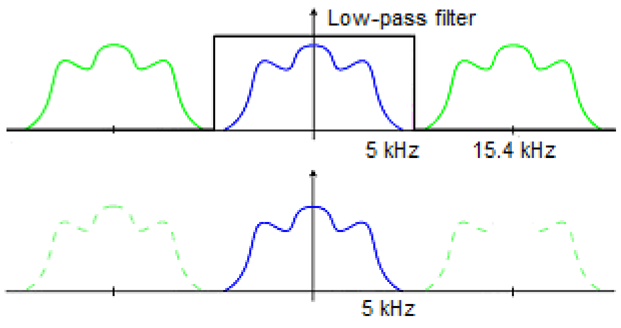

Figure 3-10 Reconstruction of resolver signals by low-pass filtering

Digital filters may be classified according to duration of their impulse responses: Finite-Impulse Response (FIR) filters and Infinite-Impulse Response (IIR) filters. Even though both filters can be implemented in an FPGA, implementing FIR filters seems easier and more reliable. FIR filtering in FPGA is easier because FIR filters have an open loop structure. On the other hand, IIR filters require feedback from output. The need for feedback not only complicates the FPGA software but also opens the doors to stability problems and makes the filter much more sensitive to quantization errors. Therefore, utilizing an FIR filter will be more easy and reliable due to its simple structure, stability and robustness against quantization effects [29, 30].

The FIR filter parameters such as sampling rate, F_{stop} and F_{pass} frequencies, coefficient resolution and filter arithmetic is adjusted such that;

- Sampling rate is adjusted according to the performed trade-off between demanded FPGA code efficiency and maximum allowable error due to quantization,

- Coefficient resolution and filter arithmetic are selected according to the analog-to-digital conversion resolution and arithmetic,
- F_{stop} and F_{pass} frequencies are adjusted according to the resolver signal carrier frequency.

Firstly, in order to decide on the sampling rate of the interpolation filter, a trade-off between the filtering performance and the code efficiency should be resolved. Choosing higher sampling rates for the filter is better to minimize the quantization error in the reconstructed sinusoidal. On the other hand, lower sampling rates are better for feasibility of the filter in FPGA. As the ratio of the FPGA clock frequency (constant) to the filter sampling frequency increases, the filter covers less area in FPGA since it needs making use of less parallel structures. Taking both factors into consideration, sampling frequency of the up sampled signal is optimized at 768 kHz (i.e. an up-sampling factor of 49.87 is used) in the experimental system. At this rate, the quantization error at the demodulator output becomes less than 0.5×10^{-5} percent which is negligibly small compared to ΔS and ΔC values (15.24%).

Secondly, since analog-to-digital conversion resolution is 16 bit in signed fixed-point arithmetic, filter coefficients are also generated in 16 bit fixed-point signed arithmetic in the experimental system.

Thirdly, the filter F_{stop} and F_{pass} parameters are adjusted to 5500 Hz and 9500 Hz respectively to filter out only the higher-frequency components above the resolver carrier frequency and not to suppress the fundamental component at 5 kHz. Filter parameters and filter's demanded magnitude response are given in Figure 3-11.

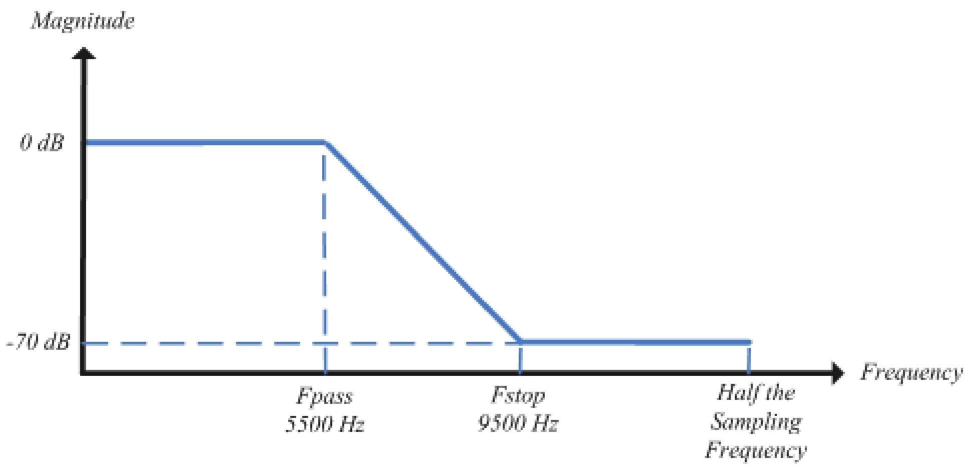

Figure 3-11 Digital interpolation filter parameters and demanded magnitude response

The filter is realized using Filter Design and Analysis (FDA) tool of Matlab and filter coefficients are loaded into FPGA software design environment (ISE). The filter order is realized as 433. The filter is implemented using Finite Impulse Response filter cores (MAC FIR version 5.1 of Xilinx). The details related to FPGA programming issues are given in Appendix A. Filter's realized magnitude and phase responses are seen in Figure 3-12. Figure 3-13 illustrates the real-time reconstruction of a resolver signal in the experimental system.

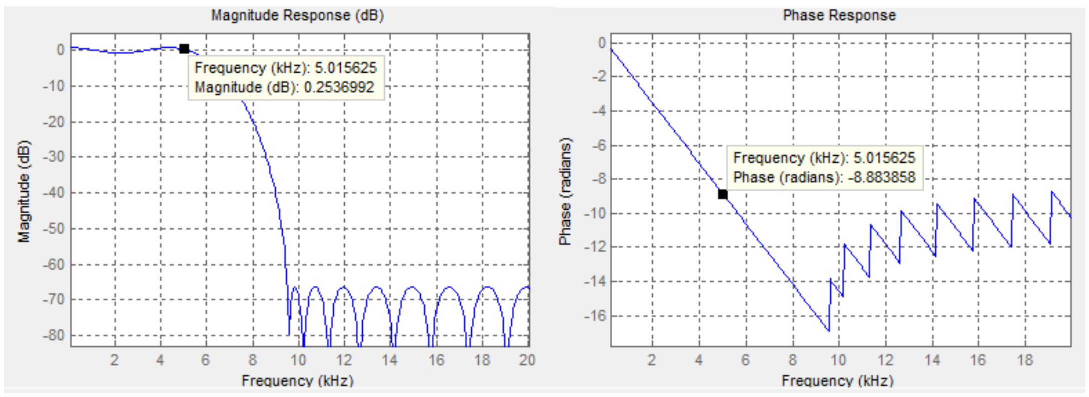

Figure 3-12 Realized magnitude and phase responses of digital interpolation filter implemented in FPGA

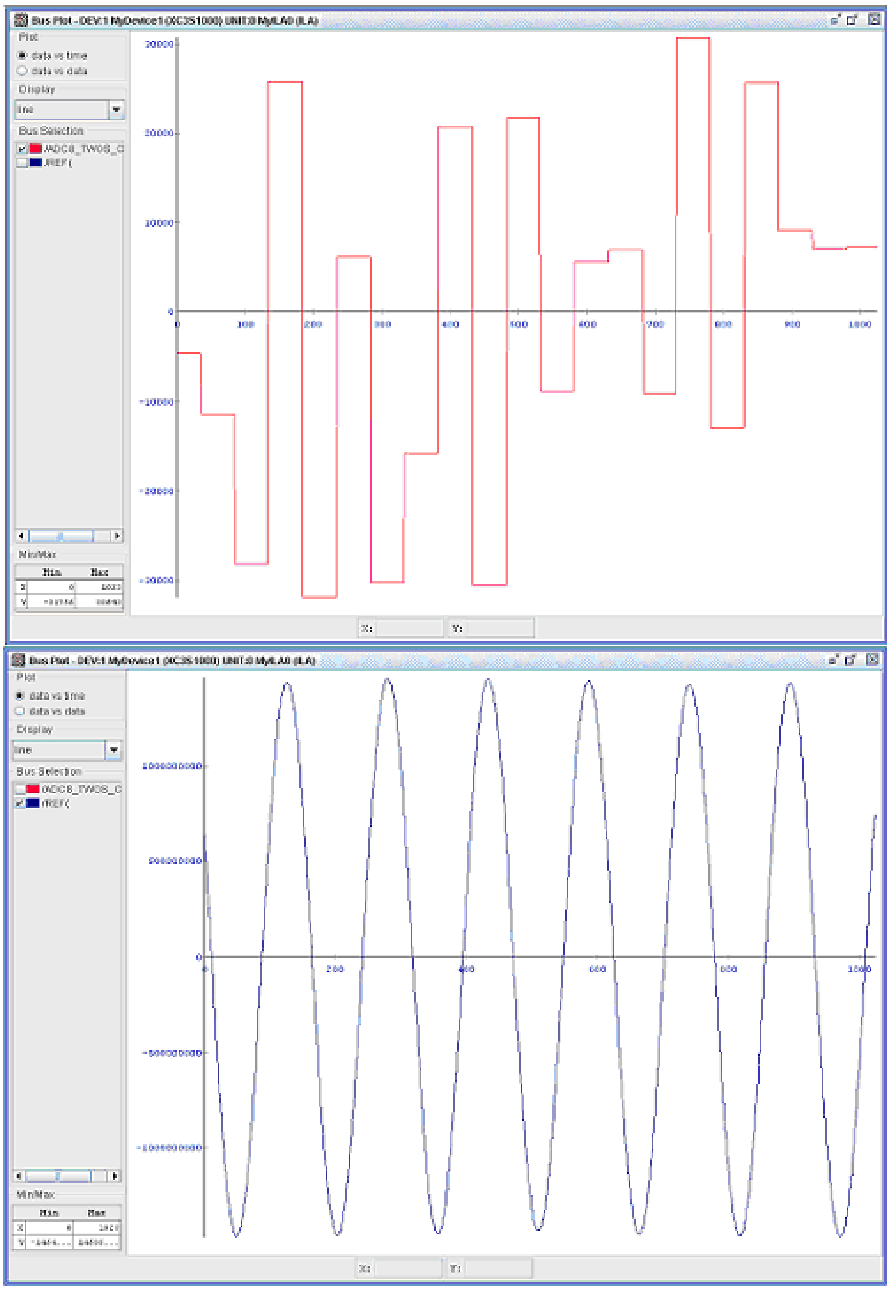

Figure 3-13 Sampled resolver signal (red signal) and reconstructed resolver signal (blue signal) observed in real-time by the help of Chipscope software

3.2.3.3 Elimination of Low-Frequency Harmonic Distortions (Non-aliasing Components) in Reconstructed Resolver Signals using Digital High-Pass Filters Implemented in FPGA

Suppressing low-frequency distortion components and DC offset present in resolver signals will improve the software-based RDC performance considerably as proved previously. For this purpose, a digital high-pass filter is designed and implemented in FPGA.

Since the high-pass filter is applied to the output of the interpolation filter, the sampling frequency of the filter is adjusted as the same with the interpolation filter which has been optimized at 768 kHz. Since analog-to-digital conversion resolution is 16 bit in signed fixed-point arithmetic, filter structure is also formed in 16 bit fixed-point signed arithmetic. Filter's F_{stop} and F_{pass} parameters are adjusted to 200 Hz and 4500 Hz to filter out only the lower-frequency components below the resolver carrier frequency. Filter's demanded magnitude response and related parameters are given in Figure 3-14.

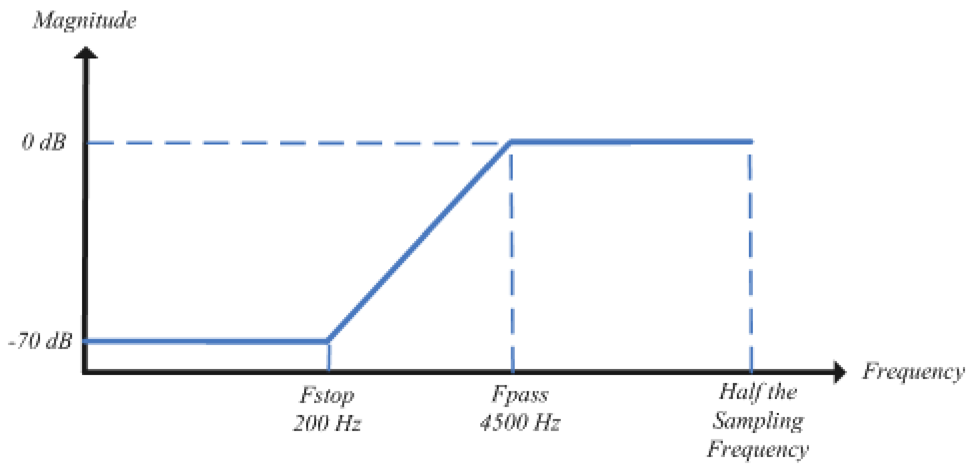

Figure 3-14 Digital high-pass filter parameters and demanded magnitude response

The filter is realized using Filter Design and Analysis (FDA) tool of Matlab and filter coefficients are loaded into FPGA software design environment (ISE). The filter order is realized as 436. The filter is implemented using Finite Impulse Response filter cores (MAC FIR version 5.1 of Xilinx). The details related to FPGA programming issues are given in Appendix A. Filter's realized magnitude and phase responses are seen in Figure 3-15.

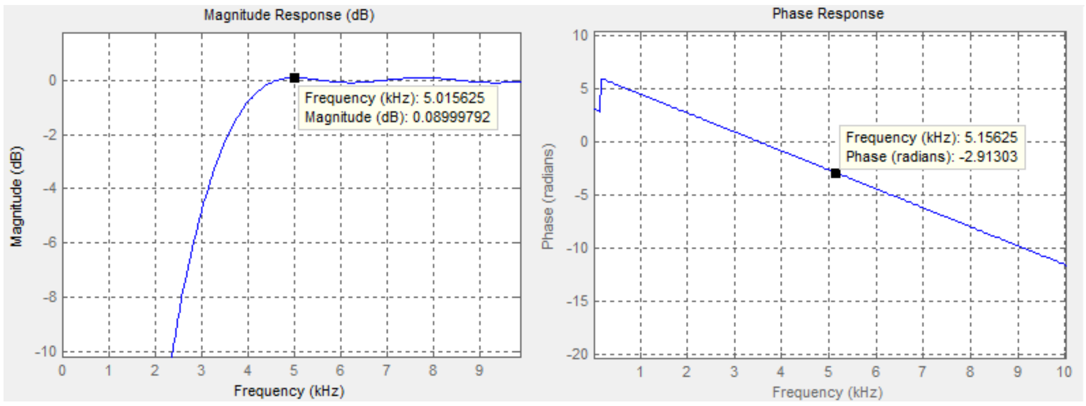

Figure 3-15 Realized magnitude and phase responses of the high-pass filter implemented in FPGA

The filter suppresses low-frequency harmonics and DC offset by a factor -70 dB. Hence, it will be reasonable to assume that there will be zero low-frequency harmonic distortions and zero DC offset at the output of the high-pass filter. Table 3-7 gives the details related to the performance of the filter.

Figure 3-16 shows the resolver signal's states through the analog and digital filters implemented in the experimental system.

Table 3-7 Performance of the digital high-pass filter

Before High-Pass Filtering			
Frequency	Amplitude of Harmonic Dist. dB	Amplitude of Harmonic Dist. %	Error at demodulator output ΔD
DC	-23.6	6.66	10.35%
After High-Pass Filtering			
Frequency	Amplitude of Harmonic Dist. dB	Amplitude of Harmonic Dist. %	Error at demodulator output ΔD
DC	-93.6	0.0000208	0.00%
Suppression of disturbance of Low-frequency Harmonic Distortions at Demodulator Output	Eliminated completely		

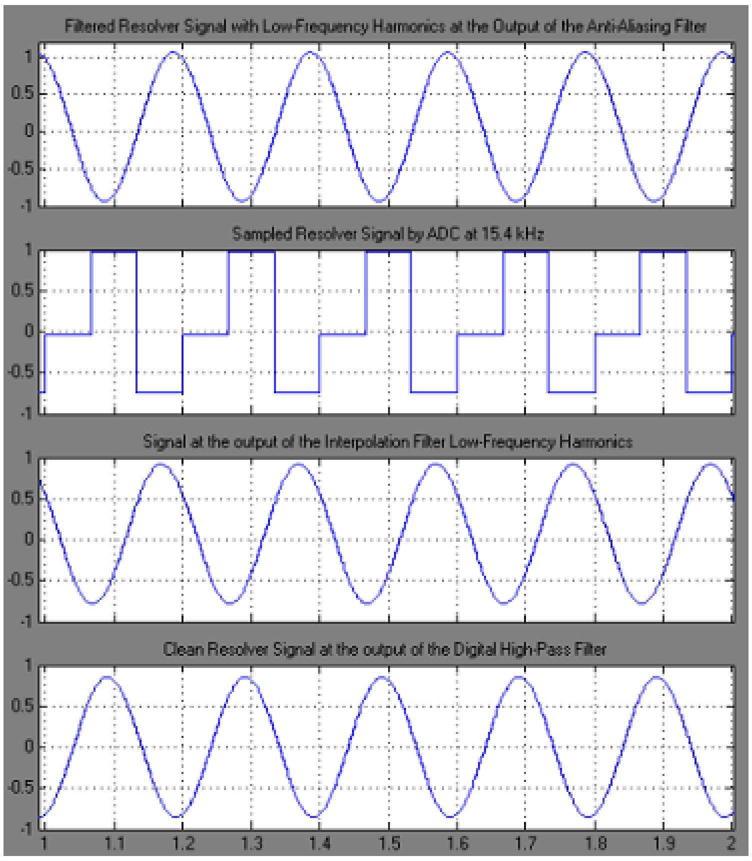

Figure 3-16 Resolver signal's states from output of the anti-aliasing filter to the input of the demodulator passing through the interpolation filter and digital high-pass filter

3.2.4 Improvement in Position Estimation Accuracy with Minimization of Resolver Signal Imperfections in the Experimental System

After the implemented analog and digital filters are applied to resolver channels, the error term coming from the low-frequency distortions (ΔD) is eliminated completely and the error term coming from the high-frequency distortions (ΔE) is minimized. Based on the data given in Table 3.6 and Table 3.7, new value for maximum demodulator output error becomes

$$\Delta S = \Delta C = \Delta D + \Delta E = 0\% + 1.84\% = 1.84\%$$

Therefore, with the minimization of resolver signal imperfections, the demodulator output errors (ΔS and ΔC) are decreased to 1.84%. Using these new values, improvement in position estimation accuracy is calculated by the help of previously derived formula for position estimation error (3.10). The formula was

$$\sin(\theta - \phi) \approx \theta - \phi = \Delta\theta = \Delta C \cos\theta \sin\phi - \Delta S \sin\theta \cos\phi \qquad (3.10)$$

In order to avoid iterations in solving (3.10), it is assumed that ϕ is equal to θ in calculation of the multiplicative terms $\cos\theta\sin\phi$ and $\sin\theta\cos\phi$. In the calculations, the resolver rotor is assumed to be rotating with a speed of 2π rad/s and ΔS and ΔC are assumed to be normally distributed with mean zero and variance 0.005% (corresponding to a maximum error of 1.8%). Figure 3-17 shows the variation of the calculated position estimation error. With the minimization of the resolver signal imperfections, the upper limit for position estimation error is decreased to 0.015 rad (0.85 deg) as seen in Figure 3-17. Furthermore, the upper limit for torque estimation error is decreased from 1% to 0.02% as seen in Figure 3-18.

The new and old values for demodulator output error, position estimation error and torque estimation error are given in Table 3-8.

Table 3-8 Improvement in error values with minimization of resolver signal imperfections

Error at	**Before Minimization of Resolver Signal Imperfections**	**After Minimization of Resolver Signal Imperfections**
Demodulator Output	15.24%	1.84%
Position Estimation	0.1 rad (5.732 deg)	0.015 rad (0.85 deg)
Torque Estimation	1%	0.02%

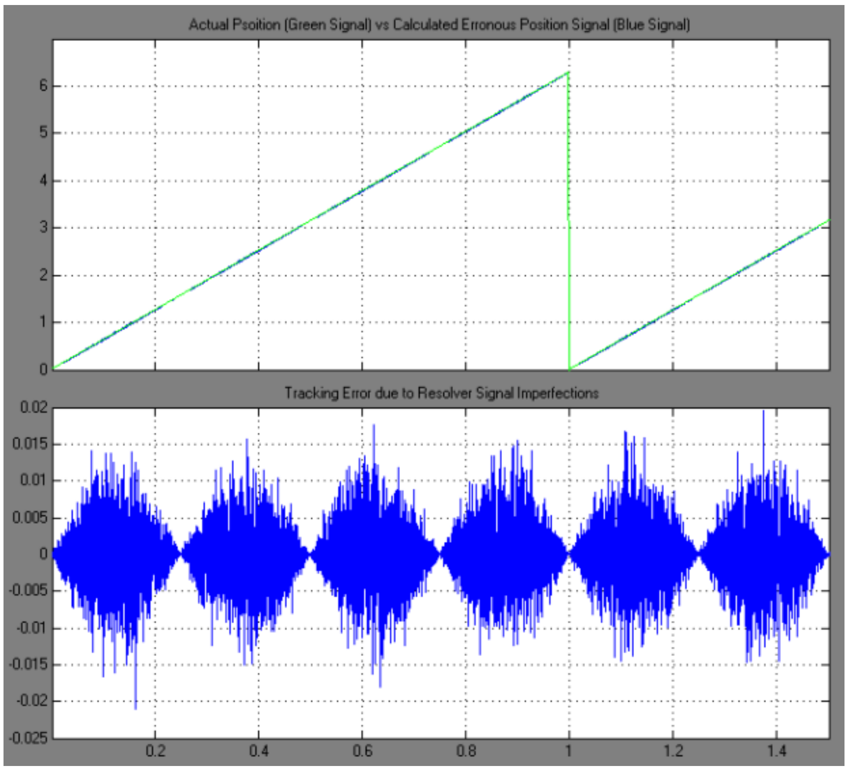

Figure 3-17 Actual position, estimated position and position estimation error when resolver signal imperfections are minimized

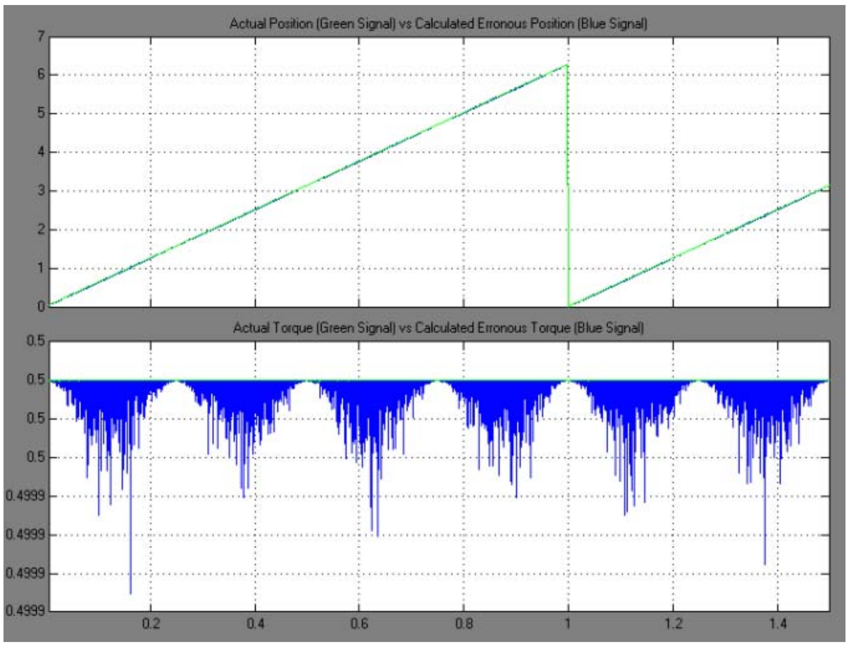

Figure 3-18 Effect of erroneous position signal on torque estimate signal after resolver signal imperfections are minimized

Effects of Attenuations and Delays in the Fundamental Component

Some other error sources will arise in the proposed system with the usage of the filters; attenuations and delays in the fundamental component (5 kHz). Since the filters are applied to all resolver channels (sine, cosine and reference channels), attenuation levels will be the same for all channels and this guarantees that no differential effect due to signal attenuations will exist. The following simple analysis shows that common mode attenuation will not affect the conversion accuracy. Let us assume that A is the attenuation factor common to all resolver signals. Then the error in the converter will be

$$A\sin wt\sin\theta\cos\phi - A\sin wt\cos\theta\sin\phi = 0 \tag{3.13}$$

$$A\sin wt(\sin\theta\cos\phi - \cos\theta\sin\phi) = 0 \tag{3.14}$$

$$\sin\theta\cos\phi - \cos\theta\sin\phi = \sin(\theta-\phi) = \theta-\phi = 0 \tag{3.15}$$

Therefore, the position estimation error $\theta - \phi$ due to common signal attenuation becomes zero. However, another error source will arise due to common phase shifts in the channels. The common mode phase shift will result in constant duration delays in resolver channels and as a result it will incur position estimation error. This error in position estimate is proportional to the speed of the resolver rotor because as the speed increases the resolver rotor travels larger angles during the constant duration delay.

The amount of the common mode phase shift can be calculated by summing up three filters' phase contributions at 5 kHz which are given in Table 3-5 for the anti-aliasing filter, in Figure 3-12 for the interpolation filter and in Figure 3-15 for the high-pass filter. Table 3-9 gives the calculated delays and corresponding position estimation errors in the experimental system when the resolver rotor rotates with a speed of 100 rad/s (5732 deg/sec) which is the maximum achievable resolver speed in the experimental system.

Table 3-9 Delays and position estimation errors due to filtering in the experimental system

	Anti-aliasing Filter	Interpolation Filter	High-Pass Filter	Total
Phase at 5 kHz	-76.7 deg	-504.4 deg	-166.8 deg	-747.9 deg
Delay in seconds	42 us	280 us	92 us	324 us
Max. Tracking Error when Res. Rotor speed is 5732 deg/sec	0.240 deg	1.605 deg	0.527 deg	2.349 deg

Total Maximum Position Estimation Error in the Experimental System

We have two main error sources in the proposed system. The former is the increasing non-linearity in the system with the introduction of parasitic multiplicative terms at the demodulator outputs ($\sin\theta + \Delta S \sin\theta$ and $\cos\theta + \Delta C \cos\theta$) due to resolver signal imperfections. The latter is the filtering delays introduced by the analog and digital filters applied to resolver channels. The first error is limited to 0.015 rad with the minimization of the resolver signal imperfections. The second error is proportional to the resolver speed and it delays the measurements. Based on the data in Table 3-8 and Table 3-9, the position estimation error due to distortions, noise and delays can be formulated as follows

$$MaxPositionEstimationError < (0.015 + 0.00040965 \times \omega)\ \text{rad} \tag{3.16}$$

where ω is the resolver speed in rad/s. Since the maximum achievable resolver rotor speed is 100 rad/s in the experimental system, the maximum position estimation error becomes

$$0.015\ \text{rad} + 0.00040965\ \text{s} \times 100\ \text{rad/s} = 0.019\ \text{rad}$$

Even if the system has this level of error in position estimation, torque control loop will be affected so negligibly that error in torque estimation will be 0.02% of the demanded torque.

3.3 FPGA-Based Phase-Sensitive Demodulator

Processing the reconstructed resolver signals $\sin wt \sin\theta$, $\sin wt \cos\theta$ and $\sin wt$, the phase-sensitive demodulator gives out $\sin\theta$ and $\cos\theta$ signals. In order to realize the said function, the proposed structure makes use of two modulus functions, two half-period integrators and one phase-detector. The block diagram of the system is seen in Figure 3-19.

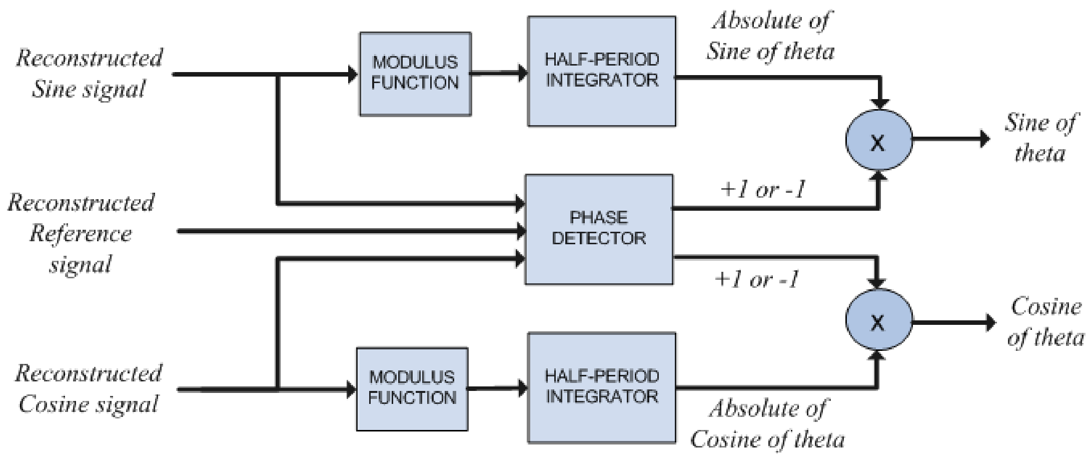

Figure 3-19 Phase-sensitive demodulator implemented in FPGA

Since half-period integration of a sinusoidal signal produces an output proportional to the amplitude of the signal, we can estimate $|\sin\theta|$ and $|\cos\theta|$ by integrating $|\sin wt \sin\theta|$ and $|\sin wt \cos\theta|$ signals between two successive zero-crossings of the signal. This is exactly what the half-period integrators do in the proposed system. However, the phase of the resolver format signals with respect to the reference signal should also be known to construct $\sin\theta$ and $\cos\theta$ signals from $|\sin\theta|$ and $|\cos\theta|$ signals. Therefore, a phase-detector which senses the phases of sine and cosine signals with respect to the reference signal is also utilized in the proposed system. The phase-detector produces two outputs which can take discrete values +1 or -1. The values of the outputs actually express the position signal's quadrant on the unit circle.

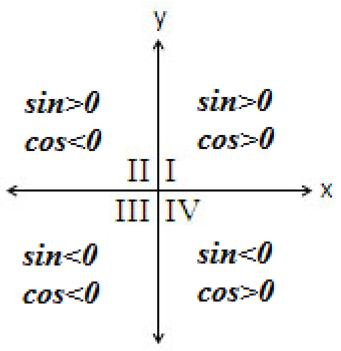

Figure 3-20 Quadrants

3.3.1 Realization of Modulus Function and Half-Period Integrator in FPGA

The function of modulus and half-period integrator can be expressed mathematically by

$$\begin{aligned} \int_{t_0}^{t_0+1/2f} \left|\sin\theta \sin wt\right| dt &= \frac{\left|\sin\theta\right|}{\pi f} \\ \int_{t_0}^{t_0+1/2f} \left|\cos\theta \sin wt\right| dt &= \frac{\left|\cos\theta\right|}{\pi f} \end{aligned} \qquad (3.17)$$

where t_0 represents any zero-crossing instant of the resolver signal and f stands for the fundamental frequency. $\left|\sin\theta \sin wt\right|$ and $\left|\cos\theta \sin wt\right|$ in (3.17) are modulus of the reconstructed resolver signals. Hence, finding the positive amplitude of the resolver signal turns into just finding the area between the resolver signal and time axis as shown in Figure 3-21.

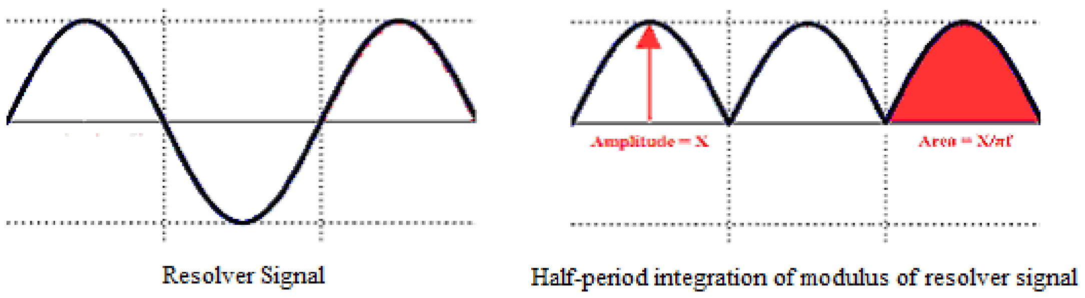

Figure 3-21 Demodulation by modulus and half-period integration

The discretization of the integration term in (3.17) yields

$$\sum_{kT_s=t_0}^{kT_s=t_0+\frac{1}{2f}} \left|\sin\theta \sin(wkT_s)\right| T_s$$
$$\sum_{kT_s=t_0}^{kT_s=t_0+\frac{1}{2f}} \left|\cos\theta \sin(wkT_s)\right| T_s \qquad (3.18)$$

where $T_s = 1/f_s$ and f_s is the sampling frequency. The discrete form of the integration requires multiplication with T_s whose implementation in FPGA makes it necessary to use multiplier cores. However, multiplier cores cover much area in FPGA and decreases the FPGA code efficiency considerably. On the other hand, DSP with its highly parallel multiplier-accumulator (MAC) units can realize the multiplication without exhausting much computational power. Therefore, in order to increase the efficiency of the proposed system, the discrete model is rewritten without the multiplication as follows

$$\sum_{kT_s=t_0}^{kT_s=t_0+\frac{1}{2f}} \left|\sin\theta \sin(wkT_s)\right|$$
$$\sum_{kT_s=t_0}^{kT_s=t_0+\frac{1}{2f}} \left|\cos\theta \sin(wkT_s)\right| \qquad (3.19)$$

The resultant operation is just an accumulation of the input signal. Therefore, the modification prevents multiplications in FPGA and increases FPGA code efficiency. However, accumulation will not yield $|\sin\theta|$ and $|\cos\theta|$ signals directly but it will give out linear functions of $|\sin\theta|$ and $|\cos\theta|$ such as

$$A_s = \sum_{kT_s=t_0}^{kT_s=t_0+1/2f} |\sin\theta \sin(wkT_s)| = f_s \frac{|\sin\theta|}{\pi f}$$
$$A_c = \sum_{kT_s=t_0}^{kT_s=t_0+1/2f} |\cos\theta \sin(wkT_s)| = f_s \frac{|\cos\theta|}{\pi f} \tag{3.20}$$

where fundamental frequency f is 5 kHz and sampling frequency f_s is 768 kHz in the experimental system.

The conversion from A_s and A_c to $|\sin\theta|$ and $|\cos\theta|$ is realized in DSP because the conversion given by the equation set (3.21) will exhaust much more resource in FPGA due to multiplications and division included.

$$|\sin\theta| = \frac{A_s}{\sqrt{A_s^2 + A_c^2}}$$
$$|\cos\theta| = \frac{A_c}{\sqrt{A_s^2 + A_c^2}} \tag{3.21}$$

Figure 3-22 shows the software components to realize modulus function and half-period integrator in FPGA.

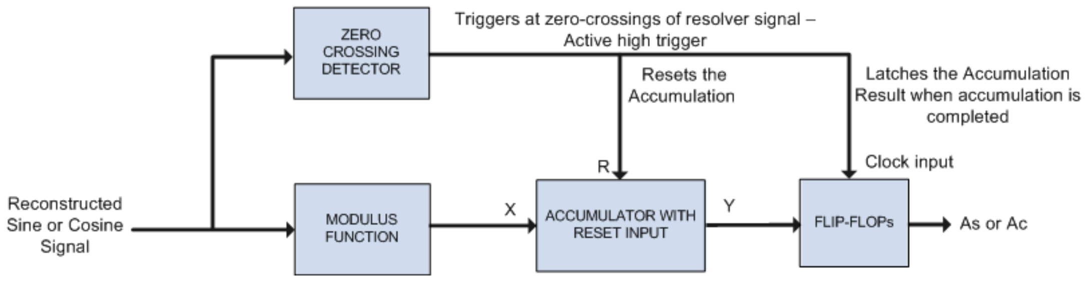

ZERO CROSSING DETECTOR
Triggers at zero-crossings of resolver signal – Active high trigger
Resets the Accumulation
Latches the Accumulation Result when accumulation is completed
R
Clock input
Reconstructed Sine or Cosine Signal
MODULUS FUNCTION
X
ACCUMULATOR WITH RESET INPUT
Y
FLIP-FLOPs
As or Ac

Figure 3-22 Structure realizing modulus function and half-period integration in FPGA

Modulus Function

The modulus function is realized using three blocks as seen in Figure 3-23. Its input (X) is $A\sin wt$ and output (Y) is $|A\sin wt|$ where A may be $\sin\theta$ or $\cos\theta$. The negative-cycle detector in the structure gives out a digital low when the input is positive and a digital high when the input is negative. The switch passes either $A\sin wt$ or $-A\sin wt$ according to the negative-cycle detector's output (S) where $-A\sin wt$ supplied by the two's complementer block. Two's complementer negates the input in two's complement form since the input signal is in two's complement form.

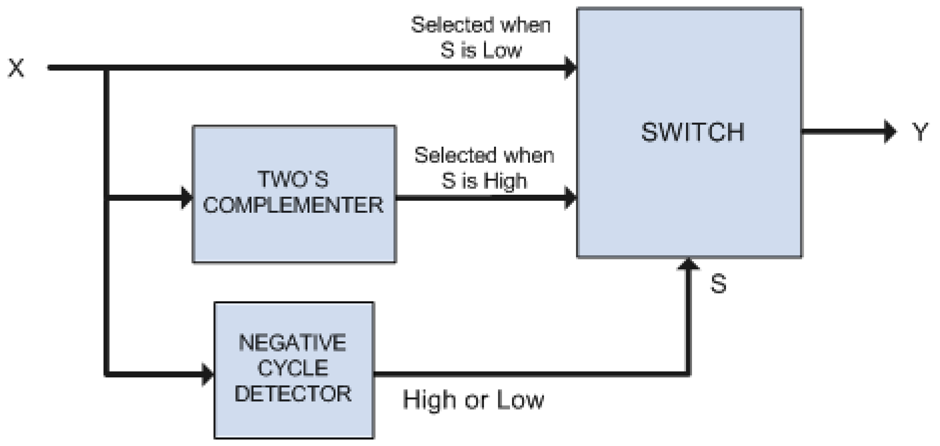

Figure 3-23 Modulus function realized in FGPA

Accumulator with Reset Input

The accumulator in the proposed system is a backward Euler type accumulator and it is used as the integrator in the demodulator (Figure 3-24). Its input (X) is $|A\sin wt|$ and its output (Y) is the accumulation of the input throughout the time. It calculates its recent output by summing its recent input with its previous output at each sampling instant unless reset input (R) is not triggered. If reset input is triggered, the switch resets the accumulation and starts to accumulate from zero level.

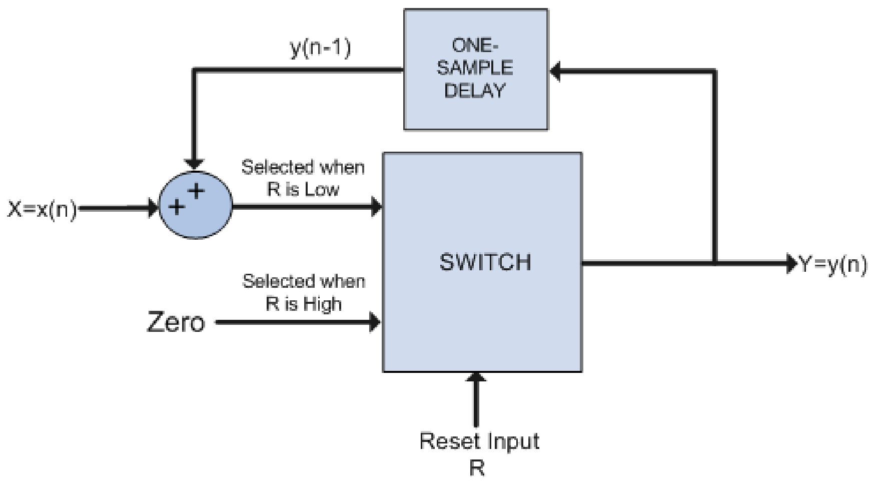

Figure 3-24 Realization of the Backward Euler accumulator with reset input in FPGA

Zero-crossing Detector

The zero-crossing detector produces a trigger signal at each zero-crossing instant of the resolver signal. This trigger signal latches the accumulator output by the help of the flip-flops and resets the internal accumulator signal through the reset input of the accumulator. This structure guarantees that the estimator filter will not be confused by the internal accumulation result and it will always be provided by the most recent completed half-period integration result.

3.3.2 Phase-Detector

Accumulation is necessary but not enough for phase sensitive demodulation of resolver signals. Accumulators will yield signals A_S and A_C which are proportional to $|\sin\theta|$ and $|\cos\theta|$ signals. However, the phases of the signals with respect to the reference signal are also necessary to detect the quadrant of the position, namely to construct $\sin\theta$ and $\cos\theta$ signals from $|\sin\theta|$ and $|\cos\theta|$ signals.

For instance, in Figure 3-25 reconstructed reference, sine and cosine signals are seen when the rotor position is within fourth and first quadrants. Phase-detector can determine the quadrant of the position by comparing resolver format signals' states with respect to zero at each time instant when the reference signal reaches its positive peak. This guarantees that the quadrant detection is not affected from phase shifts up to 90°. The duration from the the zero crossing to the peak of the reference signal is embedded into the code before programming. This duration is dependent on the resolver carrier frequency (one fourth of the reference signal's period) and should be updated if the carrier frequency of the system changes. Hence, the demodulator has a single adjusting parameter. The quadrant detection algorithm is explained schematically in Figure 3-26.

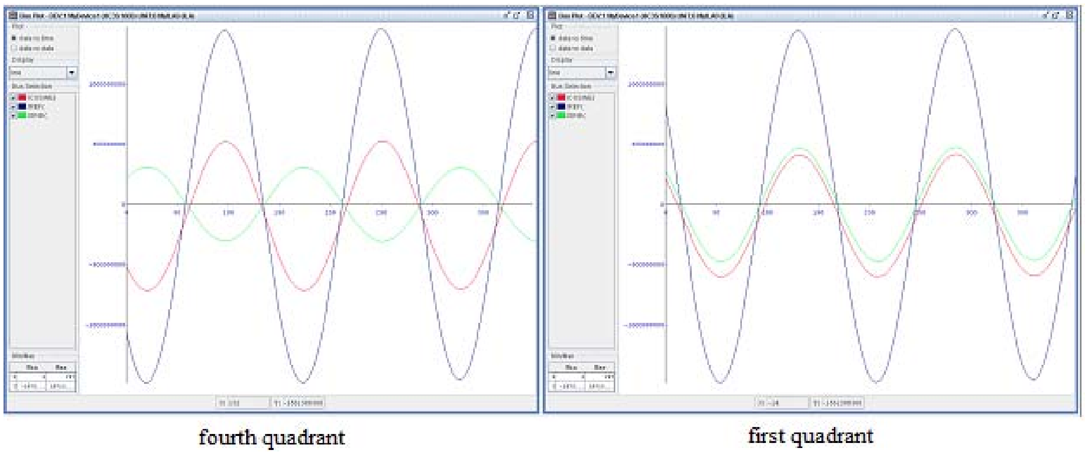

Figure 3-25 Reconstructed reference signal (blue), sine signal (green) and cosine signal (red) when the position is within the fourth and first quadrant

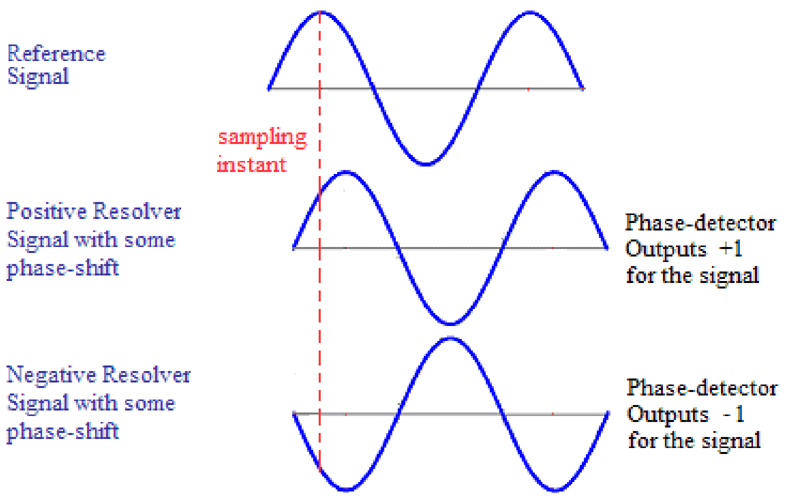
Reference Signal
sampling instant
Positive Resolver Signal with some phase-shift
Phase-detector Outputs +1 for the signal
Negative Resolver Signal with some phase-shift
Phase-detector Outputs -1 for the signal

Figure 3-26 Detection of the phase of resolver format signals with respect to reference signal

Phase-detector has two outputs such that one output is dedicated for sine signal and one output is dedicated for cosine signal. At the time instant when the reference signal is at its peak, phase-detector will output +1 for any positive resolver format signal or -1 for any negative resolver format signal.

Table 3-10 Phase-detector's outputs for position signal's quadrant

θ in	output for sine channel	output for cosine channel
the first quadrant	+1	+1
the second quadrant	+1	-1
the third quadrant	-1	-1
the fourth quadrant	-1	+1

3.3.3 Construction of Demodulated Signals in DSP

DSP continually reads the outputs of phase-detector (+1+1, +1-1, -1-1 or -1+1) and A_s and A_c through the parallel bus between DSP and FPGA at a sampling rate of 10 kHz. After each reading operation is completed, DSP firstly calculates $|\sin\theta|$ and $|\cos\theta|$ from A_s and A_c by using the formula (3.21). Then, it constructs $\sin\theta$

by multiplying $|\sin\theta|$ with phase-detector's output for sine signal and it constructs $\cos\theta$ by multiplying $|\cos\theta|$ with phase-detector's output for cosine signal. The constructed $\sin\theta$ and $\cos\theta$ signals are processed by the estimator filter and resolver position θ and speed $d\theta/dt$ are estimated.

3.3.4 Benefit of the Proposed FPGA-based Phase-Sensitive Demodulator

The benefit of the proposed software-based demodulation structure is that the servo controller can provide interface with any type of resolver easily with a slight modification in FPGA and DSP software. The demodulator has only one parameter which is dependent on the resolver carrier frequency. Therefore, the demodulator can be adapted to operate with changing resolver carrier frequencies by adjusting this single parameter. Hence, there is no longer a need for hardware modifications which exhaust much more resources.

This structure of demodulation also enables a complete solution for software-based Resolver-to-Digital conversion. It makes resolver conversion possible without needing any component specialized to resolver conversion process and by using only generic components such as ADCs, and FPGA which can be found almost in all processor and data acquisition boards.

3.4 Position and Speed Estimation from Demodulated Resolver Signals

In servo applications, using a speed sensor to form up a speed control loop is avoided to minimize system costs when a position sensor is already available. System speed is estimated from position signal in such systems. Pure differentiation to obtain speed signal from position signal generally fails since direct differentiation amplifies the noise components in the signal. The following figure shows the result of pure differentiation of the position signal.

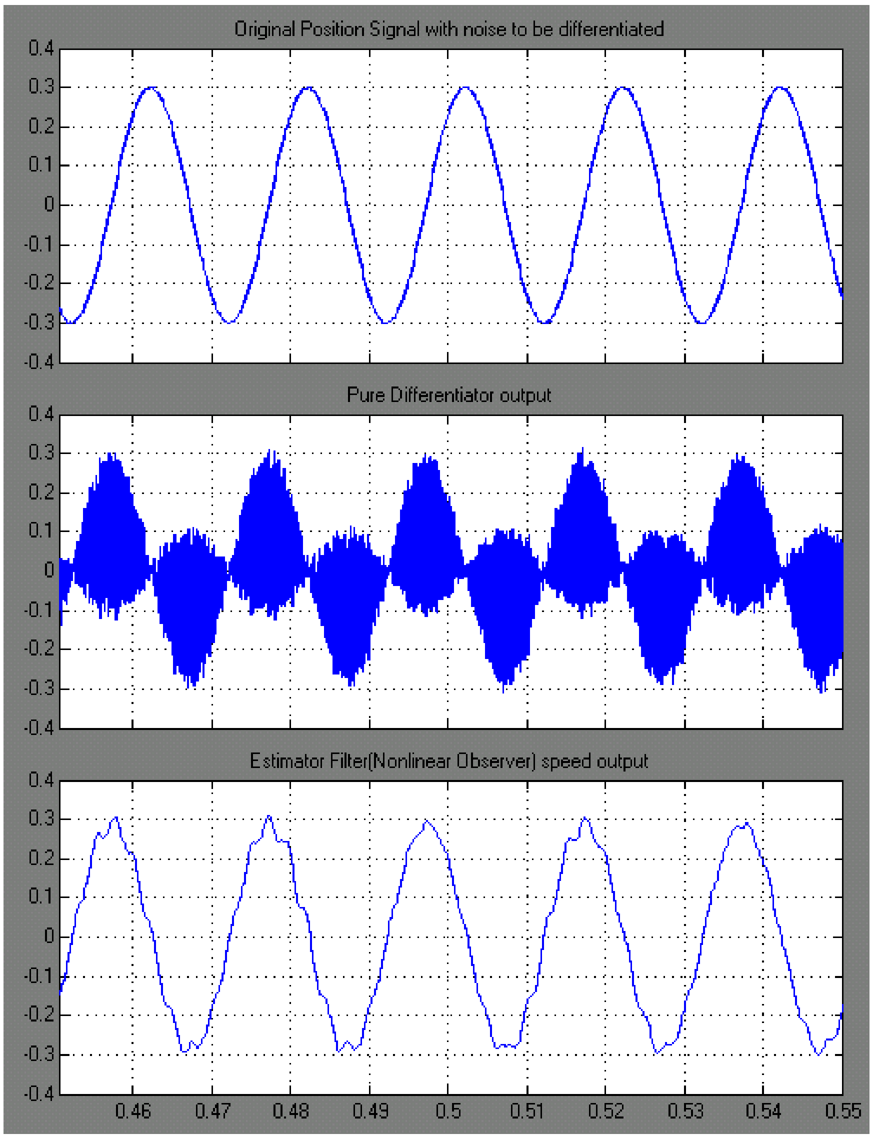

Figure 3-27 Pure differentiation of servo position signal versus speed estimate by an estimator filter

Figure 3.27 also shows the speed estimate of an estimator filter and the estimate seems much more clean and suitable to be utilized in the servo loop. Hence, estimation techniques predominate over pure differentiation when a digital servo control system is the point at issue. In the thesis, five different estimation methods are implemented and estimation performances of them are examined in both simulation and real-time. These inspected methods include;

- Nonlinear Observer recommended for resolver position and speed estimation by Harnefors in [21],
- Tracking Differentiator (TD) adapted to resolver position and speed estimation,
- Linear Kalman Filter (LKF) approach to resolver position and speed estimation,
- Extended Kalman filter (EKF) approach to resolver position and speed estimation,
- Unscented Kalman filter (UKF) approach to resolver position and speed estimation.

3.4.1 Implementation of the Estimator Filters

In this section, the estimator filters' mathematics are explained in summary. Furthermore, implementations of them in DSP are also shown with block diagrams and algorithmic state machines.

3.4.1.1 Nonlinear Observer for Resolver Position and Speed Estimation

The algorithm is proposed by Harnefors in [21]. The algorithm is in type of a nonlinear observer described by the following equations;

$$\begin{aligned}
&\varepsilon = \sin\theta\cos\phi - \cos\theta\sin\phi = \sin(\theta-\phi) \\
&\frac{d\omega}{dt} = \gamma_1\varepsilon \\
&\frac{d\phi}{dt} = \omega + \gamma_2\varepsilon
\end{aligned} \tag{3.22}$$

where ε is the error signal, ω is the estimated speed and ϕ is the estimated position. γ_1 and γ_2 are tuning parameters of the filter.

The filter is realized in DSP as shown in Figure 3-28. The model has an error calculation block and two integrators. The mod operator is needed to generate a position signal between 0 and 2π. $\sin\theta$ and $\cos\theta$ signals are supplied by the phase-sensitive demodulator.

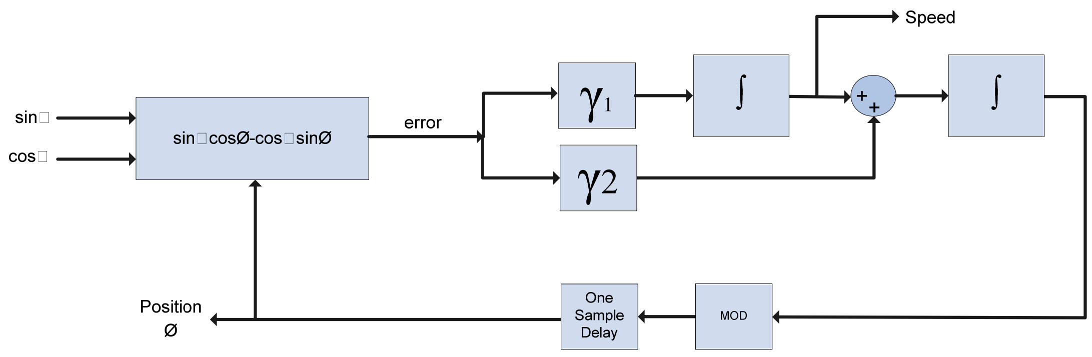

Figure 3-28 Block diagram showing the implementation of the Nonlinear Observer in DSP

3.4.1.2 Tracking Differentiator Approach to Resolver Position and Speed Estimation

Tracking differentiation is a nonlinear means of finding time-based derivative of a noisy signal without using direct differentiation. It is first introduced by Han Jingqing for military target information processing. The advantage of it is that it does not need the system and noise models [31]. The original filter can be modeled by the equation set

$$\begin{aligned} \frac{dx_1}{dt} &= x_2 \\ \frac{dx_2}{dt} &= -Rsat\left(x_1 - v + \frac{x_2|x_2|}{2R}, \lambda\right) \end{aligned} \tag{3.23}$$

where function *sat* is described as

$$sat(x,\lambda) = \begin{cases} \operatorname{sgn}(x), & |x| > \lambda \\ x/\lambda, & |x| \le \lambda \end{cases} \tag{3.24}$$

where *v* is the input for the filter and x_1 tracks the input while x_2 tracks the time-based derivative of *v*. R and λ are tuning parameters of the filter.

The filter is adapted to resolver conversion process by replacing the error term $x_1 - v$ with sinusoidal error calculator described as

$$\sin\theta\cos\phi - \cos\theta\sin\phi = \sin(\theta-\phi) \tag{3.25}$$

where ϕ is the position estimate of the filter and $\sin\theta$ and $\cos\theta$ signals are demodulated resolver signals. Then, the adapted tracking differentiator model is given by the following equations;

$$\begin{aligned} \frac{d\phi}{dt} &= \omega \\ \frac{d\omega}{dt} &= -Rsat\left((\sin\theta\cos\phi - \cos\theta\sin\phi) + \frac{\omega|\omega|}{2R}, \lambda \right) \end{aligned} \tag{3.26}$$

The adapted algorithm is implemented in DSP as shown in Figure 3-29. The model has two integrators and two feedback branches. The nonlinear function is realized using simple functions and switches.

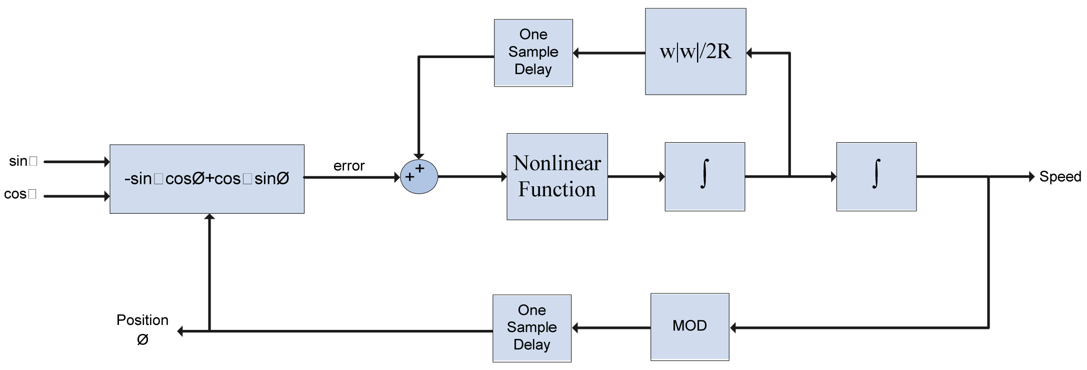

Figure 3-29 Block diagram showing the realization of the Tracking Differentiator in DSP

3.4.1.3 LKF, EKF and UKF for Resolver Position and Speed Estimation

Detailed investigation of Kalman filtering is given in Chapter 2. In this section, some additional properties of Kalman filtering will be given and it will be adapted to resolver conversion process in three different forms.

Assuming constant acceleration, the resolver can be modeled as a dynamical system described by the following equation set

$$\begin{aligned} &dx/dt = Ax \\ &\begin{bmatrix} d\theta/dt \\ d\omega/dt \\ da/dt \end{bmatrix} = \begin{bmatrix} 0 & 1 & 0 \\ 0 & 0 & 1 \\ 0 & 0 & 0 \end{bmatrix} \begin{bmatrix} \theta \\ \omega \\ a \end{bmatrix} \end{aligned} \tag{3.27}$$

where θ is position , ω is velocity and a is acceleration. Then, the noise-free discrete form of this continuous time state-space representation is

$$\begin{aligned} x_{k+1} &= Fx_k \\ &= \exp(A)x_k \\ &= \left(I + AT_s + \frac{(AT_s)^2}{2!} + \dots \right) x_k \\ &= \begin{bmatrix} 0 & T_s & T_s^2/2 \\ 0 & 1 & T_s \\ 0 & 0 & 1 \end{bmatrix} x_k \end{aligned} \tag{3.28}$$

where T_s is the sampling period of the filter. The output equation is

$$\begin{aligned} y_k &= h(x_k) \\ y_k &= \begin{pmatrix} \cos\theta_k \\ \sin\theta_k \end{pmatrix} \end{aligned} \tag{3.29}$$

where h is the nonlinear function in resolver conversion process. If the process noise and measurement noise are also taken into consideration, the system equations will be of the form

$$\begin{aligned} x_{k+1} &= Fx_k + \varpi_k \\ y_k &= h(x_k) + v_k \end{aligned} \tag{3.30}$$

where ϖ is the process noise and v is the measurement noise. The error covariance matrices for process noise and measurement noise are represented by Q_k and R_k respectively.

$$\begin{aligned} E\{\varpi_k \varpi_j^T\} &= Q_k \\ E\{v_k v_j^T\} &= R_k \end{aligned} \tag{3.31}$$

This mathematical model of the resolver conversion is used in the derived Kalman filter equations implemented as a part of the thesis (i.e. LKF, EKF and UKF).

3.4.1.3.1 Linear Kalman Filter Approach to Resolver Position and Speed Estimation

The advantage of this filter arises in real-time because the algorithm does not require continuous update for the Kalman gain. The Kalman gain is solved once before the filter actually runs and then the filter runs using this constant Kalman gain. Therefore, the real-time algorithm does not exhaust any processing power for solving Kalman gain continually. However, to derive this computationally efficient Kalman filter algorithm, we should make use of "one-step Kalman filter equations".

One-Step Kalman Filter Equations

One-step Kalman filter equations are given in the literature for obtaining efficient Kalman filter algorithms [12]. The aim is to get a priori estimate without calculating posteriori estimate.

Priori state estimate is

$$x_{k+1}^- = F_k(x_k^- + K_k(y_k - H_k x_k^-)) \tag{3.32}$$

where the term $(y_k - H_k x_k^-)$ is named as *innovation*. It is the error between real output of the system and the estimate.

Priori error covariance is

$$P_{k+1}^- = F_k P_k^- F_k^T - F_k P_k^- H_k^T (H_k P_k^- H_k^T + R_k)^{-1} H_k P_k^- F_k^T + Q_k \tag{3.33}$$

This is called discrete-time Algebraic Riccati Equation (DARE). If components of (3.33) are linear and time-invariant, the DARE would converge to a steady-state solution and it will be possible to calculate the Kalman gain offline before the system actually runs.

$$K_k = P_k^- H_k^T (H_k P_k^- H_k^T + R_k)^{-1} \tag{3.34}$$

However, resolver conversion process has nonlinear dynamics with measurements carried by nonlinear functions of θ, that is, $\sin\theta$ and $\cos\theta$.

Linearizing Resolver Conversion Process and LKF for Resolver Conversion

To be able to use linear Kalman filter in resolver conversion, nonlinear dynamics of the model should be linearized. In fact, it is simply writing the innovation term as

$$\varepsilon_k = \sin\theta_k \cos\theta_k^- - \cos\theta_k \sin\theta_k^- = \sin(\theta_k - \theta_k^-) \tag{3.35}$$

where θ_k^- is priori position estimate at *k*'th sample, $\sin\theta_k$ and $\cos\theta_k$ are measurements at *k*'th sample and $\cos\theta_k^-$ and $\sin\theta_k^-$ are cosine of priori position estimate and sine of priori position estimate respectively. The innovation term expressed by (3.35) can be approximated by $\theta_k - \theta_k^-$ for small ε.

$$\sin(\theta_k - \theta_k^-) \cong \theta_k - \theta_k^- \tag{3.36}$$

Then, (3.36) will yield the equality given by

$$\varepsilon_k = y_k - H_k x_k^- = \theta_k - \theta_k^- \tag{3.37}$$

Then the linearized h, that is, H_k of the system becomes

$$H_k = H = \begin{pmatrix} 1 & 0 & 0 \end{pmatrix} \tag{3.38}$$

Since the system is linear and time-invariant with this modification, the steady-state solution for discrete-time algebraic Riccati equation can be used in Kalman filtering algorithm. (3.33) can be rewritten for steady-state solution as follows

$$P = FPF^T - FPH^T (HPH^T + R)^{-1} HPF^T + Q \tag{3.39}$$

While solving for (3.39), process noise covariance matrice is assumed to be constant and measurement noise covariance matrice is tuned to improve the disturbance rejection ability of the filter. Hence, the algorithm has a single tuning parameter a.

$$Q = \begin{pmatrix} 0 & 0 & 0 \\ 0 & 0 & 0 \\ 0 & 0 & 1 \end{pmatrix} \qquad R = \begin{pmatrix} a & 0 \\ 0 & a \end{pmatrix} \tag{3.40}$$

Steady-state solution of the algebraic Riccati equation can be found using Matlab's *dare* function. Since a steady-state solution for DARE is present, steady-state solution for Kalman gain can also be calculated by using (3.41).

$$K = PH^T (HPH^T + R)^{-1} \tag{3.41}$$

Solving for (3.41) will yield a Kalman gain in the form of

$$K = \begin{pmatrix} k_1 \\ k_2 \\ k_3 \end{pmatrix} \tag{3.42}$$

Hence, using one-step Kalman filter equation given by (3.32), the mathematical model for the discrete-time linear Kalman filter for resolver conversion process can be written as

$$\begin{pmatrix} \theta_{k+1}^{-} \\ \omega_{k+1}^{-} \\ a_{k+1}^{-} \end{pmatrix} = \begin{pmatrix} 1 & T_s & T_s^2/2 \\ 0 & 1 & T_s \\ 0 & 0 & 1 \end{pmatrix} \begin{pmatrix} \theta_k^{-} \\ \omega_k^{-} \\ a_k^{-} \end{pmatrix} + \begin{pmatrix} k_1 \\ k_2 \\ k_3 \end{pmatrix} \varepsilon_k \tag{3.43}$$

The filter is implemented in DSP as shown in Figure 3-30.

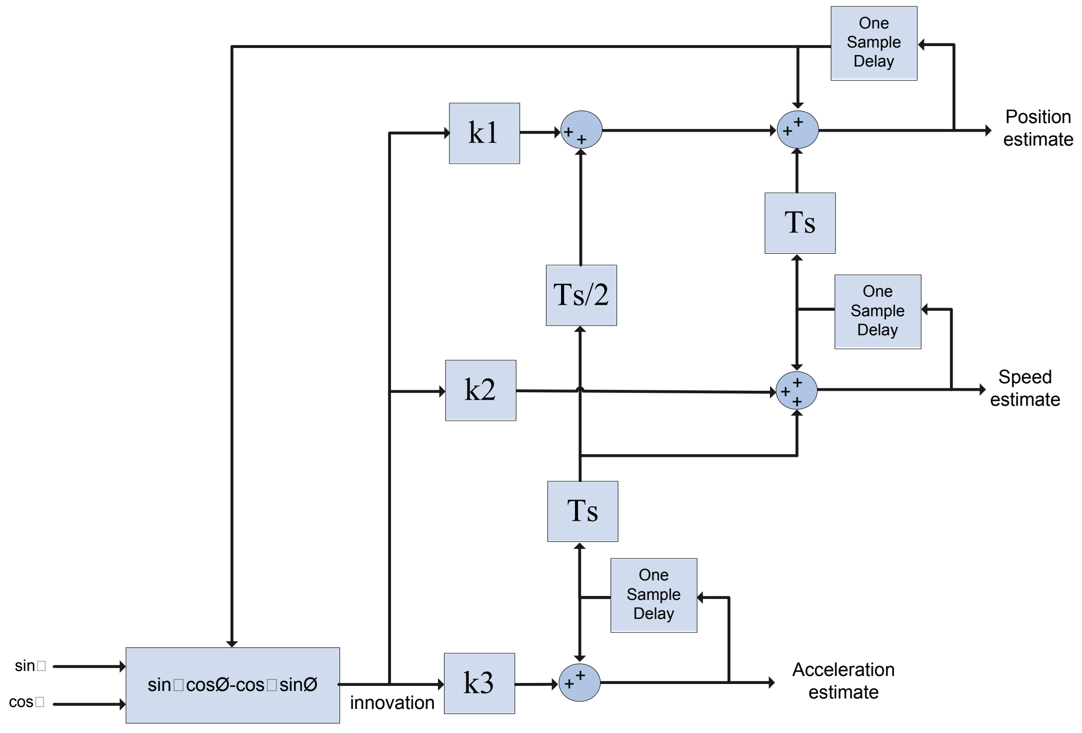

Figure 3-30 Block diagram showing the implementation of LKF in DSP

3.4.1.3.2 Extended Kalman Filter Approach to Resolver Position and Speed Estimation

EKF requires calculation of partial derivatives of the non-linear function *h* with respect to *x* at mean points at each time step.

$$H_k = \frac{\partial h_k}{\partial x}(x = x_k^-) = \begin{pmatrix} -\sin(\theta_k^-) & 0 & 0 \\ \cos(\theta_k^-) & 0 & 0 \end{pmatrix} \tag{3.44}$$

Since H_k is position and time dependent, this modification results in a time-varying algebraic Riccati equation. As a result, Kalman gain will also be time-varying. This implies that the algorithm will continuously solve the DARE and calculate the Kalman gain at each time step. This will increase computational burden considerably. Solving the nonlinearity by the help of the partial derivative, the Kalman algorithm is implemented by the continuous update of the steps given in Figure 3-31. The mathematical formulation for each step is given in section 2.5.2.2 where Extended Kalman Filter algorithm is explained in details.

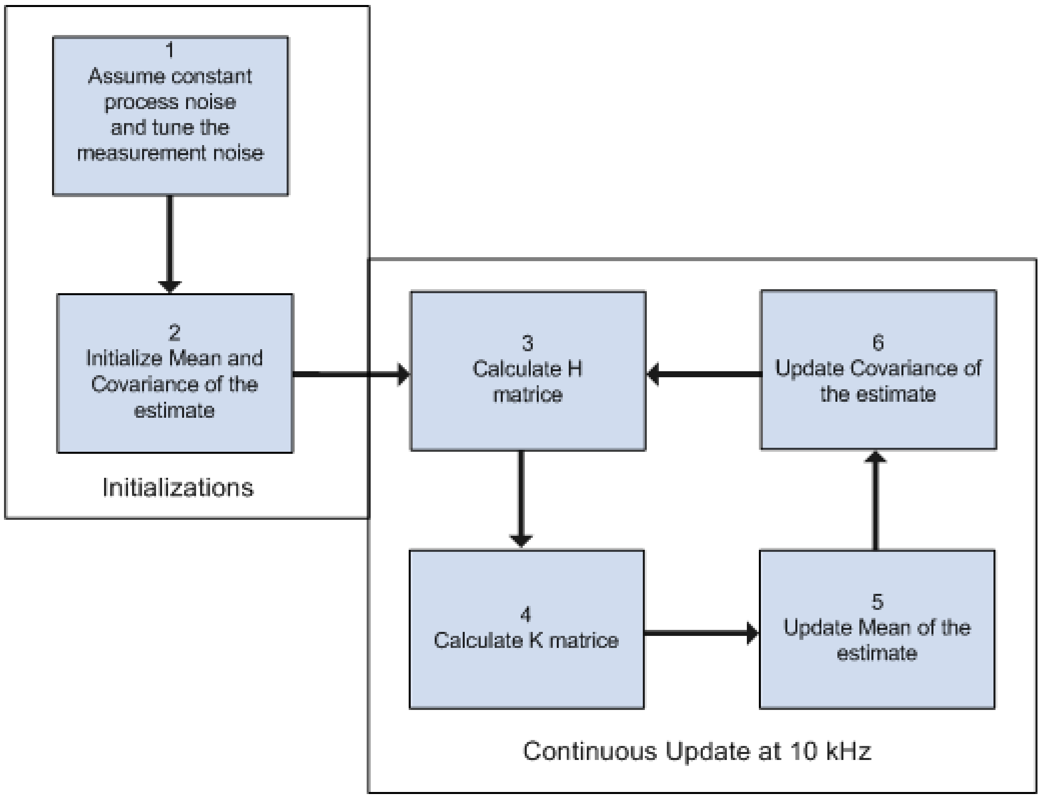
1
Assume constant process noise and tune the measurement noise
2
Initialize Mean and Covariance of the estimate
Initializations
3
Calculate H matrice
4
Calculate K matrice
5
Update Mean of the estimate
6
Update Covariance of the estimate
Continuous Update at 10 kHz

Figure 3-31 Algorithmic state machine showing the realization of the EKF in DSP

Similar to LKF, process noise covariance matrice is assumed to be constant and measurement noise covariance matrice is tuned to improve disturbance rejection ability of the filter. Hence, the EKF has a single tuning parameter a .

$$Q = \begin{pmatrix} 0 & 0 & 0 \\ 0 & 0 & 0 \\ 0 & 0 & 1 \end{pmatrix}$$
$$R = \begin{pmatrix} a & 0 \\ 0 & a \end{pmatrix} \tag{3.45}$$

3.4.1.3.3 Unscented Kalman Filter Approach to Resolver Position and Speed Estimation

UKF is similar to EKF when the computational complexity is considered. On the other hand, it is more successful when the system has severe nonlinearities [12]. In hope of a better estimation performance, UKF algorithm is implemented for resolver conversion process.

The unscented transformation is a way of passing Gaussian signals through nonlinear functions. Instead of linearization with differentiation as the EKF, the UKF makes use of unscented transforms while passing Gaussian signals through nonlinear functions. Hence, the unscented transformation is applied to *h* in the proposed system.

Assuming a Gaussian with dimension *n* with mean μ and covariance $\sum$, there will be 2*n*+1 sigma points symmetrically located with respect to the mean. This selection of sigma points relies on a deterministic method and some parameters are needed to locate these deterministic points. For resolver conversion, there are 7 sigma points since the dimensionality of the state vector is 3. Each sigma point has two weights which are used in recovering mean and covariance after the sigma points are passed through the nonlinear function *h*.

The equations to choose sigma points X^i for a Gaussian $N(\mu,\Sigma)$ are given as

$$\begin{aligned}
&X^0 = \mu, \quad \text{for i=0} \\
&X^i = \mu + (\sqrt{(n+\lambda)\Sigma}), \quad \text{for i=1,2,3} \\
&X^i = \mu - (\sqrt{(n+\lambda)\Sigma}), \quad \text{for i=4,5,6}
\end{aligned} \tag{3.46}$$

where $\lambda = \alpha^2(n+\kappa) - n$ and α and κ are the parameters which determine the locations of the symmetrical sigma points. For each sigma point, there exist two weights w_m^i and w_c^i which are calculated according to the following rules

$$w_m^0 = \frac{\lambda}{n+\lambda}$$
$$w_c^0 = \frac{\lambda}{n+\lambda} + (1-\alpha^2+\beta) \tag{3.47}$$
$$w_m^i = w_c^i = \frac{1}{2(n+\lambda)}, \text{ for i=1,..,7}$$

where the parameter β is optimally 2 when the distribution is an exact Gaussian. Second step of unscented transform is passing sigma points through the nonlinear function *h*.

$$Y^i = h(X^i) \tag{3.48}$$

Y^i is the output of the nonlinear function for each sigma point. The third and final step of the unscented transform is to calculate new mean μ' and covariance Σ' of the resultant Gaussian. The parameters can be calculated from the equations

$$\mu' = \sum_{i=0}^{2n} w_m^i Y^i$$
$$\Sigma' = \sum_{i=0}^{2n} w_c^i (Y^i - \mu')(Y^i - \mu')^T \tag{3.49}$$

The equations are simple but they will be enough to increase the computational complexity considerably because the algorithm calculates sigma points and weights at each time step. Solving the nonlinearity by the help of unscented transform, the Kalman algorithm is implemented by the continuous update of the steps given in Figure 3-32. The mathematical formulation for each step is given in section 2.5.2.3 where Unscented Kalman Filter algorithm is explained in details.

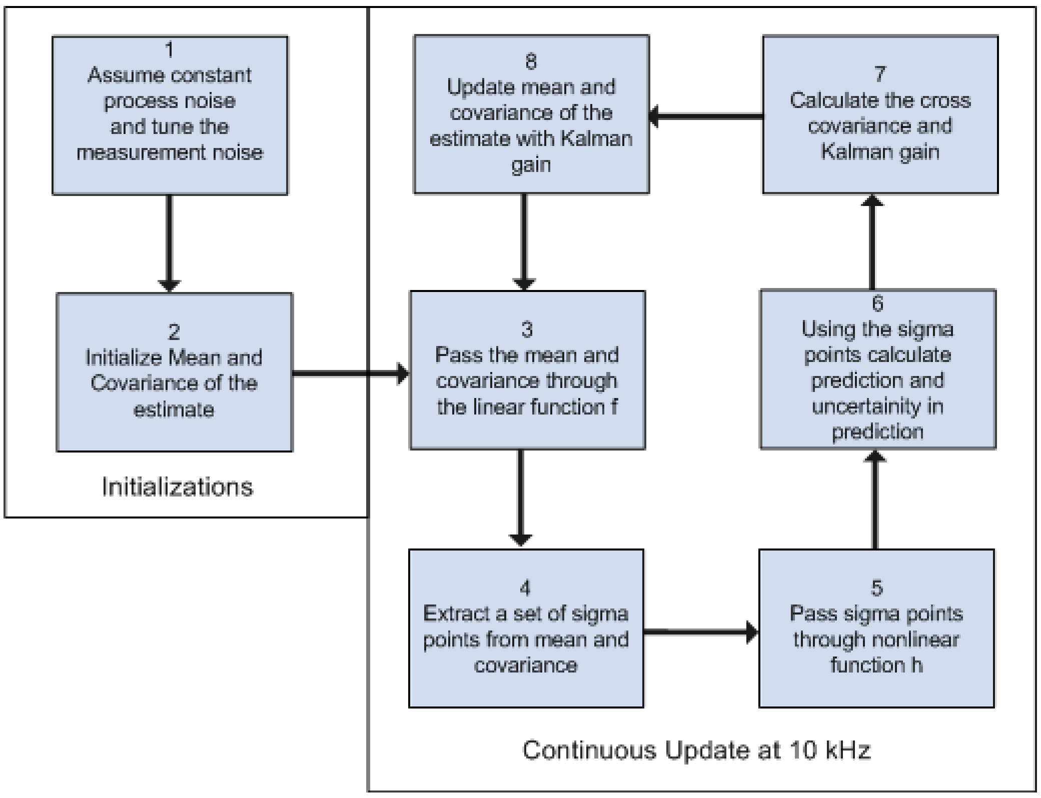
1
Assume constant process noise and tune the measurement noise
2
Initialize Mean and Covariance of the estimate
Initializations
3
Pass the mean and covariance through the linear function f
4
Extract a set of sigma points from mean and covariance
5
Pass sigma points through nonlinear function h
6
Using the sigma points calculate prediction and uncertainity in prediction
7
Calculate the cross covariance and Kalman gain
8
Update mean and covariance of the estimate with Kalman gain
Continuous Update at 10 kHz

Figure 3-32 Algorithmic state machine showing the realization of the UKF in DSP

Similar to LKF and EKF, process noise covariance matrice is assumed to be constant and measurement noise covariance matrice is tuned to improve disturbance rejection ability of the filter. Hence, UKF has four tuning parameters; *γ, α, β* and *κ.*

$$Q = \begin{pmatrix} 0 & 0 & 0 \\ 0 & 0 & 0 \\ 0 & 0 & 1 \end{pmatrix} \qquad (3.50)$$

$$R = \begin{pmatrix} \gamma & 0 \\ 0 & \gamma \end{pmatrix}$$

CHAPTER 4

PERFORMANCE ANALYSIS OF THE PROPOSED RESOLVER-TO-DIGITAL CONVERTER

One of the most important performance criterions for resolver converters is the conversion bandwidth. External disturbances coming from sea have a bandwidth of 0.5 Hz according to both Pierson & Moskowitz and JONSWAP spectrums as analyzed in Chapter 2. Hence, stabilization at sea requires that the position sensor utilized on the stabilization system, for instance a resolver with a RDC, track input signals coming at a frequency spectrum 0.5 Hz.

Noise suppression ability is another important performance criterion for resolver converters since a resolver, operating in a noisy environment where high motor phase currents are flowing closely, generates electromagnetically contaminated output signals. Moreover, disturbances coming from the resolver channels and demodulator degrade the conversion performance. Hence, the converter should be robust against the noise and said disturbances to maintain high-performance tracking.

Taking above mentioned performance criterions into consideration, models for simulation and real-time tests are constructed in this chapter. The estimator filters are tuned in simulation environment and tuned filters are implemented in an experimental STAMP system. Filters' performances are observed in real-time in the experimental system and results are given. Stability and sensitivity analyses are also given in this chapter.

4.1 Constructing Models for Simulative and Real-time Performance Tests and Tuning the Estimator Filters

Before running the estimator filters in real-time, we should make sure that they work properly and their parameters are adjusted optimally. For this purpose, simulation models of the estimator filters are constructed in Simulink. Once the filters are verified and tuned in simulation environment, they are applied to real-time models running in the experimental system.

4.1.1 Constructing Simulation Models of the Estimator Filters for Tuning Procedure

A simulative resolver position trajectory based on a realistic scenario is determined and the trajectory is passed through sine and cosine functions to simulate the resolver and the phase-sensitive demodulator. Some amount of white noise is added to signals and noisy signals are fed to the estimator filters. Simulation models of the estimator filters are constructed as described in section 3.4. The simulation model is summarized schematically in Figure 4-1. In the performance tests, position and speed estimates of the estimator filters are compared to the constructed position and speed trajectories and performance parameters such as position and speed estimation errors are calculated.

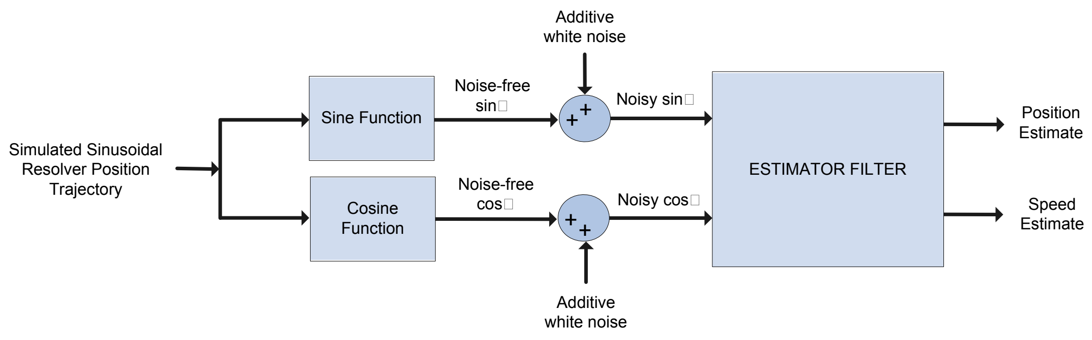

Figure 4-1 Simulation model

A servo system can be modeled as a gear box transmitting the motion from servo motors to servo system as shown in Figure 4-2. In order to construct a realistic position trajectory, system gear ratio, system maximum speed, system maximum acceleration and system bandwidth all should be taken into consideration.

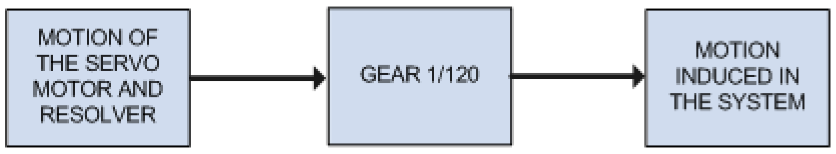
MOTION OF THE SERVO MOTOR AND RESOLVER
GEAR 1/120
MOTION INDUCED IN THE SYSTEM

Figure 4-2 Gun-stabilization system block diagram

Since the resolver is mounted to shaft of the servo motor, maximum acceleration and maximum speed that the estimator filters should be able to track are evaluated by multiplying system maximum acceleration and maximum speed values by the system gear ratio. The gear ratio is 120 and maximum speed and maximum acceleration values are 60°/s (1.0467 rad/s) and 120°/s^2 (2.0933 rad/ s^2) respectively in the experimental system. Hence, for a sinusoidal resolver position trajectory, amplitude of the signal should be adjusted such that;

- Peak of the second order time based derivative of resolver position trajectory signal (acceleration of the resolver) does not exceed $120 \times 120°/\mathrm{s}^2$ (120×2.0933 rad/s^2),

- Peak of the first order time based derivative of resolver position trajectory signal (speed of the resolver) does not exceed $120 \times 60°/\text{s}$ ($120 \times 1.0467\ \text{rad/s}$).

Regarding above mentioned considerations and system bandwidth (0.5 Hz), simulative resolver position trajectory is constructed as

$$\theta = \left[39.8\sin(2\pi ft)\right]_0^{2\pi}\ \text{rad} \tag{4.1}$$

where f is chosen as $0.4Hz$. Then, simulative resolver speed trajectory can be found by taking derivative of the position trajectory with respect to time such that

$$d\theta/dt = \omega = 100\cos(2\pi ft)\ \ \text{rad/s} \tag{4.2}$$

where f is $0.4Hz$.

In the simulation model, noise process is assumed to be white, uncorrelated and zero mean Gaussian process. Variance of the noise is extracted from real noise data collected from the stabilized gun system while resolver is stationary and resolver position is close to 45° (Figure 4-3). Using *var* and *mean* functions of Matlab, variance of the signal is found as 6.90735x10^{-5} where mean of it is found as 0.6589 corresponding to a resolver position of 41.22°. Hence, white noise signals with the same variance are added to noise-free $\cos\theta$ and $\sin\theta$ signals. Then, noisy resolver signals are fed to the estimator filters and filters are tuned based on the performance observations made in simulation environment.

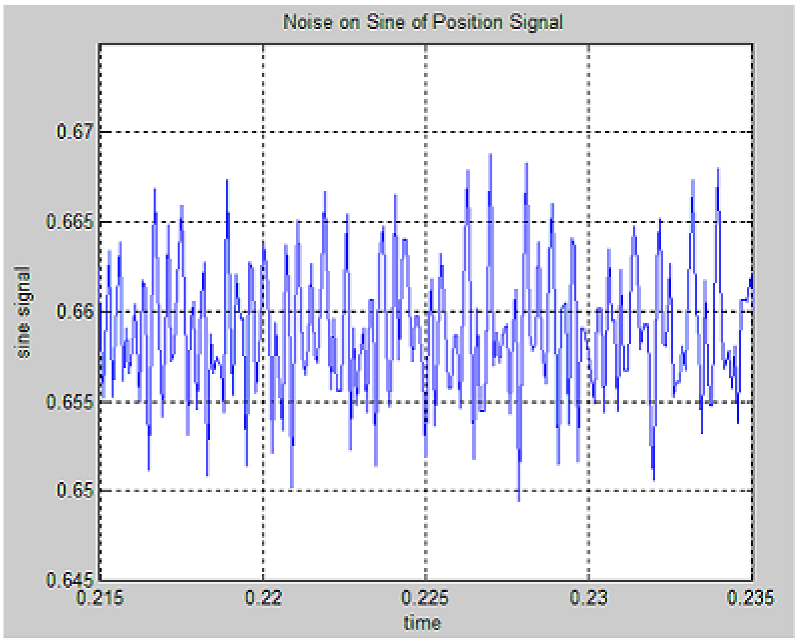

Figure 4-3 Noise on the resolver channel in the gun stabilization system when resolver speed is zero and position is 41.22°

Figure 4-4 shows the simulative position trajectory (θ) and constructed $\sin\theta$ and $\cos\theta$ signals with additive white noise.

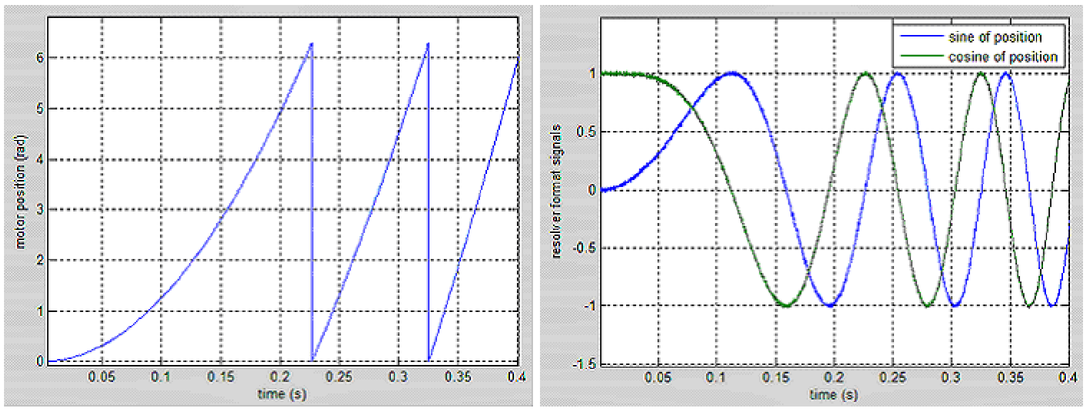

Figure 4-4 Noise-free position signal and noisy sine and cosine signals used as input to estimator filters in simulation environment

4.1.2 Tuning the Filters

The filters are tuned in simulation environment and the same parameters are used in real-time performance tests. To make the performance tests fair, parameters of each filter are adjusted such that the error between the speed estimate and the true speed has the same level of noise amplification (variance) for each filter. This level is set to 2.75 rad/s corresponding to 2.75% of maximum achievable resolver speed in the experimental system. The tuned parameters of the estimator filters and corresponding performance parameters are shown in Table 4-1.

Table 4-1 Tuned Parameters of the estimator filters and corresponding performance parameters obtained in simulation environment

				Filters' Performance Parameters			
Filter	**Environ.**	**Filters' Tuning Params**	**Tuned Values**	**Mean of Position Estimation Error (rad)**	**Variance of Position Estimation Error (rad)**	**Mean of Speed Estimation Error (rad/s)**	**Variance of Speed Estimation Error (rad/s)**
Nonlinear Observer	Simulation	γ1	350000	-0.00461	0.07252	0.00136	2.75671
		γ2	200				
Tracking Differentiator	Simulation	R	50000	-0.01379	0.66366	-0.00189	2.75944
		λ	0.071				
SSLKF	Simulation	α	1.8E-09	-0.00854	0.08826	0.00037	2.75536
EKF	Simulation	α	1.8E-09	-0.00779	0.05207	0.00025	2.75846
UKF	Simulation	γ	0.15	-0.00829	0.08361	0.00027	2.75441
		α	1.41				
		β	2				
		κ	1				

All in all, the tracking differentiator has the maximum average position estimation error which is 0.01379 rad (0.79 deg). This error level is acceptable since it will incur a negligible amount of torque ripple (<0.01%) in the experimental system. Hence, it is concluded that the filters are tuned well enough to run in real-time.

4.1.3 Running the Estimator Filters in the Experimental System for Real-time Performance Tests

The estimator filters with the other necessary components of the converter are implemented in an experimental STAMP system. The experimental system has a servo motor with a resolver sensor, a resolver reference generator, a DSP board and a motor drive board. The block diagram of the experimental system is shown in Figure 4-5.

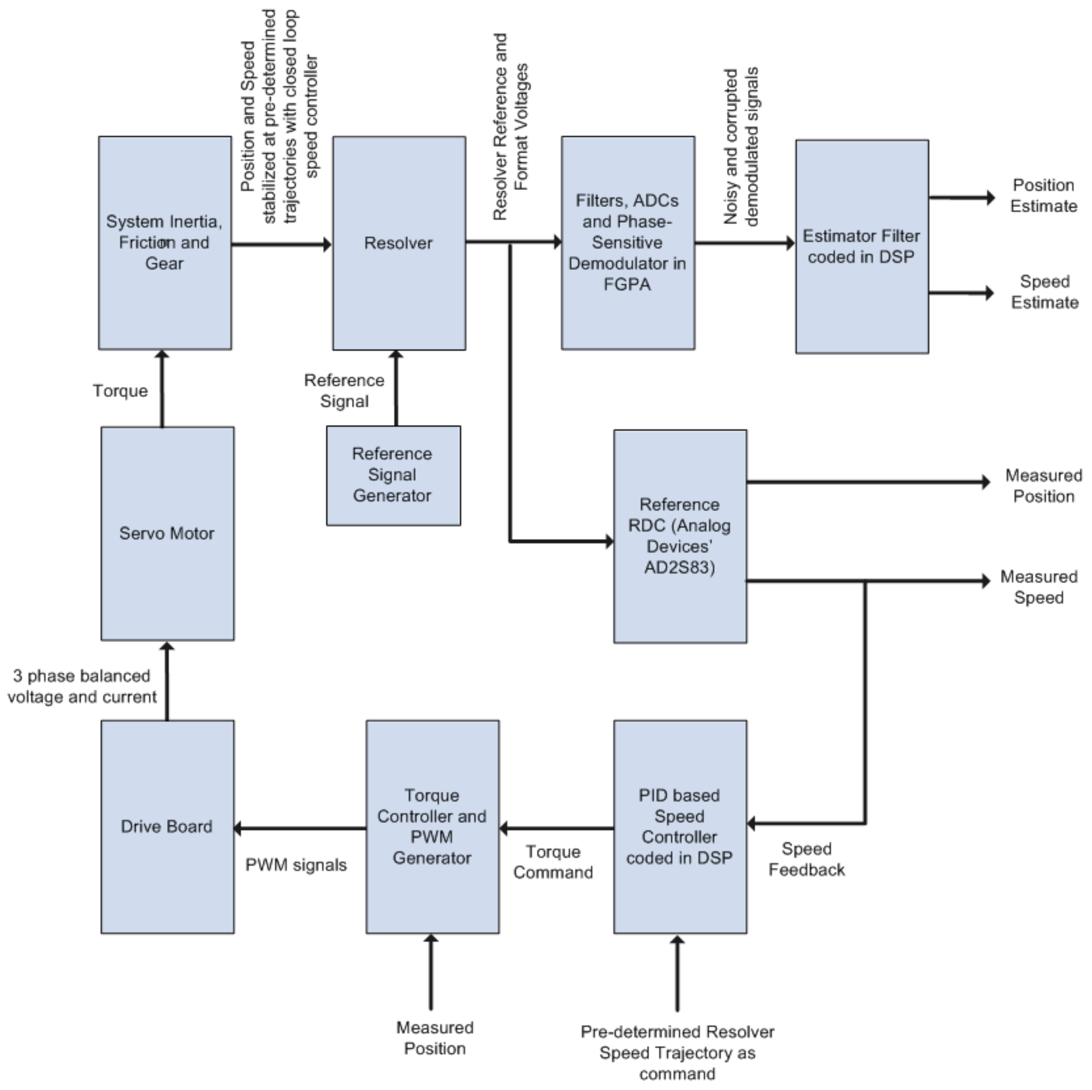
Position and Speed stabilized at pre-determined trajectories with closed loop speed controller
Resolver Reference and Format Voltages
Noisy and corrupted demodulated signals
System Inertia, Friction and Gear
Resolver
Filters, ADCs and Phase-Sensitive Demodulator in FGPA
Estimator Filter coded in DSP
Position Estimate
Speed Estimate
Torque
Reference Signal
Reference Signal Generator
Servo Motor
Reference RDC (Analog Devices' AD2S83)
Measured Position
Measured Speed
3 phase balanced voltage and current
Drive Board
PWM signals
Torque Controller and PWM Generator
Torque Command
PID based Speed Controller coded in DSP
Speed Feedback
Measured Position
Pre-determined Resolver Speed Trajectory as command

Figure 4-5 Experimental system for real-time performance tests

After filtered by the anti-aliasing filters, resolver signals are sampled by the analog-to-digital converters on the DSP board and sampled signals are carried to the FPGA through serial interfaces. Then, the resolver signals are reconstructed from the sampled signals by the interpolation filters and filtered by the high-pass filters for elimination of low-frequency distortions. The reconstructed resolver signals are demodulated by the phase-sensitive demodulator and demodulated resolver signals are delivered to the estimator filters running in the DSP.

The position trajectory for real-time performance tests is formed as

$$\theta = \left[11.25\sin(2\pi ft)\right]_0^{2\pi} \quad \text{rad} \tag{4.3}$$

where f is chosen as $0.4Hz$. Then, resolver speed trajectory can be found by differentiating the position trajectory with respect to time such that

$$d\theta/dt = \omega = 9\pi\cos(2\pi ft) \quad \text{rad/s} \tag{4.4}$$

where f is $0.4Hz$. In order to stabilize the position and speed of the motor at the determined position and speed trajectories expressed by (4.3) and (4.4) respectively, a PID based closed-loop speed controller is embedded into the servo drive controller software and speed feedback is obtained from the reference RDC (Analog Devices' AD2S83). The experimental system can be summarized schematically as shown in Figure 4-6.

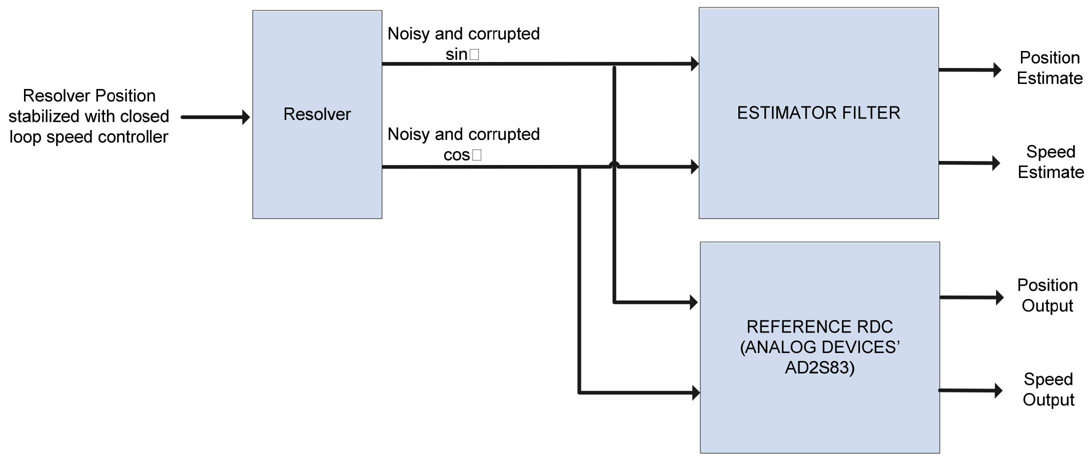

Figure 4-6 Schematically summary of the experimental system used in real-time performance tests

4.2 Simulative and Real-time Estimation Performances of the Filters

Simulative and real-time performance tests are performed with the pre-determined position and speed trajectories. The estimation errors in simulation environment are calculated by subtracting the estimate signals from the pre-determined trajectories while estimation errors in real-time are calculated by subtracting the estimate signals from the measurements of the reference RDC.

4.2.1 Simulative and Real-time Performances of the Nonlinear Observer

The estimation performances of the Nonlinear Observer in simulation and real-time are shown in Figure 4-7, Figure 4-8, Figure 4-9 and Figure 4-10.

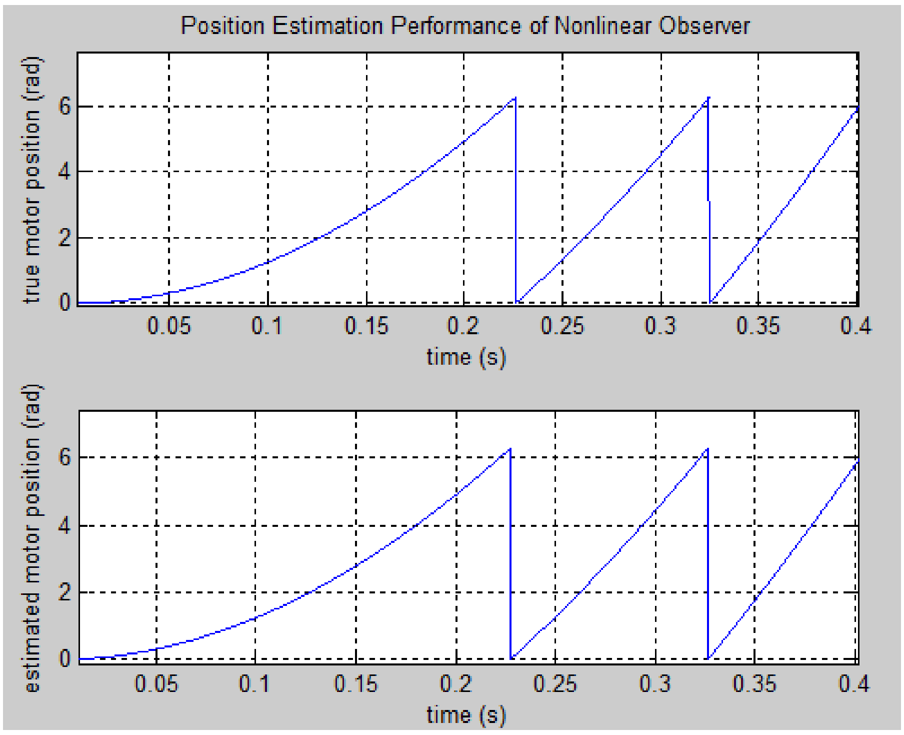

Figure 4-7 Position estimation performance of the Nonlinear Observer in simulation

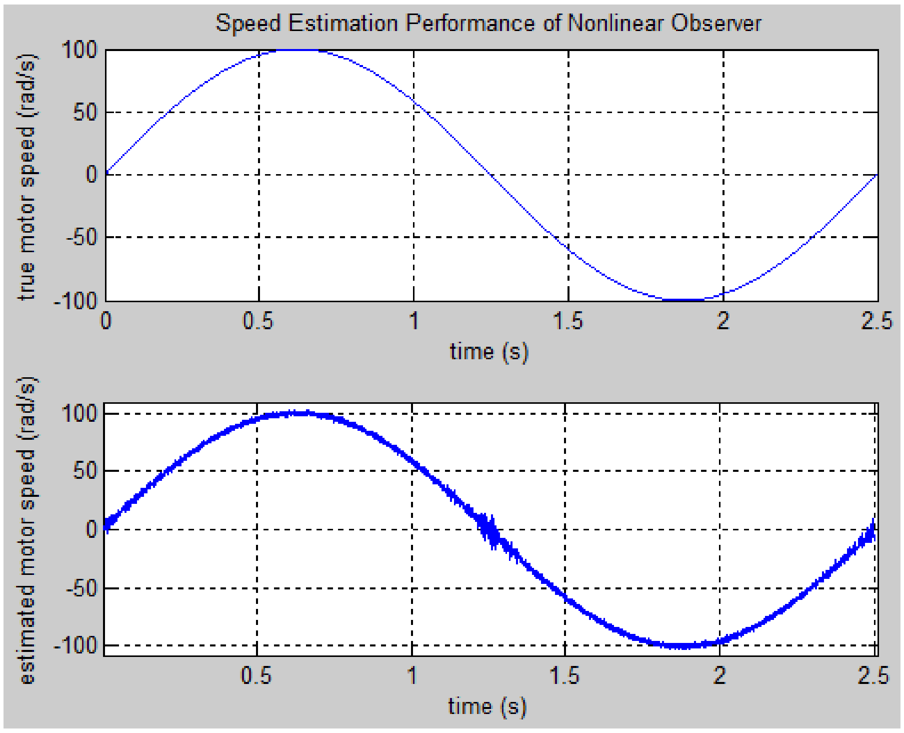

Figure 4-8 Speed estimation performance of the Nonlinear Observer in simulation

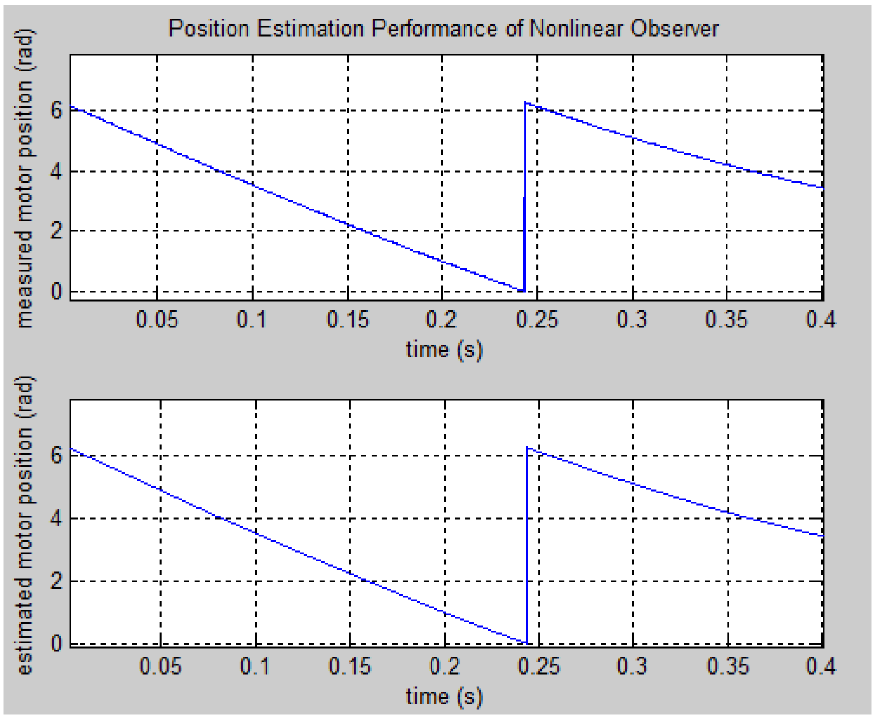

Figure 4-9 Position estimation performance of the Nonlinear Observer in real-time

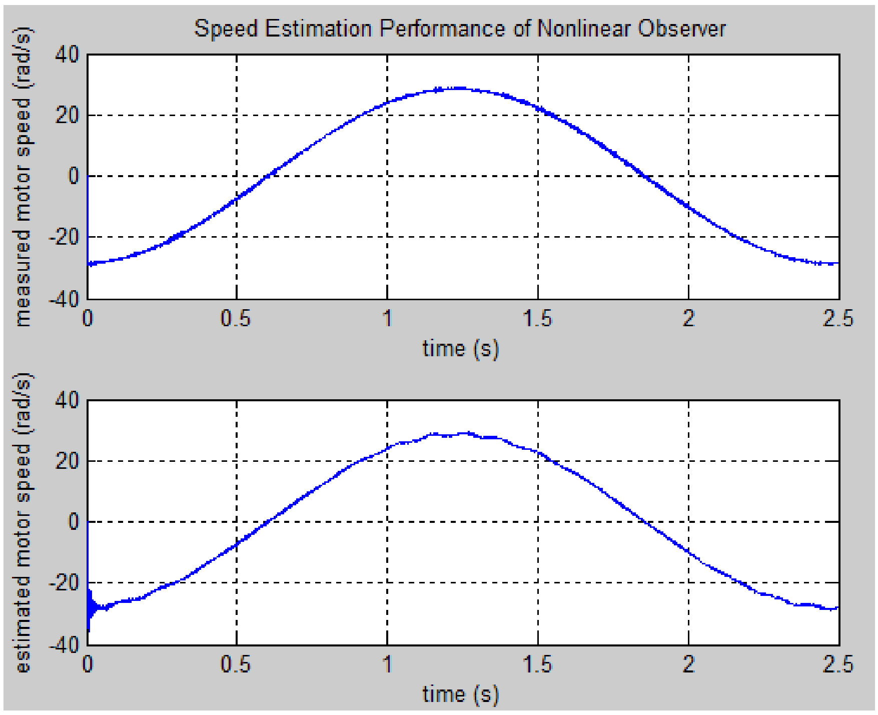

Figure 4-10 Speed estimation performance of the Nonlinear Observer in real-time

Table 4-2 gives the filter's performance parameters calculated using Matlab's *mean* and *var* functions.

Table 4-2 Performance parameters of the Nonlinear Observer in simulation and real-time

Environment	**Filter Params**	**Filter Params' Values**	**Mean of Position Estimation Error (rad)**	**Variance of Position Estimation Error (rad)**	**Mean of Speed Estimation Error (rad/s)**	**Variance of Speed Estimation Error (rad/s)**
Simulation	$\gamma 1$	350000	-0.00461	0.07252	0.00136	2.75671
	$\gamma 2$	200				
Real-time	$\gamma 1$	350000	-0.00197	0.01424	-0.23219	0.43378
	$\gamma 2$	200				

4.2.2 Simulative and Real-time Performances of the Tracking Differentiator

The estimation performances of the Tracking Differentiator in simulation and real-time are shown in Figure 4-11, Figure 4-12, Figure 4-13 and Figure 4-14.

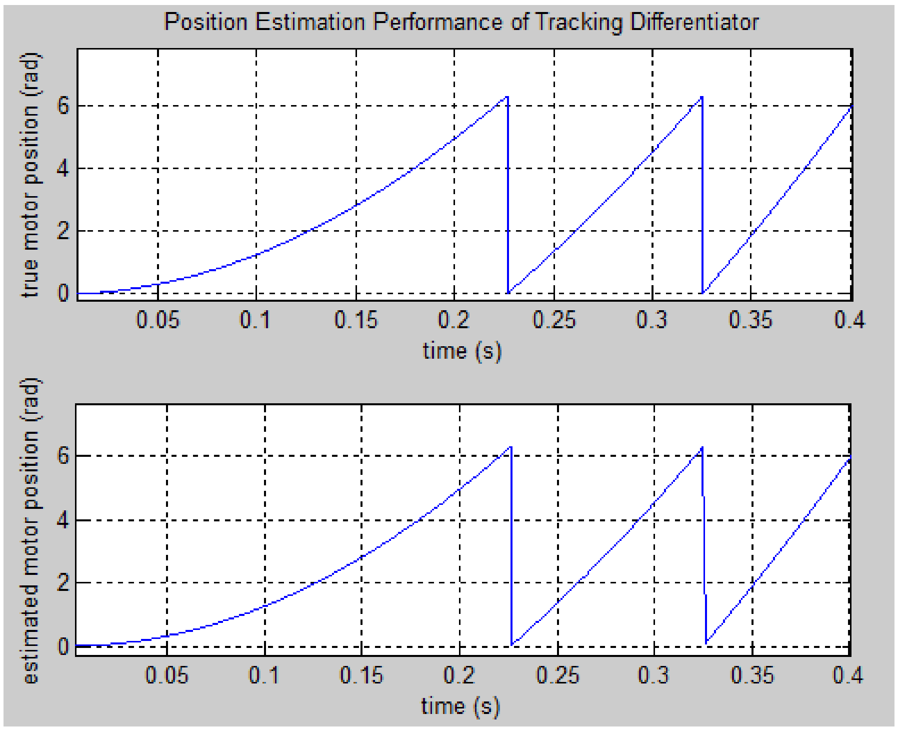

Figure 4-11 Position estimation performance of the Tracking Diff. in simulation

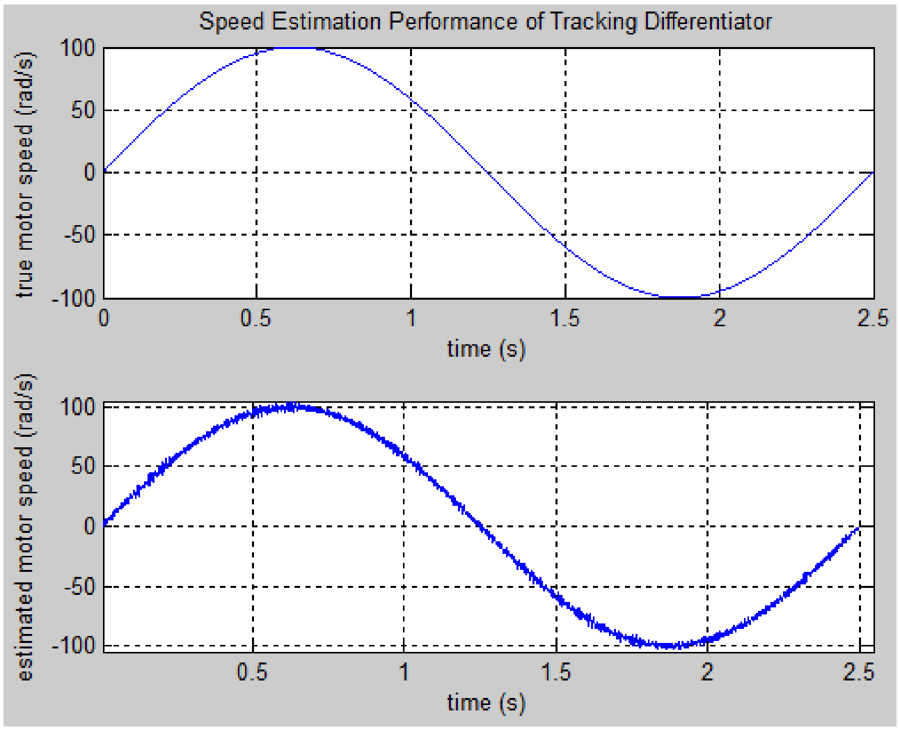

Figure 4-12 Speed estimation performance of the Tracking Diff. in simulation

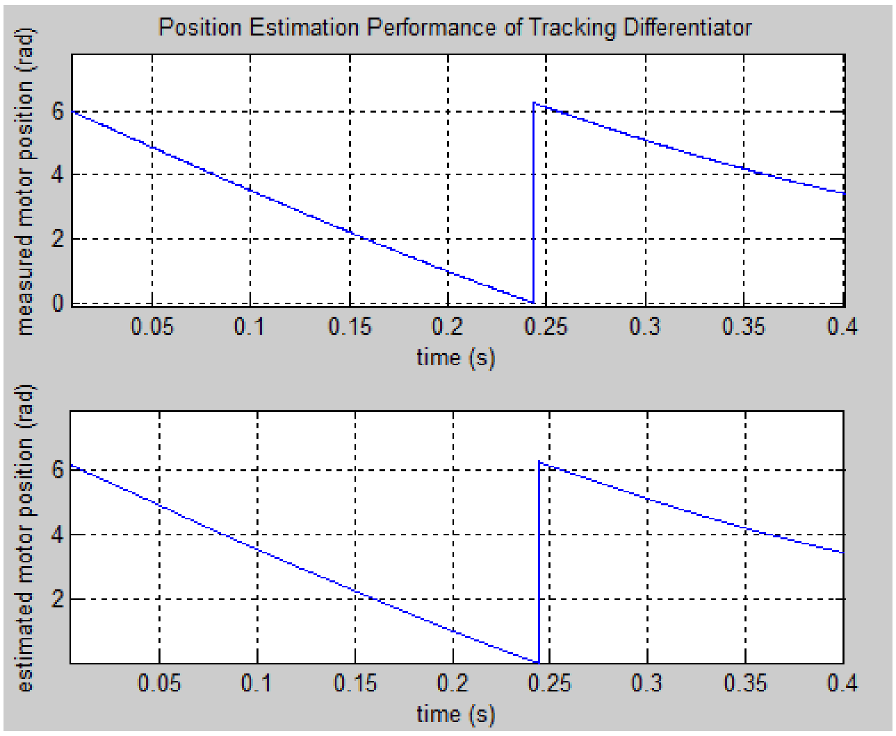

Figure 4-13 Position estimation performance of the Tracking Diff. in real-time

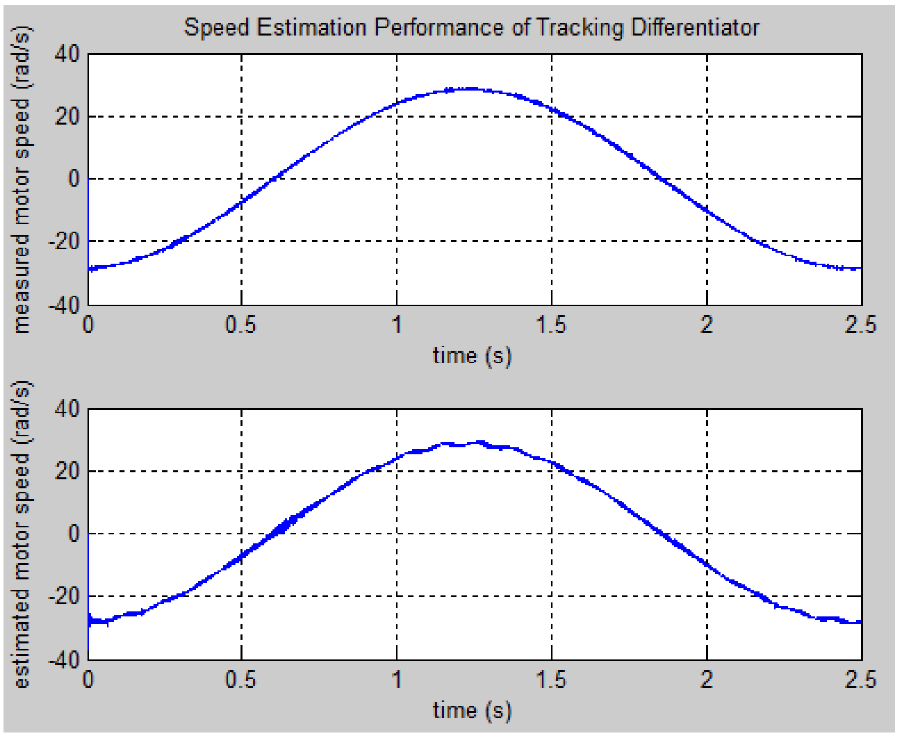

Figure 4-14 Speed estimation performance of the Tracking Diff. in real-time

Table 4-3 gives the filter's performance parameters calculated using Matlab's *mean* and *var* functions.

Table 4-3 Performance parameters of the Tracking Differentiator in simulation and real-time

Environment	**Filter Params**	**Filter Params' Values**	**Mean of Position Estimation Error (rad)**	**Variance of Position Estimation Error (rad)**	**Mean of Speed Estimation Error (rad/s)**	**Variance of Speed Estimation Error (rad/s)**
Simulation	R	50000	-0.01379	0.66366	-0.00189	2.75944
	λ	0.071				
Real-time	R	50000	-0.00329	0.0552	-0.23207	0.59698
	λ	0.071				

4.2.3 Simulative and Real-time Performances of the LKF

The estimation performances of the LKF in simulation and real-time are shown in Figure 4-15, Figure 4-16, Figure 4-17 and Figure 4-18.

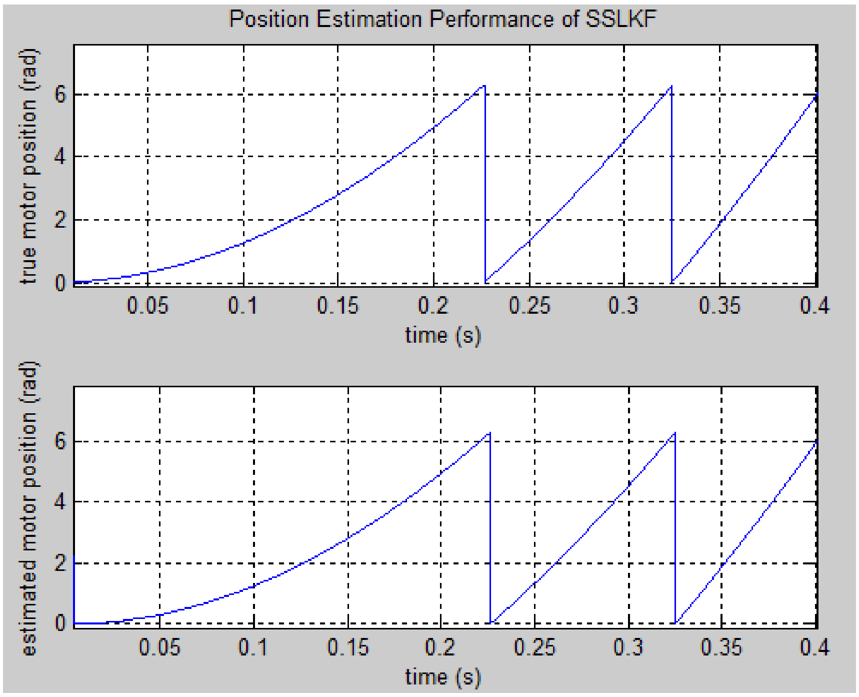

Figure 4-15 Position estimation performance of the LKF in simulation

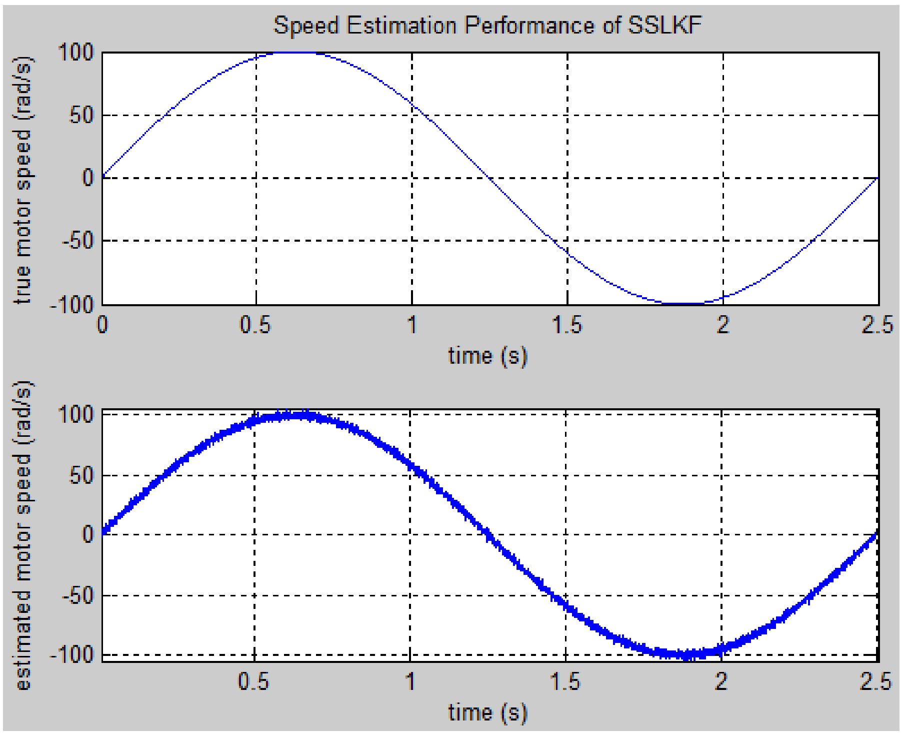

Figure 4-16 Speed estimation performance of the LKF in simulation

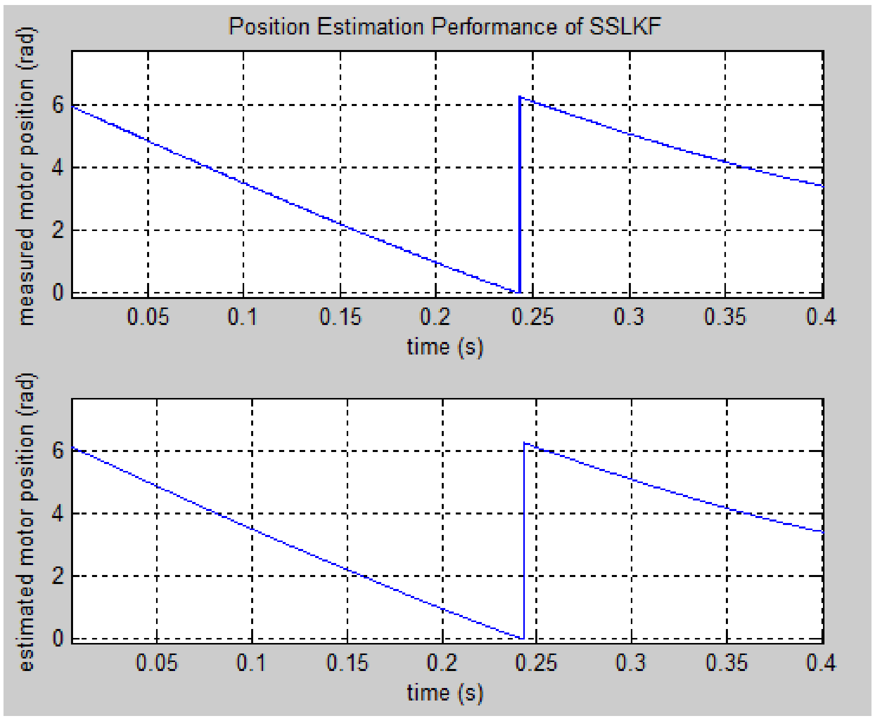

Figure 4-17 Position estimation performance of the LKF in real-time

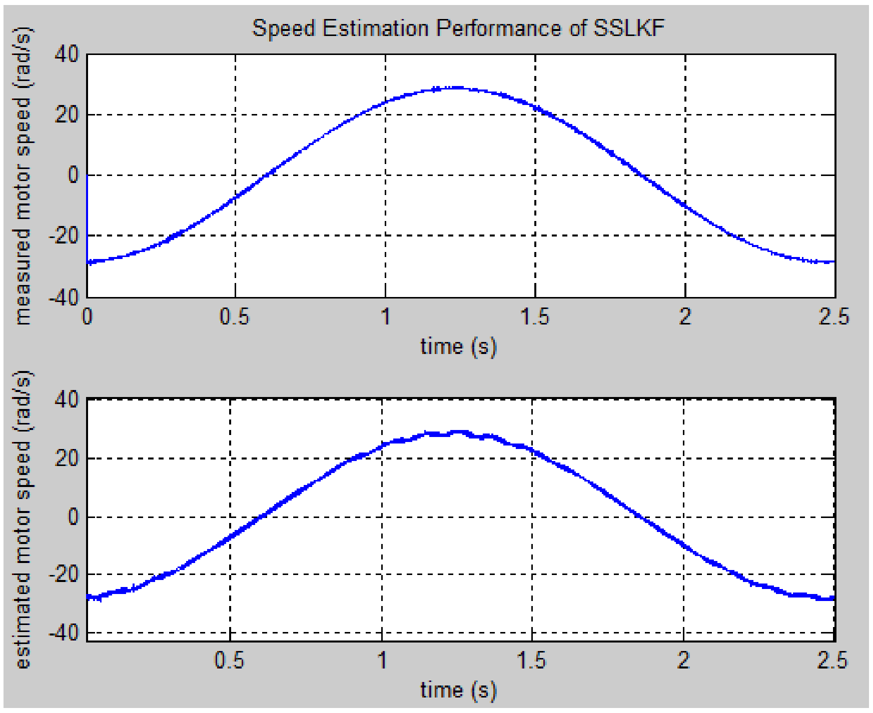

Figure 4-18 Speed estimation performance of the LKF in real-time

Table 4-4 gives the filter's performance parameters calculated using Matlab's *mean* and *var* functions.

Table 4-4 Performance parameters of the LKF in simulation and real-time

Environment	**Filter Params**	**Filter Params' Values**	**Mean of Position Estimation Error (rad)**	**Variance of Position Estimation Error (rad)**	**Mean of Speed Estimation Error (rad/s)**	**Variance of Speed Estimation Error (rad/s)**
Simulation	α	1.8E-09	-0.00854	0.08826	0.00037	2.75536
Real-time	α	1.8E-09	-0.00192	0.01734	-0.22581	1.00329

4.2.4 Simulative and Real-time Performances of the EKF

The estimation performances of the EKF in simulation and real-time are shown in Figure 4-19, Figure 4-20, Figure 4-21 and Figure 4-22.

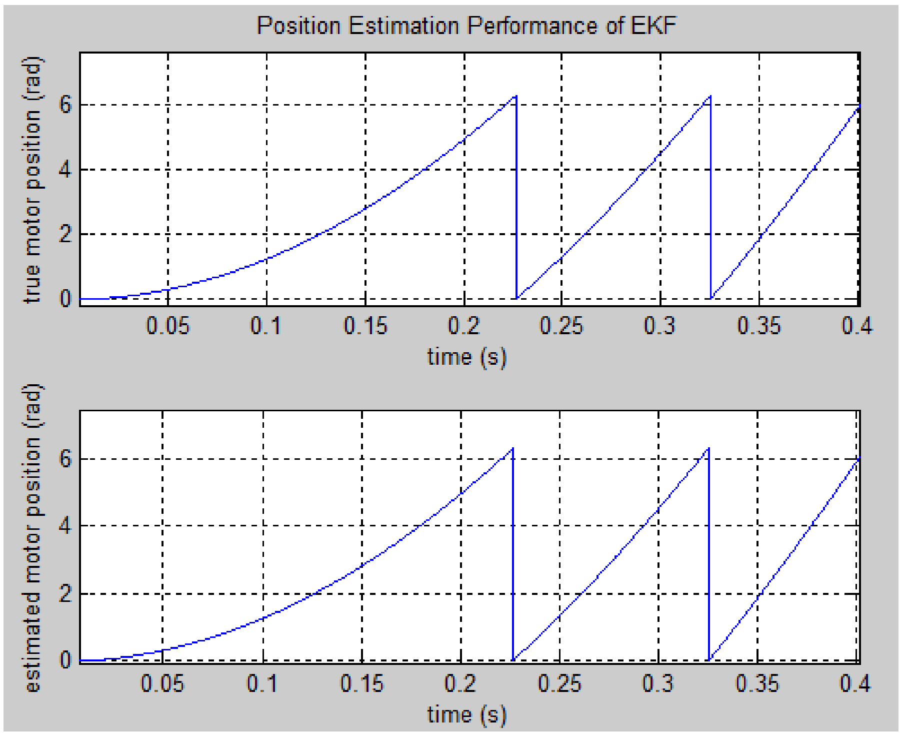

Figure 4-19 Position estimation performance of the EKF in simulation

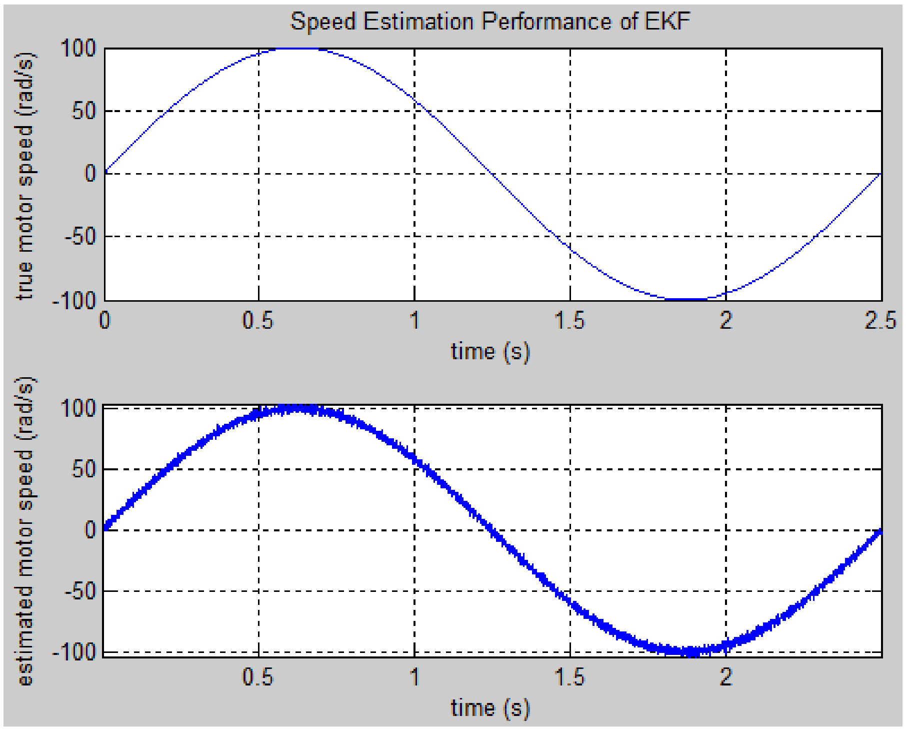

Figure 4-20 Speed estimation performance of the EKF in simulation

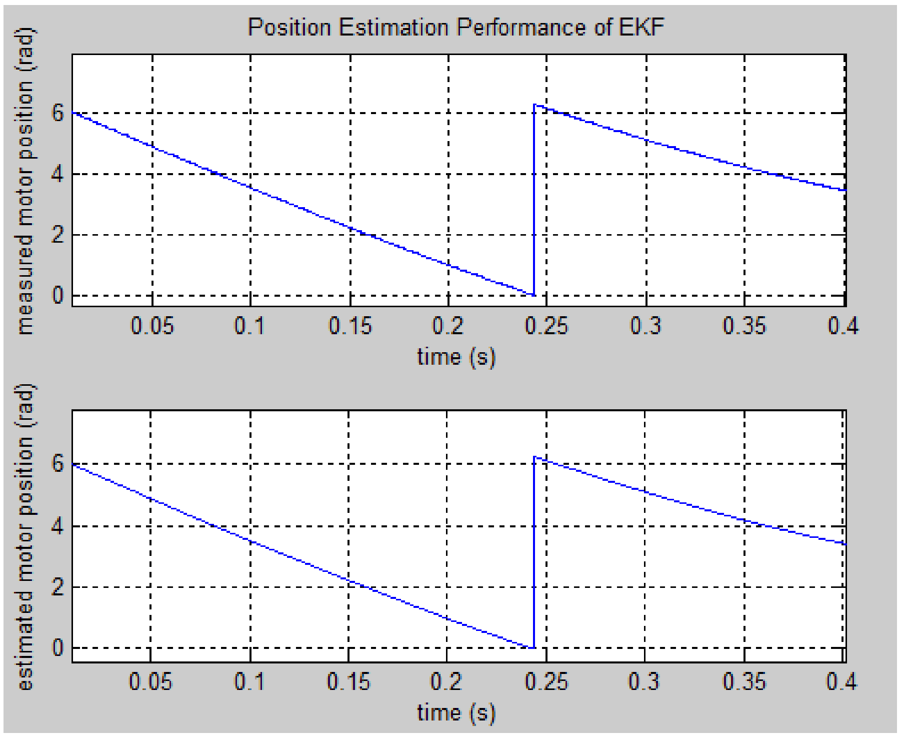

Figure 4-21 Position estimation performance of the EKF in real-time

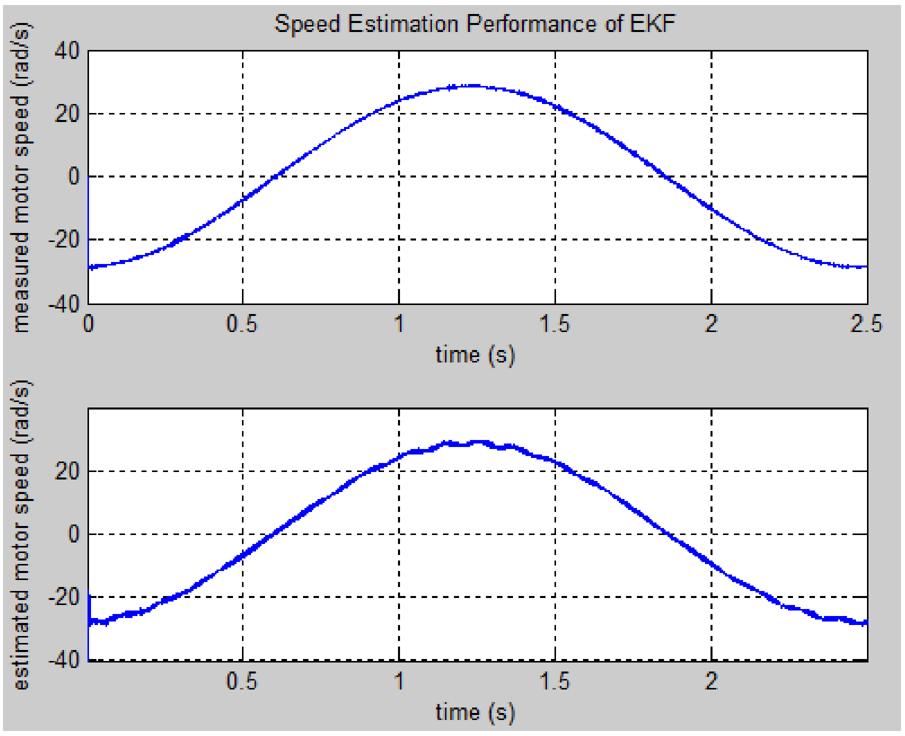

Figure 4-22 Speed estimation performance of the EKF in real-time

Table 4-5 gives the filter's performance parameters calculated using Matlab's *mean* and *var* functions.

Table 4-5 Performance parameters of the EKF in simulation and real-time

Environment	**Filter Params**	**Filter Params' Values**	**Mean of Position Estimation Error (rad)**	**Variance of Position Estimation Error (rad)**	**Mean of Speed Estimation Error (rad/s)**	**Variance of Speed Estimation Error (rad/s)**
Simulation	α	1.8E-09	-0.00779	0.05207	0.00025	2.75846
Real-time	α	1.8E-09	-0.00097	0.03001	-0.20787	2.79309

4.2.5 Simulative and Real-time Performances of the UKF

The estimation performances of the UKF in simulation and real-time are shown in Figure 4-23, Figure 4-24, Figure 4-25 and Figure 4-26.

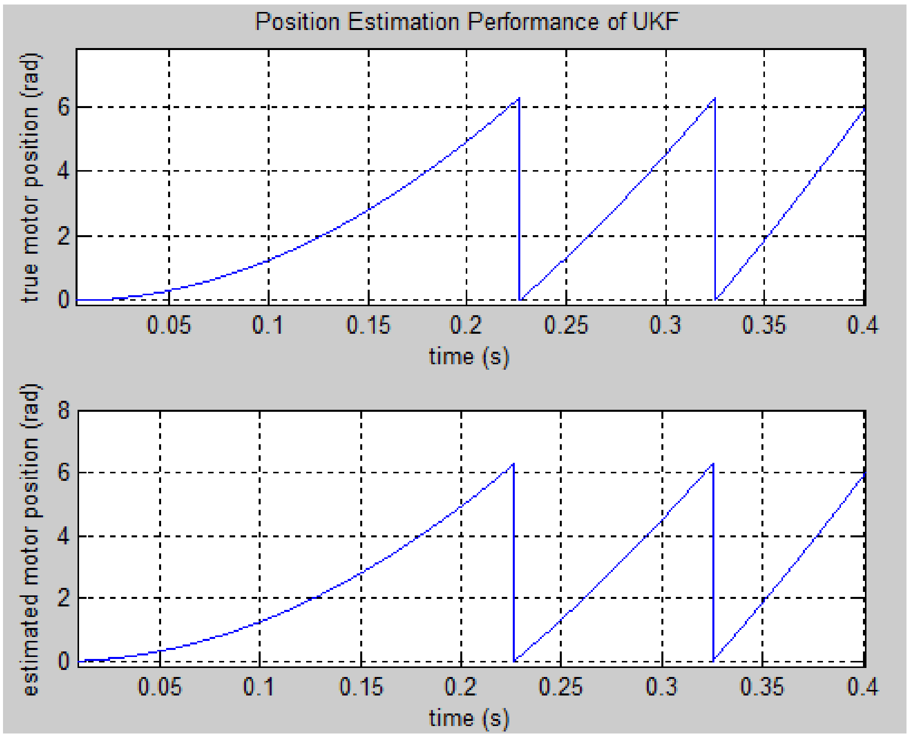

Figure 4-23 Position estimation performance of the UKF in simulation

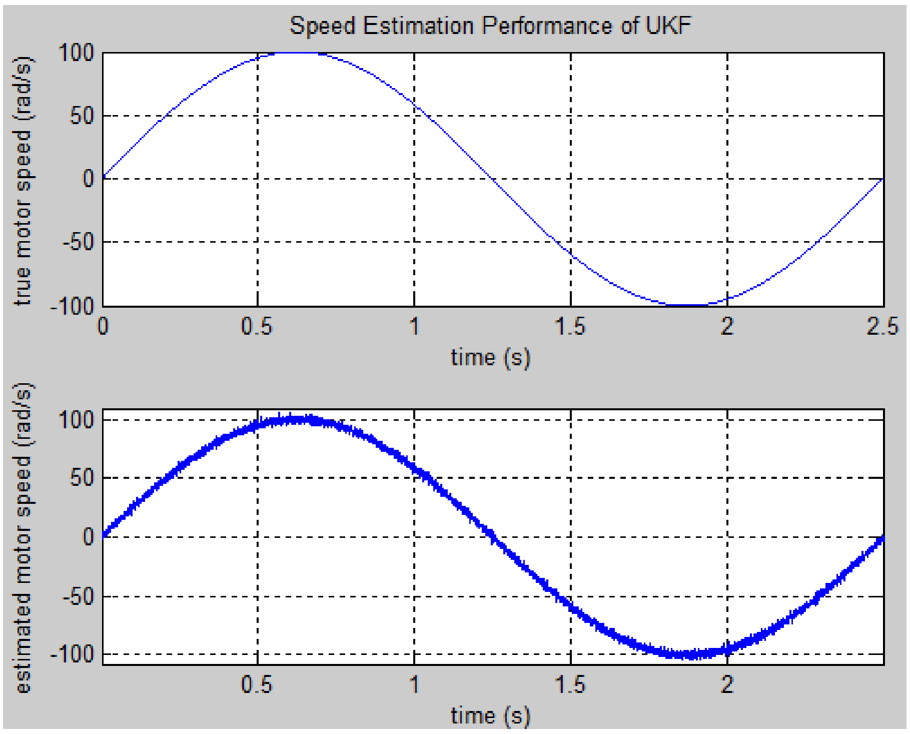

Figure 4-24 Speed estimation performance of the UKF in simulation

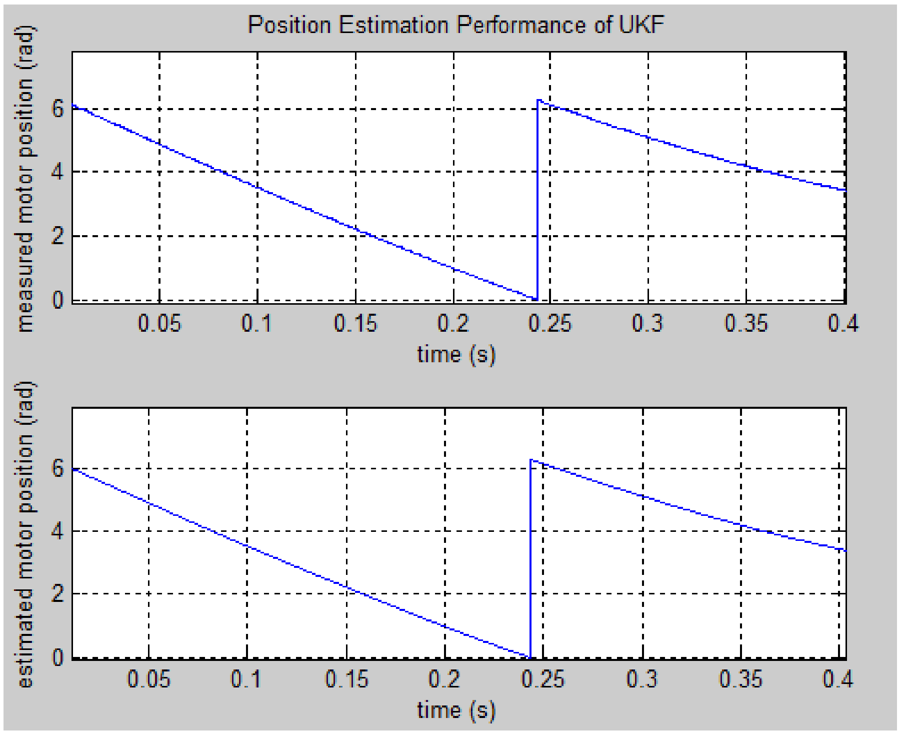

Figure 4-25 Position estimation performance of the UKF in real-time

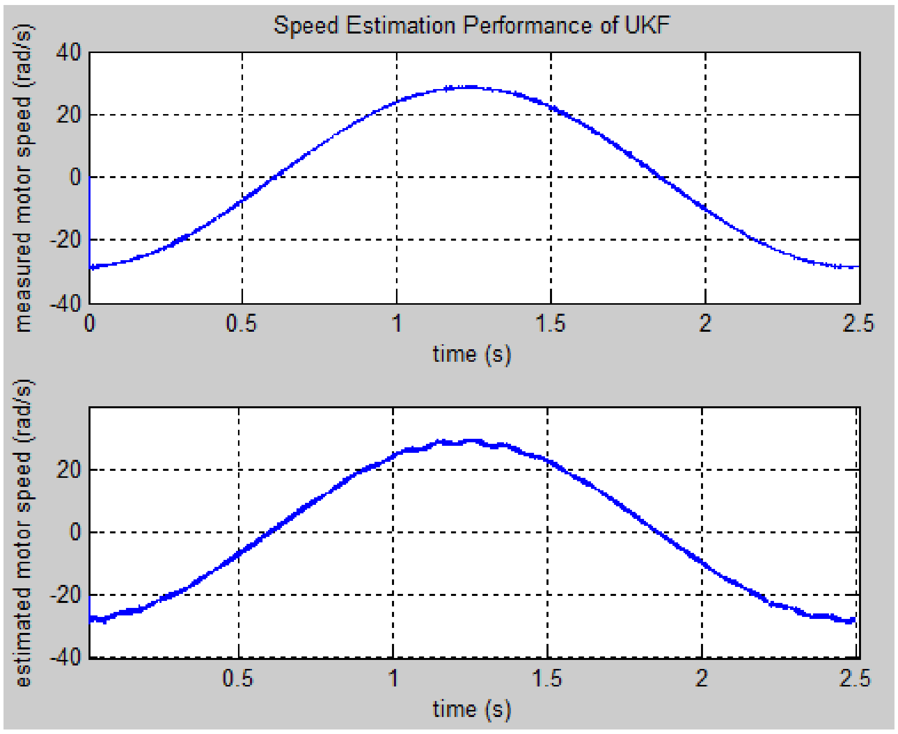

Figure 4-26 Speed estimation performance of the UKF in real-time

Table 4-6 gives the filter's performance parameters calculated using Matlab's *mean* and *var* functions.

Table 4-6 Performance parameters of the UKF in simulation and real-time

Environment	**Filter Params**	**Values**	**Mean of Position Estimation Error (rad)**	**Variance of Position Estimation Error (rad)**	**Mean of Speed Estimation Error (rad/s)**	**Variance of Speed Estimation Error (rad/s)**
Simulation	γ	0.15	-0.00829	0.08361	0.00027	2.75441
	α	1.41				
	β	2				
	κ	1				
Real-time	γ	0.15	-0.0022	0.03158	-0.2158	2.18465
	α	1.41				
	β	2				
	κ	1				

4.3 Comparative Analysis of the Real-time Estimation Performances of the Estimator Filters

Estimation performances in simulation and real-time differ due to changing noise and signal characteristics.

- Noise injected to resolver signals in simulation models is white, uncorrelated and zero-mean Gaussian. However, noise in the servo system does not satisfy these conditions. For instance, Figure 4-27 shows Power Spectral Density (PSD) analysis of real-time cosine signal. Since the signal has not a flat power spectral density, it is concluded that noise is not white in the experimental system.
- Simulation models have idealized characteristics such that nonlinearities present in the experimental system do not exist in simulation models. For instance, real-time demodulated cosine and sine signals have multiplicative distortion terms ($\sin\theta + \Delta S \sin\theta$ and $\cos\theta + \Delta C \cos\theta$) whereas simulation models do not have such terms.
- Simulation models do not suffer from delays in the demodulated sine and cosine signals whereas real-time models are exposed to them.

Therefore, the goal of the real-time comparative performance analysis is to find the most robust estimator filter against system non-linearities, signal distortions and non-ideal noise characteristics. If a filter is more sensitive to the said disturbing effects, it is less suitable to be utilized in the servo system.

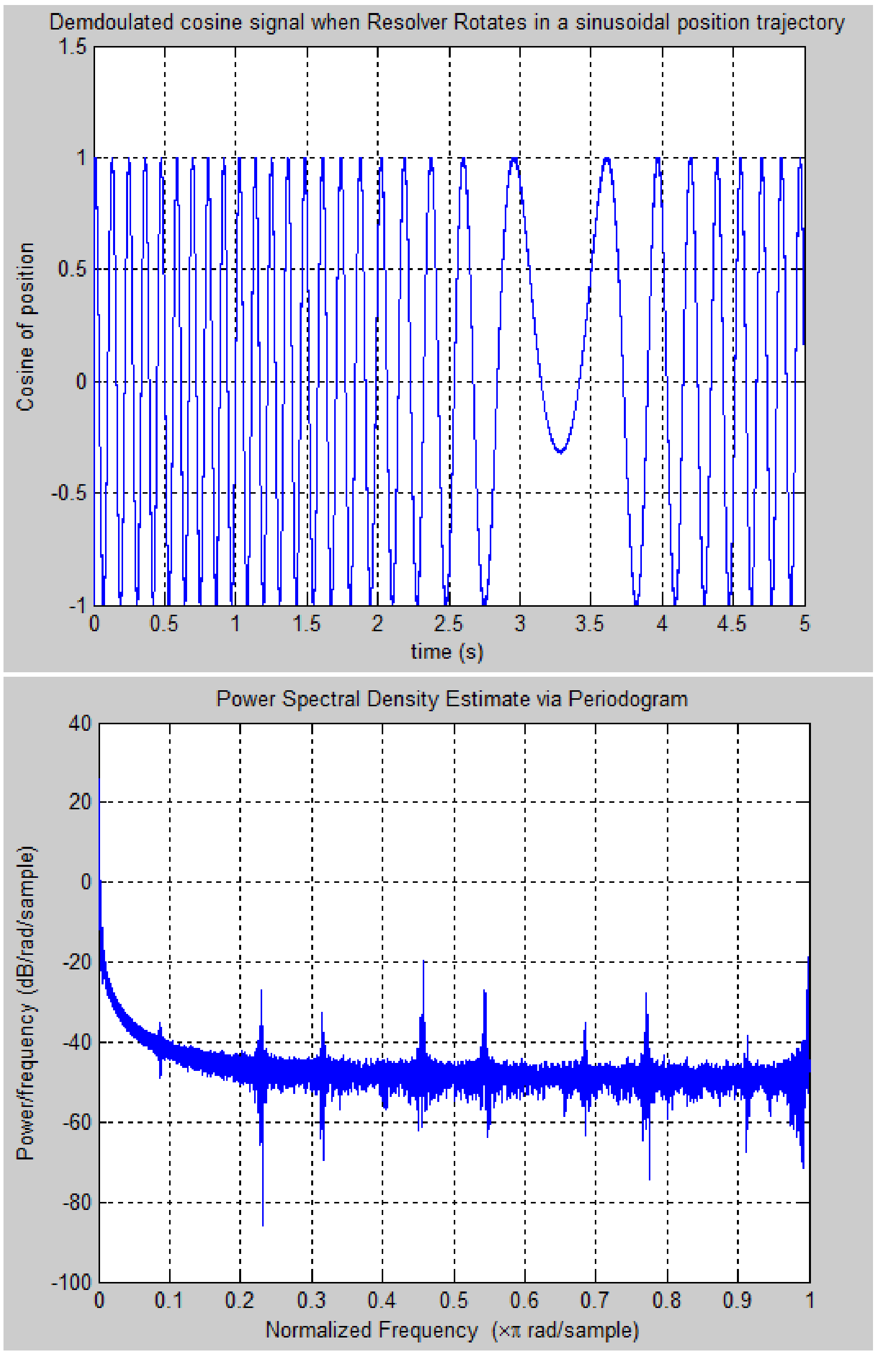

Figure 4-27 Real-time demodulated cosine signal and its Power Spectral Density estimate

Since the noise in resolver process is not white, it is expected that Kalman filters in real-time will not be as successful as they are in simulation environment. Contrary to this expectation, Kalman filters performed better than the nonlinear observer and the tracking differentiator with smaller estimation errors in both position estimate and speed estimate. However, evaluating position and speed estimation performances of the estimator filters alone does not give enough insight into replaceability of the designed software-based RDC with the ready-to-use RDC ICs. Hence, effects on torque, speed and position loops' performances should also be inspected. Table 4-7 includes all the data related to real-time performances of the filters.

Table 4-7 Results of the real-time performance tests of the estimator filters

Filter	**Environ.**	**Params**	**Values**	**Mean of Position Estimation Error (rad)**	**Mean of Speed Estimation Error (rad/s)**
Nonlinear Observer	Real-time	γ1	350000	-0.00197	-0.23219
		γ2	200		
Tracking Differentiator	Real-time	R	50000	-0.00329	-0.23207
		λ	0.071		
LKF	Real-time	α	1.8E-09	-0.00192	-0.22581
EKF	Real-time	α	1.8E-09	-0.00097	-0.20787
UKF	Real-time	γ	0.15	-0.0022	-0.2158
		α	1.41		
		β	2		
		κ	1		

4.3.1 Comparison of the Estimator Filters for Torque Loop's Performance

Since resolver rotor position (motor shaft position) signal is utilized for calculation of the produced torque in the servo system, error in position estimate in turn will degrade the torque loop performance. The block diagram of the torque control loop of the stabilized gun system is shown in Figure 4-28.

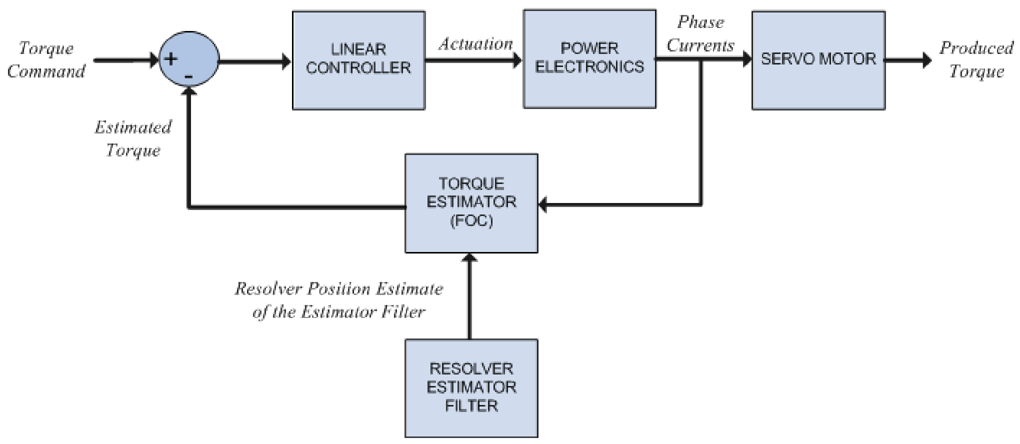

Figure 4-28 Simplified block diagram of the torque control loop with Field Orientated Control (FOC) in the servo system

(4.5) shows the relation between the torque feedback and resolver shaft position θ as

$$T = i_a\left(-\sin\theta + \tfrac{1}{\sqrt{3}}\cos\theta\right) + \tfrac{2}{\sqrt{3}} i_b \cos\theta \qquad (4.5)$$

where T stands for the produced torque and i_a and i_b stand for the motor phase currents. To observe the effect of the each filter's position estimation error on torque loop's performance, a simulation is performed by using (4.5).

Simulation Model

In the simulation model, a one pole pair synchronous motor with a resolver sensor rotating with a speed of 2π rad/s is simulated. The model has Inverse Park and Inverse Clarke transforms in order to simulate the motor phase currents i_a and i_b. The true torque estimate is calculated by using the correct position signal whereas the erroneous torque estimate is calculated by using the position signal with the estimation error. The simulation is repeated for each estimator filter by changing the position estimation error value of the model according to the data given in Table 4-7. The simulation model is shown in Figure 4-29.

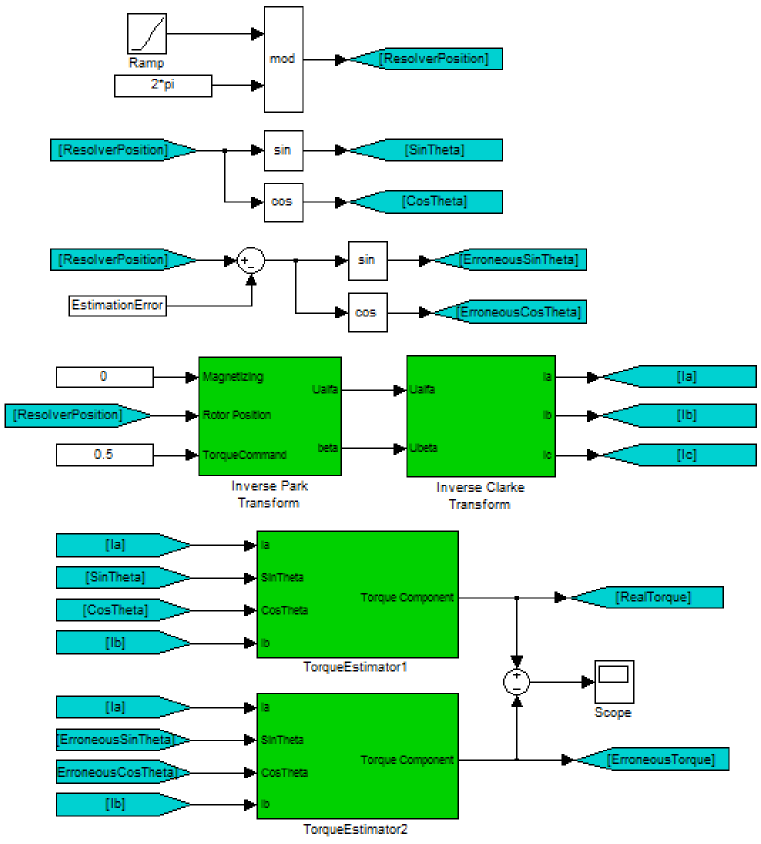

Figure 4-29 Simulation model in Simulink to observe the torque estimation error for filters' position estimation errors

Torque Estimation Performance for Different Estimator Filters

Using the derived simulation model, torque estimation error for each estimator filter is observed in simulation environment as shown in Figure 4-30.

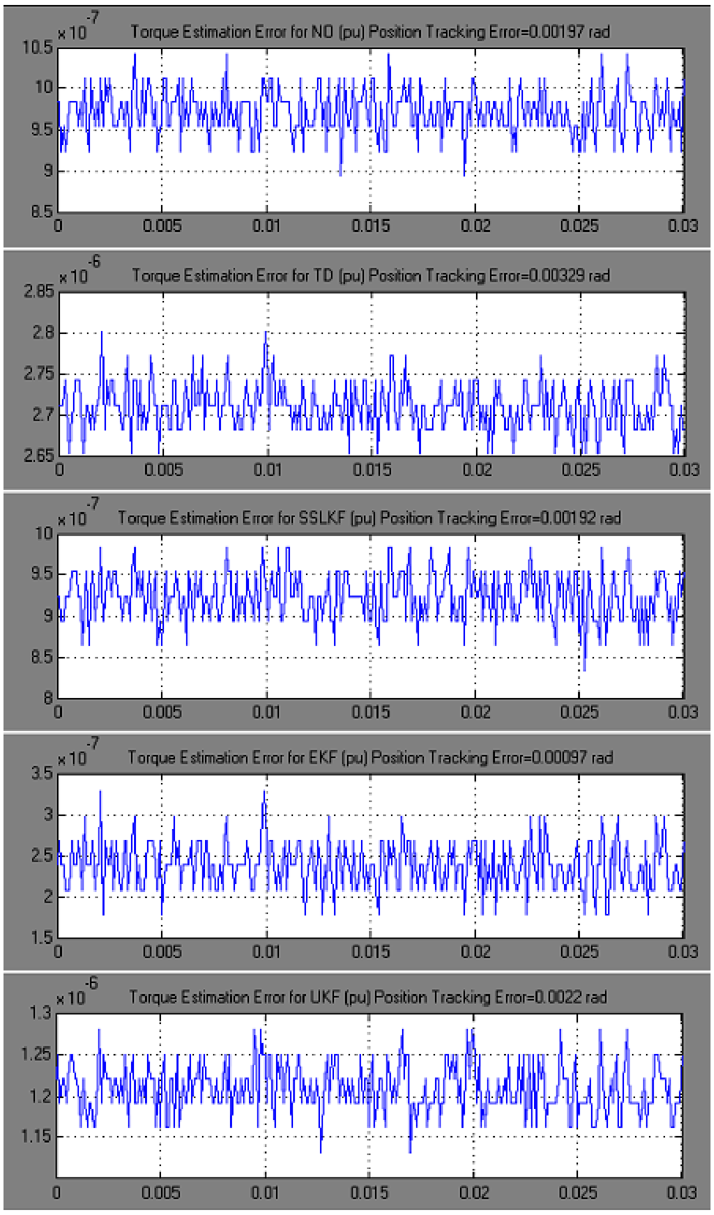

Figure 4-30 Torque estimation errors for estimator filters' position outputs

All in all, torque estimation error values are so small ($< 2.85 \times 10^{-4}\%$) that torque loop's performance will be affected negligibly with utilization of any estimator filter.

4.3.2 Comparison of the Estimator Filters for Speed and Position Loops' Performances

Velocity output of the estimator filter may be utilized to form up a closed-loop speed controller for a non-stabilized servo system as shown in Figure 4-31. One example for such a system may be stationary gun control systems deployed at battle field.

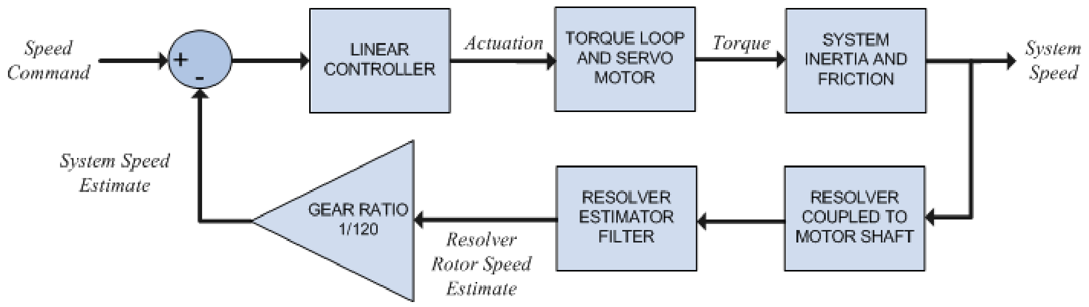
Speed Command
+
-
LINEAR CONTROLLER
Actuation
TORQUE LOOP AND SERVO MOTOR
Torque
SYSTEM INERTIA AND FRICTION
System Speed
System Speed Estimate
GEAR RATIO 1/120
Resolver Rotor Speed Estimate
RESOLVER ESTIMATOR FILTER
RESOLVER COUPLED TO MOTOR SHAFT

Figure 4-31 Block diagram of the speed control loop in the non-stabilized servo system

Since the system speed estimate is directly fed to the loop without encountering any transformation, an error in this signal will induce the same amount of tracking error in system speed loop. Therefore, feasibility of the estimator filters' velocity output in the servo system should be examined in terms of the resultant deterioration in speed and position tracking performance of the gun system.

The main goal of a gun control system is to keep the gun orientation at the target while the target is not stationary. In general, fire control systems utilize radars and electro-optical sensors which sense the target angular position with respect to the gun. Hence, in general, a position controlled servo system is preferred in gun control systems to stabilize the gun position. The most precise and reliable way of realizing the position controlled servo system is to use nested three control loops two of whom are above mentioned speed control and torque control loops. The third and the last loop of the position controlled servo system is the position loop.

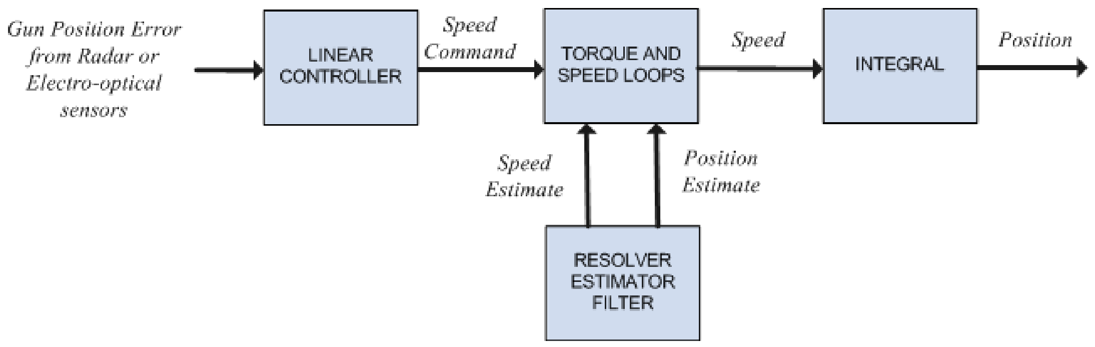

Figure 4-32 Position error controlled non-stabilized servo system

In the position controlled non-stabilized servo system, speed estimation error's disturbing effect on target tracking performance will be tolerated and reduced by the position loop. In order to observe the amount of this tolerance, a simulation is performed in Simulink using the real estimation error data given in Table 4-7.

Simulation Model

The simulation model is constructed by using nested loops of speed and position and modeling the torque loop's transfer function as a gain. The gun control system can be modeled as a differentiator between torque signal and speed signal as

$$T(s) = JsW(s) \tag{4.6}$$

where *T(s)* and *W(s)* are the torque and speed signals in Laplace domain and *J* is the inertia of the system. Together with the zero-order hold, the system transfer function in Laplace domain can be written as

$$\frac{W(s)}{T(s)} = \frac{1-e^{-T_s}}{s}\frac{1}{Js} = \frac{1-e^{-T_s}}{Js^2} \tag{4.7}$$

The discrete-time model in Z domain can be found using the Pulse transfer Function method described in [11], namely by the operation

$$\frac{W(z)}{T(z)} = Z\left(\frac{1-e^{-T_s}}{Js^2}\right) = (1-z^{-1})Z\left\{\frac{1}{Js^2}\right\} = \frac{T_s z^{-1}}{J(1-z^{-1})} \tag{4.8}$$

where Z stands for Pulse Transfer Function operator and T_s stands for the sampling period. The numerical values for T_s and J are 0.001 s and 34 kgm^2 respectively yielding a system transfer function of

$$\frac{W(z)}{T(z)} = 2.9412\times10^{-5}\frac{z^{-1}}{(1-z^{-1})} = \frac{2.9412\times10^{-5}}{z-1} \tag{4.9}$$

Using the system transfer function expressed by (4.9), the simulation model is constructed as seen in Figure 4-33. The model is supported by the realistic system parameters collected from the experimental system. For instance, the torque gain is set to 420 since the maximum achievable system torque is 420 Nm. Speed scale gain is set to 1.0467 since the maximum achievable system speed is 1.0467 rad/s. Lastly, friction torque is set to 85 Nm as measured in the experimental system.

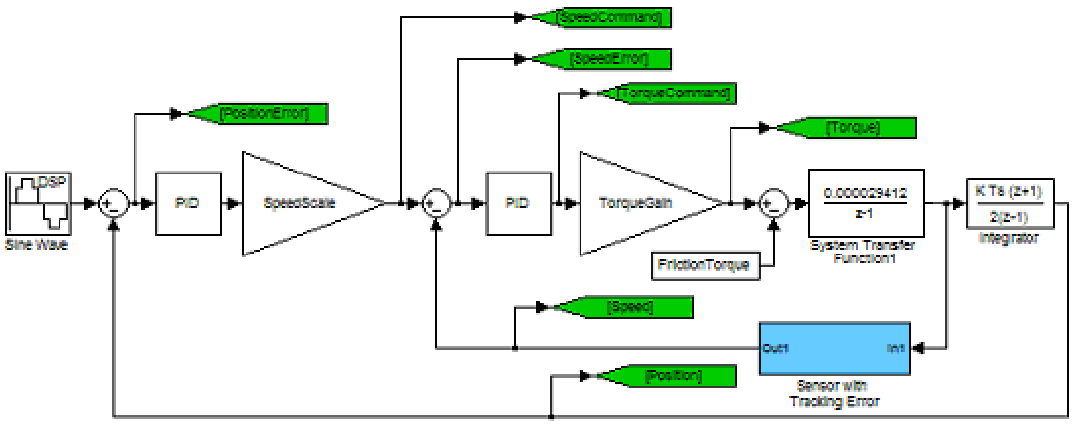

Figure 4-33 Non-stabilized gun control system's simulation model

The system speed estimation error values for each estimator filter are calculated from the data given in Table 4-7. The calculated system speed estimation error values are given in Table 4-8.

Table 4-8 System speed estimation error values calculated by multiplying real-time resolver speed estimation error values by system gear ratio (1/120)

Filter	**Mean of Resolver Speed Estimation Error (rad/s)**	**Mean of System Speed Estimation Error (rad/s)**
Nonlinear Observer	-0.23219	-0.00193492
Tracking Differentiator	-0.23207	-0.00193392
LKF	-0.22581	-0.00188175
EKF	-0.20787	-0.00173225
UKF	-0.21580	-0.00179833

In the simulation model, the software-based RDC is modeled as a speed sensor with non-zero speed estimation error. The simulation is repeated for each estimator filter by changing the system speed estimation error value of the model according to Table 4-8. System position command trajectory in simulation model is formed as the same with the position trajectory used in real-time performance tests. Namely, it is $0.09375\sin(2\pi 0.4t)$ rad. In the simulation, it is assumed that the radar or electro-optical sensor produces the position error at a sampling frequency of 25 Hz.

Comparison of the Estimator Filters for Speed and Position Loops' Performances

Making use of the derived simulation model, speed and position tracking errors are measured for different estimator filters by using running mean method. The results are given in Table 4-9. Transient responses of the loops are also taken into consideration during the measurements.

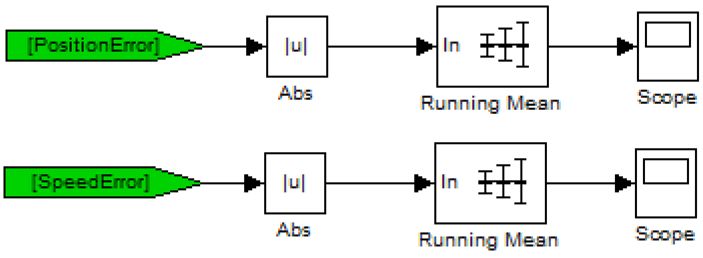

Figure 4-34 Measuring servo system speed and position tracking errors in simulation environment using running mean method in Simulink

Table 4-9 Position and speed loops' performances with different estimator filters for a position command trajectory of $0.09375\sin(2\pi ft)$ rad

Filter	**Average System Speed Estimation Error (rad/s)**	**Simulation Time**	**Running Mean of Position Tracking Error (rad)**	**Running Mean of Speed Tracking Error (rad/s)**
Zero Estimation Error	0	7 s	0.017672955	0.00761063
Nonlinear Observer	-0.00193492	7 s	0.017676911	0.00761110
Tracking Differentiator	-0.00193392	7 s	0.017676909	0.00761108
LKF	-0.00188175	7 s	0.017676795	0.00761109
EKF	-0.00173225	7 s	0.017676469	0.00761105
UKF	-0.00179833	7 s	0.017676613	0.00761107

Figure 4-35 shows the position tracking performance of the servo loop for changing position estimation error values for a position command trajectory of $0.09375\sin(2\pi 0.4t)$ rad.

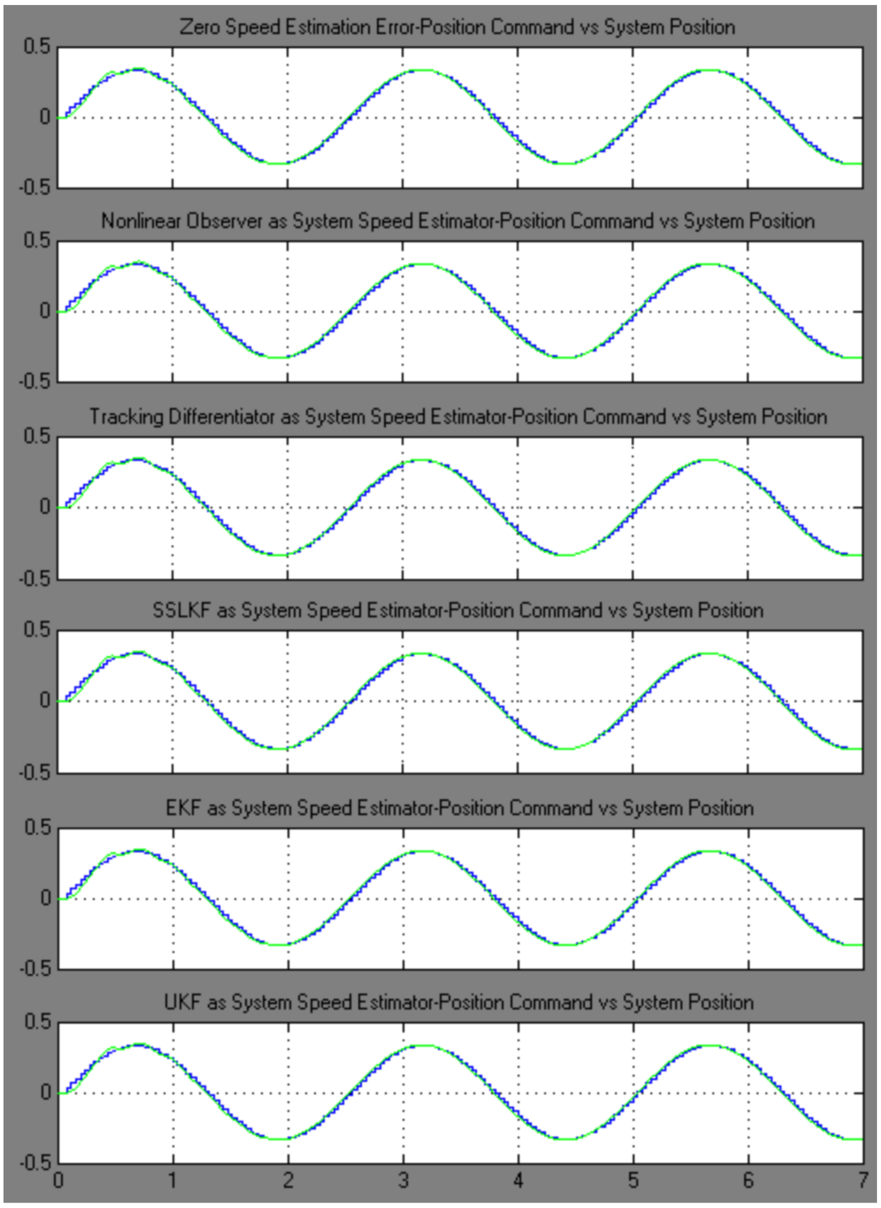

Figure 4-35 Scope screen showing position tracking performance of the servo system in transient and steady-state for changing position estimation error values when a position command trajectory of $0.09375\sin(2\pi ft)$ rad is applied to the servo system

When Table 4-9 is examined in close, it is observed that position tracking errors of the servo system with non-zero estimation errors (i.e. with estimator filters' speed estimation errors) are negligibly small compared to the position tracking error of the servo system when zero speed estimation error is applied. This proves the claim that the estimator filters can be utilized as system speed estimator in a non-stabilized servo system. Therefore, from the aspect of non-stabilized gun control system's target tracking performance, the proposed software-based RDC seem to be replaceable with the ready-to-use RDC ICs.

4.3.3 Comparison of the Estimator Filters for Filtering Performances and Computational Complexity

Kalman filters show slightly better performance in both simulation environment and in real-time when we investigate the resolver speed estimation performances of the filters. In fact, since real-time noise in resolver process is not Gaussian and it is correlated to position signal, it is expected that Kalman filters implemented in the experimental system will not be as successful as they are in simulation environment. However, although the real-time noise in the process does not satisfy the optimality criterions of the Kalman filtering, that is being white, uncorrelated and Gaussian, Kalman filters performed slightly better than the nonlinear ways of filtering such as nonlinear observer and tracking differentiator.

When we compare estimation performances of different type Kalman filters for resolver conversion process, we see that the EKF is the best filter followed by the UKF and then LKF. Although it is stated that the UKF generally performs slightly better than EKF in [13], we observed that UKF performs worse. The worse performance of the UKF may be due to tuning imperfections since the UKF has four tuning parameters and these parameters are closely dependent on the noise model which is not exactly known. Moreover, the worse performance of the UKF may also be due to the fact that system nonlinearities in resolver conversion process are not so severe that Unscented Transform could not show its dominating success in passing Gaussians through nonlinear functions. All in all, it is proved that there is not a great difference in estimation performances of LKF, UKF and EKF for resolver conversion process. Hence, UKF and EKF with their higher computational power requirements are not so feasible that LKF with its minimized computational complexity show a very similar estimation performance.

As far as the computational efficiency is thought based on the mathematical derivations of the filters, UKF is the most complex filter followed by EKF. LKF, Nonlinear Observer and Tracking Differentiator have similar computational complexities which can be stated as light compared to the EKF and the UKF. Hence, it is concluded that the ideal filter for software-based resolver-to-digital converter is the Linear Kalman filter as illustrated in Figure 4-36.

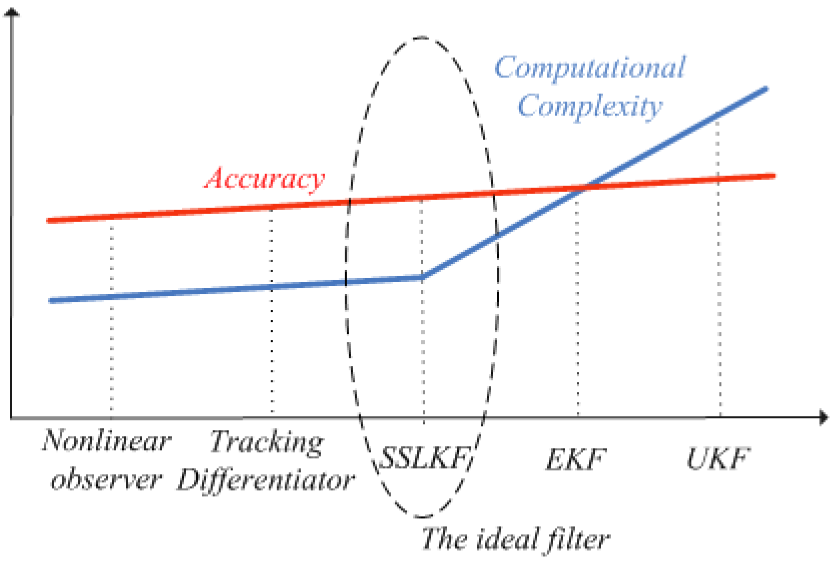

Figure 4-36 Accuracy and computational complexity graphs of the estimator filters (not scaled to real values)

One more advantage of the Kalman filters over the Nonlinear Observer and the Tracking Differentiator is that they provide an estimate of the acceleration even though it is a bit noisy. The acceleration information may be utilized to form up an acceleration-controlled servo system instead of the classical torque-controlled servo system. Acceleration control increases the stiffness of the servo system considerably [32, 33, 34].

4.4 Stability and Sensitivity Analyses

4.4.1 Stability Analysis

The stability analysis is performed for the Kalman filter by making use of the Liapunov stability criterion. The mathematical model of the Linear Kalman filter is

$$\begin{pmatrix} \theta_{k+1}^- \\ \omega_{k+1}^- \\ a_{k+1}^- \end{pmatrix} = \begin{pmatrix} 1 & T_s & T_s^2/2 \\ 0 & 1 & T \\ 0 & 0 & 1 \end{pmatrix} \begin{pmatrix} \theta_k^- \\ \omega_k^- \\ a_k^- \end{pmatrix} + K(\theta_k - \theta_k^-) \tag{4.10}$$

where θ_k^- is the filter's position estimate, ω_k^- is the filter's speed estimate, a_k^- is the filter's acceleration estimate and θ_k is the actual resolver position. Lastly, K is the pre-calculated Kalman gain and it is expressed as

$$K = \begin{pmatrix} k_1 \\ k_2 \\ k_3 \end{pmatrix} \tag{4.11}$$

Then the filter can be described by

$$\begin{pmatrix} \theta_{k+1}^- \\ \omega_{k+1}^- \\ a_{k+1}^- \end{pmatrix} = \begin{pmatrix} 1-k_1 & T_s & T_s^2/2 \\ -k_2 & 1 & T_s \\ -k_3 & 0 & 1 \end{pmatrix} \begin{pmatrix} \theta_k^- \\ \omega_k^- \\ a_k^- \end{pmatrix} + \begin{pmatrix} k_1 \\ k_2 \\ k_3 \end{pmatrix} \theta_k \tag{4.12}$$

Setting θ_k to zero, zero-input solution for the system can be found by solving the following state-space equation;

$$\begin{pmatrix} \theta_{k+1}^- \\ \omega_{k+1}^- \\ a_{k+1}^- \end{pmatrix} = \begin{pmatrix} 1-k_1 & T_s & T_s^2/2 \\ -k_2 & 1 & T_s \\ -k_3 & 0 & 1 \end{pmatrix} \begin{pmatrix} \theta_k^- \\ \omega_k^- \\ a_k^- \end{pmatrix} \tag{4.13}$$

The second method of Liapunov states that if a system has an asymptotically stable equilibrium state within a region of attraction in the state space, whatever the energy level the system is in at the beginning, it will dissipate its energy and its energy will decay within a trajectory with increasing time until the system reaches the minimum energy level at the equilibrium state. Hence, if a system has an asymptotically stable equilibrium state in a certain region in state space, then we can claim that it is asymptotically stable in this region. If asymptotic stability holds for all states in state space from which the energy trajectories start, then the equilibrium state is said to be asymptotically stable in the large. Asymptotic stability in the large is a desirable feature in control engineering. [11]

Practically, let us consider a discrete-time system described as

$$x(k+1) = Ax(k) \tag{4.14}$$

where x is the state vector of the system and A is the state matrix of the system. Let us assume that A is a nonsingular matrix. Then the equilibrium state at the origin of the system (x=0) is asymptotically stable in the large, if, given any positive definite Hermitian matrix Q, there exists a positive definite Hermitian matrix P such that

$$A^*PA - P = -Q \tag{4.15}$$

Using the above defined method, let us investigate the stability of the origin for the Kalman filter realized in the thesis. The A matrix will be

$$A = \begin{pmatrix} 1-k_1 & T_s & T_s^2/2 \\ -k_2 & 1 & T_s \\ -k_3 & 0 & 1 \end{pmatrix} \tag{4.16}$$

Writing the numerical values for k_1, k_2, k_3 and T_s which are 0.1235037, 73.98153, 22158.22 and 0.0001 s respectively, we get

$$A = \begin{pmatrix} 0.8764963 & 0.0001 & 0.00005 \\ -73.98153 & 1 & 0.0001 \\ -22158.32 & 0 & 1 \end{pmatrix} \tag{4.17}$$

Then, let us choose Q to be **I**. Then from the equation (4.15), the stability equation becomes

$$A^*PA - P = -\begin{pmatrix} 1 & 0 & 0 \\ 0 & 1 & 0 \\ 0 & 0 & 1 \end{pmatrix} \tag{4.18}$$

Making use of the Matlab's *dlyap* function, the solution for *P* is found as

$$P = \begin{pmatrix} 3.93\times10^{11} & -1.96\times10^{7} & -2.05\times10^{6} \\ -1.96\times10^{7} & 2.06\times10^{6} & -5\times10^{3} \\ -2.05\times10^{4} & -5\times10^{3} & 27.99 \end{pmatrix} \tag{4.19}$$

Applying the Sylvester's criterion for positive definiteness, the *P* matrix is found as to be positive definite. Hence, the equilibrium state x=0 is asymptotically stable in the large for the Kalman filter implemented in the thesis.

4.4.2 Sensitivity Analysis

In this section, sensitivity of the position tracking error of the servo system equipped with the proposed RDC to demodulator output errors (ΔS and ΔC) is analyzed. At the end of the study, robustness of the servo system is also measured by the numerical analysis.

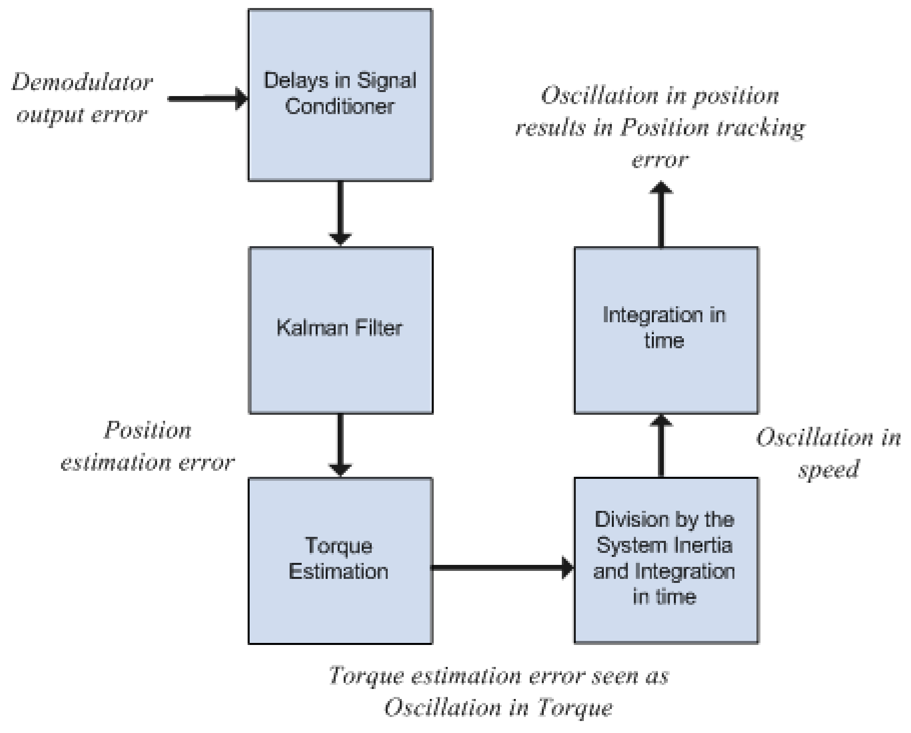
Demodulator output error
Delays in Signal Conditioner
Oscillation in position results in Position tracking error
Kalman Filter
Integration in time
Position estimation error
Oscillation in speed
Torque Estimation
Division by the System Inertia and Integration in time
Torque estimation error seen as Oscillation in Torque

Figure 4-37 Flow of the error from the demodulator to the position tracking performance of the servo system

Position Estimation Error as a Function of ΔS *,* ΔC *and Actual Position*

Kalman filter derived for the software-based RDC can be seen as to have two components; a nonlinear transfer function and a linear transfer function.

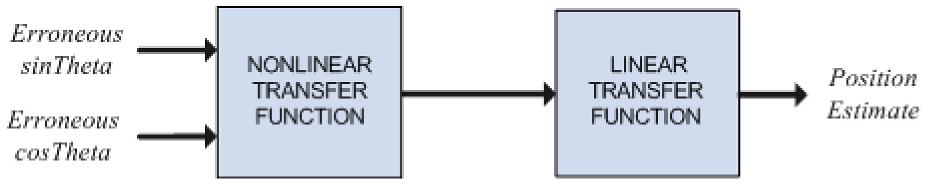

Figure 4-38 Kalman filter divided into two components for sensitivity analysis

Firstly, let us neglect the dynamics of the Kalman filter carried by the linear transfer function and express the position estimation error in terms of ΔS, ΔC and actual position by using the nonlinear transfer function. The nonlinear transfer function in Kalman filter is the error calculator function expressed by

$$\sin\theta\cos\phi - \cos\theta\sin\phi \tag{4.20}$$

where θ is the actual resolver position and ϕ is the position estimate of the filter. From the analysis performed in section 3.2.2, we know that if the Kalman filter shows zero steady-state error, the position estimation error $\Delta\theta$ will be

$$\Delta\theta = \Delta C\cos\theta\sin\phi - \Delta S\sin\theta\cos\phi \tag{4.21}$$

Then, (4.21) can be expanded as

$$\Delta\theta = \Delta C\cos\theta\sin(\theta - \Delta\theta) - \Delta S\sin\theta\cos(\theta - \Delta\theta) \tag{4.22}$$

Further expanding will yield

$$\begin{aligned}\Delta\theta(\Delta C, \Delta S, \theta) = {} & \Delta C\cos\theta(\sin\theta\cos\Delta\theta - \cos\theta\sin\Delta\theta) \\ & - \Delta S\sin\theta(\cos\theta\cos\Delta\theta + \sin\theta\sin\Delta\theta)\end{aligned} \tag{4.23}$$

Since $\Delta\theta$ will be very close to zero, we can assume $\cos\Delta\theta$ to be 1 and $\sin\Delta\theta$ to be 0. Then, (4.23) will be reduced to

$$\Delta\theta(\Delta C, \Delta S, \theta) = \Delta C\cos\theta\sin\theta - \Delta S\sin\theta\cos\theta \tag{4.24}$$

Hence, the position estimation error due to demodulator output errors and actual position can be approximated by (4.24).

This analysis gives the behavior of the filter with the assumption that the kalman filter will track the input with zero steady-state error. However, for some values of the filter parameter α the assumption may not hold, that is, filter may show non-zero steady-state error. Hence, the following analysis is performed to include the Kalman filter's dynamics in the sensitivity analysis as well.

Position Estimation Error as a Function of Filter Parameter and Resolver Speed

The Kalman filter is modeled by the following state-space representation;

$$\begin{pmatrix} \theta_{k+1}^- \\ \omega_{k+1}^- \\ a_{k+1}^- \end{pmatrix} = \begin{pmatrix} 1 & T_s & T_s^2/2 \\ 0 & 1 & T_s \\ 0 & 0 & 1 \end{pmatrix} \begin{pmatrix} \theta_k^- \\ \omega_k^- \\ a_k^- \end{pmatrix} + \begin{pmatrix} k_1 \\ k_2 \\ k_3 \end{pmatrix} (\theta_k - \theta_k^-) \tag{4.25}$$

where θ_k^- is the filter's position estimate, ω_k^- is the filter's speed estimate, a_k^- is the filter's acceleration estimate and θ_k is the actual resolver position. Lastly, K is the pre-calculated Kalman gain and it is expressed by

$$K = \begin{pmatrix} k_1 \\ k_2 \\ k_3 \end{pmatrix} \tag{4.26}$$

Let us make use of Z-transform method in extracting the transfer function of the filter. The following equations can be written in Z domain.

$$a = z^{-1}a + k_3(\theta - z^{-1}\phi) \tag{4.27}$$

$$\omega = z^{-1}\omega + k_2(\theta - z^{-1}\phi) + T_s z^{-1} a \tag{4.28}$$

$$\phi = z^{-1}\phi + k_1(\theta - z^{-1}\phi) + T_s z^{-1}\omega + \frac{T_s^2}{2} z^{-1} a \tag{4.29}$$

where the following definitions are given

$$\begin{aligned} a &= Z\{a_k^-\} \\ \omega &= Z\{\omega_k^-\} \\ \phi &= Z\{\theta_k^-\} \\ \theta &= Z\{\theta_k\} \end{aligned} \tag{4.30}$$

Writing (4.27) into (4.28), an expression for ω in terms of θ and ϕ is derived. When the derived expression and (4.27) are both written into (4.29), the following linear transfer function is obtained.

$$G(z)=\frac{\phi}{\theta}=\frac{k_1+(k_2T_s+{}^{k_3}\!/_2\,T_s^2-2k_1)z^{-1}+(k_1-k_2T_s+{}^{k_3}\!/_2\,T_s^2)z^{-2}}{1+(k_1-3)z^{-1}+(3+k_2T_s+k_3\,{}^{T_s^2}\!/_2-2k_1)z^{-2}+(-1+k_1-k_2T_s+{}^{k_3}\!/_2\,T_s^2)z^{-3}} \qquad (4.31)$$

Then, the error signal in Z-domain can be expressed as

$$E(z)=\theta-\phi=\theta-G(z)\theta=\theta(1-G(z)) \qquad (4.32)$$

For instance, for a position signal varying with constant speed $\omega_k = A$ rad/s, the error signal in Z-domain will be

$$E(z)=(1-G(z))\theta=(1-G(z))\frac{AT_sz^{-1}}{(1-z^{-1})^2} \qquad (4.33)$$

Making use of (4.33), the variation of the steady-state error with respect to filter parameter α and resolver speed is observed as shown in Figure 4-38.

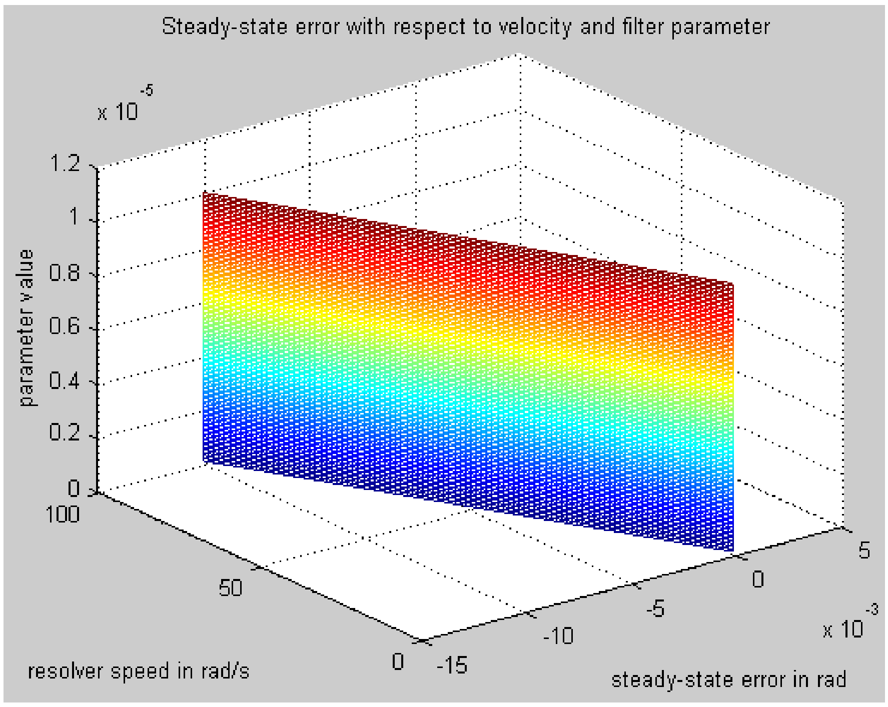

Figure 4-39 Steady-state error with respect to resolver speed and α where speed varies from 1 rad/s to 100 rad/s and α varies from 10^{-10} to 10^{-5}

From Figure 4-38, it is concluded that the steady-state error changes negligibly with changing α where α takes values between 10^{-10} to 10^{-5}. As a result, it can be assumed that $\partial\Delta\theta / \partial\alpha = 0$ where α changes in this limited region. The reason why α is limited between 10^{-10} to 10^{-5} can be explained by the trade-off performed between the filter bandwidth and noise suppression performance. If the parameter (α) is made greater than 10^{-5}, the filter's bandwidth decreases to an unacceptable level. On the other hand, if it is made smaller than 10^{-10}, the filter bandwidth increases so much that the noise suppression ability deteriorates. Figure 4-39 explains the situation with error signal's variation with different filter parameters selected between 10^{-10} to 10^{-5}.

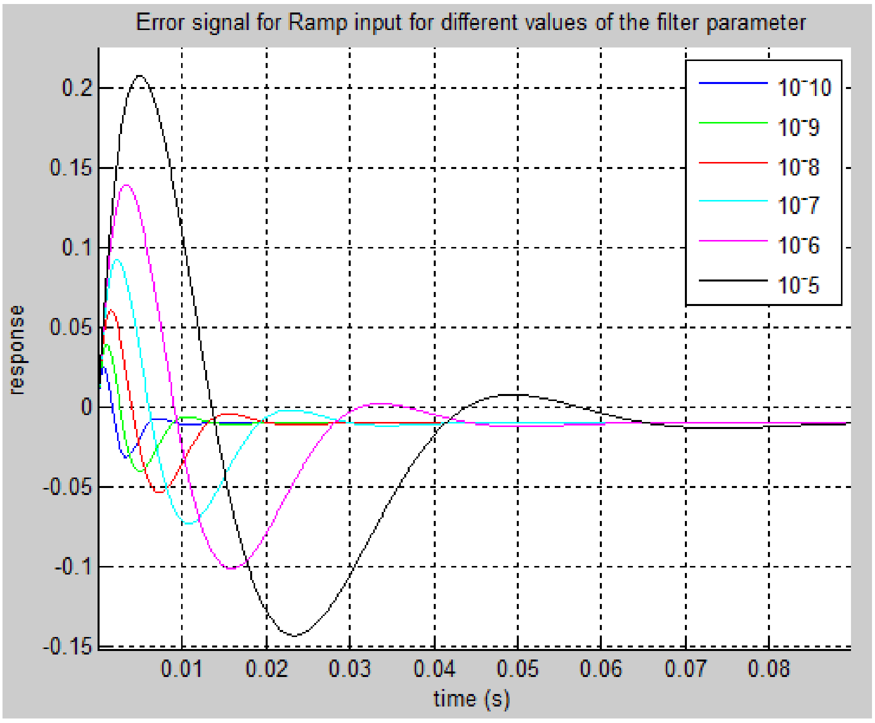

Figure 4-40 Error signal's settling for different values of the filter parameter α

Although the bandwidth changes with changing parameter value, the steady-state error does not change with changing parameter value (Figure 4-39). On the other hand, the steady-state error increases with increasing resolver speed (Figure 4-38).

Hence, we can claim that the estimation error is dependent on not only the resolver position but also resolver speed. This situation can be explained mathematically by the final-value theorem. The steady-state error will be

$$\begin{aligned}\Delta\theta(A) &= \lim_{z\to 1}\left((1-z^{-1})E(z)\right) = \lim_{z\to 1}\left(A\frac{b_0(1-b_1z^{-1})(1-b_2z^{-1})(1-b_3z^{-1})(1-b_4z^{-1})}{(1-a_1z^{-1})(1-a_2z^{-1})(1-a_3z^{-1})(1-a_4z^{-1})}\right) \\ &= A\frac{b_0(1-b_1)(1-b_2)(1-b_3)(1-b_4)}{(1-a_1)(1-a_2)(1-a_3)(1-a_4)}\end{aligned} \qquad (4.34)$$

where A is the actual resolver speed in rad/s and b_i and a_i are filter coefficients calculated with the filter parameter α. Hence, the theorem reveals that there will always be a finite steady-state error whose amplitude is proportional to resolver speed while the resolver rotates with a constant speed. By using the assumption $\partial\Delta\theta / \partial\alpha = 0$ and numerical values of b_i and a_i, position estimation error due to constant resolver speed can be formulated as

$$\Delta\theta(A) = 0.0000375A \text{ rad} \qquad (4.35)$$

Position Estimation Error Due to Filtering Delays

Another error source is the filtering delays which stem from implementation of anti-aliasing filter, interpolation filter and high-pass filter on resolver channels. The expression (4.36) has been derived in section 3.2.5 and it gives the position estimation error with respect to resolver speed as

$$\Delta\theta(\omega) = 0.00040965\omega \text{ rad} \qquad (4.36)$$

where ω is the resolver speed in rad/s.

Total Position Estimation Error

Making use of (4.24), (4.35) and (4.36), the total position estimation error can be approximated by the following expression;

$$\Delta\theta(\Delta C,\Delta S,\theta,\omega,A)=\Delta C\cos\theta\sin\theta-\Delta S\sin\theta\cos\theta \\ +0.0000375A+0.00040965\omega \text{ rad} \tag{4.37}$$

where ΔC and ΔS are demodulator output percentage errors for cosine and sine channels respectively, A is the constant resolver speed in rad/s and ω is the resolver speed in rad/s. Since the expression is derived for constant speed case, the third and the fourth terms can be unified reducing (4.37) to

$$\Delta\theta(\Delta C,\Delta S,\theta,A)=\Delta C\cos\theta\sin\theta-\Delta S\sin\theta\cos\theta+0.00044715A \tag{4.38}$$

Then, sensitivity of the position estimation error to ΔC and ΔS can be found using partial derivatives such as

$$\frac{\partial\Delta\theta}{\partial\Delta C}=\cos\theta\sin\theta \tag{4.39}$$

and

$$\frac{\partial\Delta\theta}{\partial\Delta S}=-\sin\theta\cos\theta \tag{4.40}$$

The sensitivity of the position estimation error to filter parameter α has been found as negligibly small in the region where the filter has acceptable bandwidth and noise rejection performance. Similarly, we can also neglect the sensitivity of the position estimation error to constant speed A since the related coefficient in (4.38) is negligibly small. Hence, the sensitivity of the position estimation error to filter parameter and resolver speed is assumed to be zero throughout the sensitivity analysis.

Figure 4-40 visualizes sensitivity of the nonlinear transfer function to demodulator output percentage errors ΔS and ΔC.

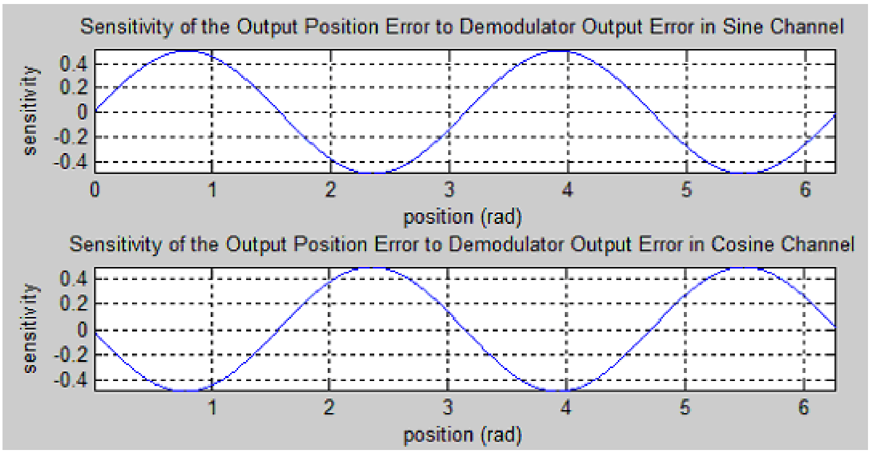

Figure 4-41 Sensitivity of the nonlinear transfer function to demodulator output percentage errors ΔS and ΔC

The position estimation error signal is visualized by using realistic ΔS and ΔC values in Figure 4-41. ΔS and ΔC are modeled as Gaussian distributed signals with mean 0 and variance 0.005% which correspond to maximum demodulator output errors of 1.8% as calculated in section 3.2.5.

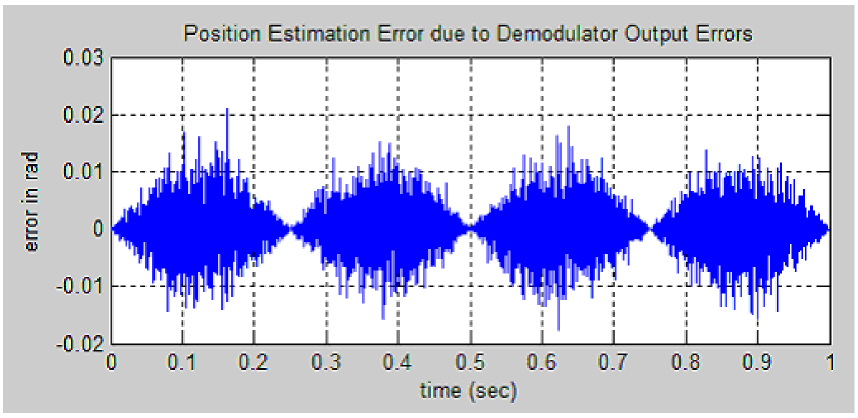

Figure 4-42 Position estimation error in steady-state due to Gaussian demodulator output errors while the resolver rotor rotates with a speed of 2π rad/s

The position estimate signal is used to form up the torque loop of the servo drive controller. The following transformation derived from (3.12) gives the relation between the torque tracking error ΔT and the position estimation error $\Delta\theta$.

$$\begin{aligned}\Delta T &= T_{\Delta T} - T \\ &= i_a\left(-\sin(\theta+\Delta\theta)+\frac{1}{\sqrt{3}}\cos(\theta+\Delta\theta)\right)+i_b\frac{2}{\sqrt{3}}\cos(\theta+\Delta\theta) \\ &\qquad -i_a\left(-\sin\theta+\frac{1}{\sqrt{3}}\cos\theta\right)+i_b\frac{2}{\sqrt{3}}\cos\theta\end{aligned} \tag{4.41}$$

where T is the demanded torque, $T_{\Delta T}$ is the erroneous actual torque, i_a and i_b are motor phase currents and θ is the actual position. Expanding (4.41) will yield

$$\begin{aligned}\Delta T = {} & i_a\left(-\sin\theta\cos\Delta\theta-\sin\Delta\theta\cos\theta+\frac{1}{\sqrt{3}}\left(\cos\theta\cos\Delta\theta-\sin\theta\sin\Delta\theta\right)\right) \\ & +i_b\frac{2}{\sqrt{3}}\left(\cos\theta\cos\Delta\theta-\sin\theta\sin\Delta\theta\right)-i_a\left(-\sin\theta+\frac{1}{\sqrt{3}}\cos\theta\right) \\ & +i_b\frac{2}{\sqrt{3}}\cos\theta\end{aligned} \tag{4.42}$$

Since $\Delta\theta$ is so small we can assume that $\cos\Delta\theta \approx 1$ and $\sin\Delta\theta \approx \Delta\theta$, which will reduce (4.42) to

$$\Delta T = i_a\left(-\Delta\theta\cos\theta-\frac{1}{\sqrt{3}}\Delta\theta\sin\theta\right)-i_b\frac{2}{\sqrt{3}}\Delta\theta\sin\theta \tag{4.43}$$

where i_a and i_b are position and torque dependent variables. They can be approximated using (2.5) and (2.6) as

$$i_a = -T\sin\theta \tag{4.44}$$

$$i_b = \frac{T}{2}\sin\theta+\frac{\sqrt{3}T}{2}\cos\theta \tag{4.45}$$

Hence, writing (4.44) and (4.45) into (4.43), the sensitivity of torque tracking error to position estimation error can be found as

$$\frac{\partial \Delta T}{\partial \Delta \theta} = 2T \sin\theta \cos\theta \tag{4.46}$$

Combining (4.46) and (4.38), we will obtain

$$\Delta T = 2T\left(\sin\theta\cos\theta\right)^2 \Delta C, S \tag{4.47}$$

Hence, the torque tracking error will be periodic and its frequency will depend on the rate of change of the actual position of the motor. That is to say, ΔT shows oscillation with a frequency four times the motor rotation frequency as seen in the Figure 4-42. Let us name this oscillation as "torque ripple".

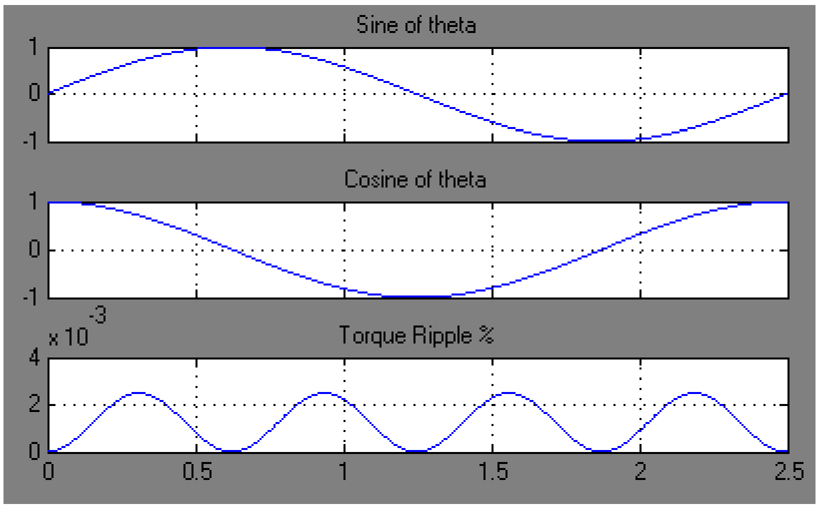

Figure 4-43 Scope screen showing torque ripple and $\sin\theta$ and $\cos\theta$ signals when a torque demand of 50% and a demodulator output error of 1% are present in the system

The following differential equation which is time domain expression of (4.6) gives the relation between the torque tracking error ΔT and speed tracking error $\Delta\omega$.

$$\Delta T = J\frac{d\Delta\omega}{dt} \tag{4.48}$$

which can also be written as

$$\Delta\omega = \frac{1}{J}\int_{t_1}^{t_2} \Delta T dt \tag{4.49}$$

where J is the inertia of the system. Then, the sensitivity of speed tracking error to torque tracking error can be derived by differentiating both sides of (4.49) with respect to ΔT.

$$\frac{\partial \Delta\omega}{\partial \Delta T} = \frac{\partial}{\partial \Delta T}\left(\frac{1}{J}\int_{t_1}^{t_2} \Delta T dt\right) = \frac{1}{J}\int_{t_1}^{t_2} \frac{\partial \Delta T}{\partial \Delta T} dt = \frac{1}{J}(t_2 - t_1) \tag{4.50}$$

Similarly, the system position tracking error $\Delta\mathrm{P}$ is the time-based integral of the system speed tracking error $\Delta\omega$.

$$\Delta\mathrm{P} = \int_{t_1}^{t_2} \Delta\omega dt \tag{4.51}$$

Hence, the sensitivity function can be written as

$$\frac{\partial \Delta\mathrm{P}}{\partial \Delta\omega} = \frac{\partial}{\partial \Delta\omega}\left(\int_{t_1}^{t_2} \Delta\omega dt\right) = \int_{t_1}^{t_2} \frac{\partial \Delta\omega}{\partial \Delta\omega} dt = (t_2 - t_1) \tag{4.52}$$

Consequently, an oscillation on the torque signal will induce an oscillation on the system speed at the same frequency. Similarly an oscillation on the speed signal will induce an oscillation on the position signal at the same frequency. Hence, t_2 and t_1 values in (4.50) and (4.52) should be determined based on the torque ripple frequency. If we perform the worst case analysis, the integration time $(t_2 - t_1)$ should be chosen as

$$(t_2 - t_1) = 1/2f_T \tag{4.53}$$

where f_T is the frequency of the torque ripple which has been determined as four times the motor rotation frequency from (4.47).

The overall sensitivity function which relates the system position tracking error to the demodulator output error can be found from the chain rule as

$$\frac{\partial \Delta \mathrm{P}}{\partial \Delta C, S} = \frac{\partial \Delta \theta}{\partial \Delta C, S} \frac{\partial \Delta T}{\partial \Delta \theta} \frac{\partial \Delta \omega}{\partial \Delta T} \frac{\partial \Delta \mathrm{P}}{\partial \Delta \omega} \tag{4.54}$$

which yields (4.55) by (4.52), (4.50), (4.46), (4.40) and (4.39).

$$\frac{\partial \Delta \mathrm{P}}{\partial \Delta C, S} = \pm \frac{2T}{J} (t_2 - t_1)^2 (\cos\theta \sin\theta)^2 \tag{4.55}$$

Then, for any value of ΔC or ΔS, let us call them $\Delta C'$ and $\Delta S'$, $|\Delta \mathrm{P}|$ can be found by the integral term

$$|\Delta \mathrm{P}| = \int_0^{\Delta C', S'} \left| \frac{\partial \Delta \mathrm{P}}{\partial \Delta C, S} \right| d\Delta C, S = \frac{2T}{J} (t_2 - t_1)^2 (\cos\theta \sin\theta)^2 \, \Delta C', S' \tag{4.56}$$

When (5.56) is inspected closely, it is observed that T and J works adversely, that is, as the torque demand T increases, position tracking error increases whereas as the inertia of the system J increases, position tracking error decreases for a constant demodulator output error. It is also concluded that the position tracking error is dependent on the actual motor position (θ). Moreover, as $(t_2 - t_1)$ increases, in other words, as the frequency of the torque tracking error decreases, position tracking error increases. This result makes it necessary that the analysis will be performed for a determined operation frequency of the motor. Hence, let us assume that the motor operates at a very low frequency, namely 1 Hz inducing a 4 Hz torque ripple. Then, $(t_2 - t_1)$ can be calculated as 0.125 s from (4.53). Let us also assume that there is a torque demand of 71.2 Nm which induces the maximum permissible acceleration in the system (120°/sec^2). This operation condition may be thought as the worst case since the operation frequency of the motor is so low that it induces a speed of 3°/s in the system where the maximum speed is 60°/s and the torque demand is at the maximum value permissible in the system. Writing the numerical values of J (34 kgm^2), T (71.2 Nm) and $(t_2 - t_1)$ (0.125 s) into (4.56), position tracking error can be found as

$$|\Delta\mathrm{P}| = 0.5235(\cos\theta\sin\theta)^2\, \Delta C', S' \text{ rad} \tag{4.57}$$

The maximum error occurs when θ is at 45°, 135°, 225° and 315° since $(\cos\theta\sin\theta)^2$ produces peaks at these angles. Writing the peak value for $(\cos\theta\sin\theta)^2$ which is 0.25 into (4.57) will yield

$$|\Delta\mathrm{P}|_{\max} = 0.13088\Delta C', S' \text{ rad} \tag{4.58}$$

The maximum acceptable position tracking error can be determined from the deviation of the projectile fired from the gun and the center point of the target located at a distance of 100 meters from the gun. The deviation can be modeled as the perimeter of a portion of a circle with radius 100 meters as illustrated in Figure 4-43.

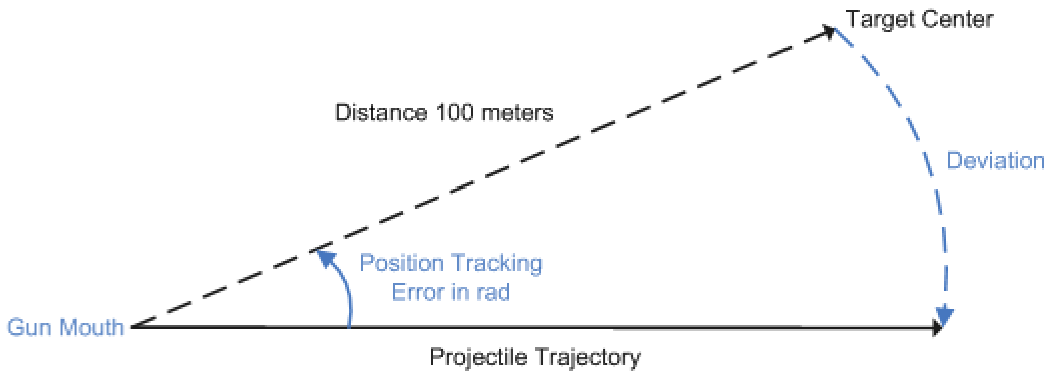

Figure 4-44 Deviation of the projectile from the target for the proposed system

The acceptable maximum deviation amount can be assumed to be 0.5 m since even the gun in the experimental system shows this amount of deviation for a target at a distance of 100 m. Then, combining (4.58) and perimeter of circle formula,

$$100|\Delta \mathrm{P}|_{\max} = 13.088\Delta C', S' = 0.5 \text{ m} \qquad (4.59)$$

the maximum permissible demodulator output error can be found as 3.8%. If the actual value for the demodulator output error which is 1.84% is compared with this calculated value, it is concluded that the proposed system is reliable against demodulator output error with a safety margin of 2%.

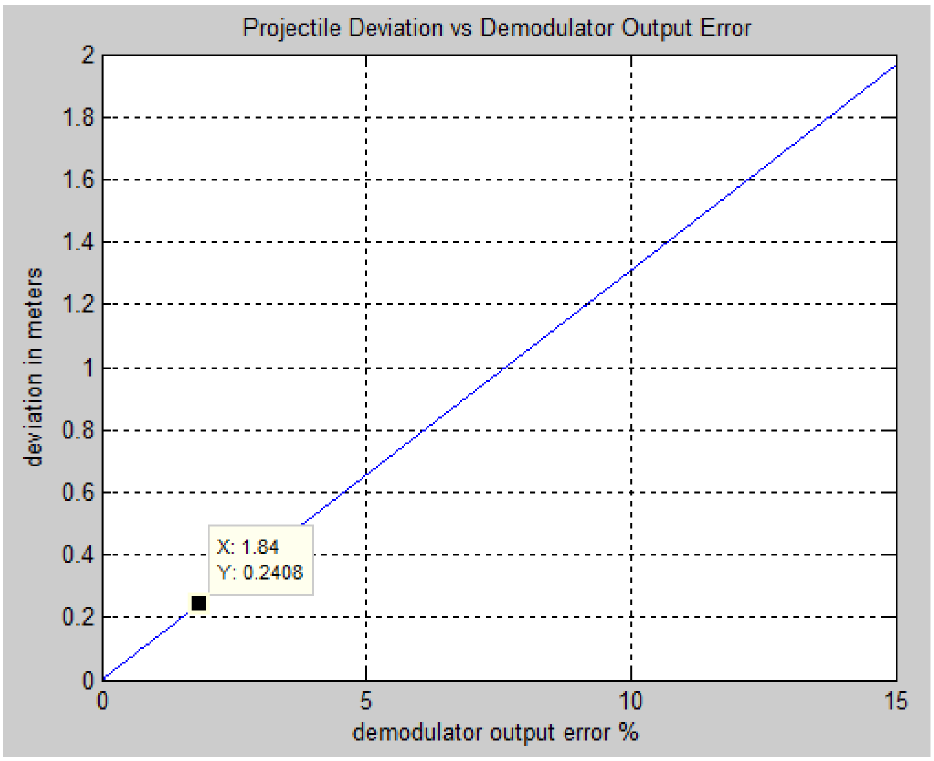

Figure 4-45 Projectile deviation with respect to the demodulator output error

Figure 4-45 shows the amount of projectile deviation with respect to the demodulator output. The value for the realized system is 0.24 m. If the signal conditioner was not applied to the resolver channels, this value would be 2 m approximately as extracted from Figure 4-45 for a demodulator output error of 15%.

It is important to state that the error values determined by this analysis are the maximum errors that the probability of seeing these levels of errors is very low because;

- The demodulator output error values has been calculated for the worst case analysis,
- Improving effects of the closed-loop control are neglected in the analysis and transients are taken into consideration since the system is more vulnerable to such imperfections in transients,
- Operating frequency and system acceleration values are selected to guarantee the worst case analysis.

In conclusion, the proposed system is claimed to be robust against the most effective imperfection, that is, demodulator output error, under the most severe condition it can face up with.

Sensitivity of Errors to Analog-to-Digital Conversion Rate

Analog-to-digital conversion rate comes up as the most important parameter of the proposed system. As the conversion rate goes towards infinity, frequency cut-off points of the anti-aliasing filter and the interpolation filter also move along the frequency axis towards the infinity. In the limit point, that is, in continuous-time domain, as a matter of fact, we neither need the anti-aliasing filter nor the interpolation filter since necessity for these filters arises from the digitization of the converter. Therefore, as the analog-to-digital conversion rate comes down along the frequency axis from infinity to Nyquist rate, the position estimation error of the software-based RDC increases due to both increasing filtering delays and increasing aliasing.

CHAPTER 5

CONCLUSION AND FUTURE WORK

5.1 Conclusion of the Thesis

The objective of this thesis has been stated to develop a software-based resolver-to-digital converter to be utilized in weapon systems. The motivation behind this objective is to enhance the servo controllers used in weapon systems in terms of adaptability to changing system structures. For this purpose, enhancing the independency of the servo system to hardware components in realization of system functions becomes more of an issue. Hence, a software-based resolver-to-digital converter which eliminates the need for special hardware components for resolver conversion contributes to this motivation.

Excited with a reference signal, a resolver gives out two amplitude modulated signals. Measuring the reference signal and the amplitude modulated signals, the software-based RDC estimates position and speed of the resolver by the help of three components. These components can be specified as signal conditioner, phase-sensitive demodulator and estimator filter.

The resolver signals have harmonic distortions and high-frequency noise due to several imperfections present in the servo system. Such imperfections may decrease the quality of the demodulation, which consequently increases the position estimation error. Increased position estimation error in turn induces oscillations on the torque signal. As a consequence of the torque oscillations, the speed of the system also oscillates, which may prevent the weapon system from realizing its main function that is stabilizing the speed of the gun. Therefore, at the beginning of the thesis study, an analysis examining the levels of harmonic distortions and noise present in resolver signals and their possible effects on torque and speed of the servo system is performed. Based on the result of the analysis, it is concluded that suppression of the harmonic distortions and noise is indispensable for the experimental system to obtain ripple-free torque and speed signals. Hence, a mixed-signal signal conditioner is designed to be used in front of the phase-sensitive demodulator. The signal conditioner suppresses the deteriorating effects of the resolver signal imperfections on the demodulation. Namely, the demodulator output error is decreased from 15.24% to 1.84% by the application of the signal conditioner. As a result, amplitude of the oscillations on the torque signal is decreased from 1% to 0.02% where the latter value is proved to be an acceptable torque error value by the sensitivity analysis.

The phase sensitive demodulator, as the name implies, demodulates the amplitude modulated resolver signals by also sensing their phases with respect to the reference signal. For realization of this function, the demodulator utilizes several components which may be specified as zero-crossing detectors, half-period integrators, a phase detector, two's complementers, negative cycle detectors and some other logic elements. The performance of the designed demodulator is highly satisfactory that the quantization error at the demodulator output becomes less than 0.5×10^{-5} percent. The developed demodulator reduces the effort consumed for adaptation of the servo system to a different sensor. Furthermore, the demodulator provides interface with any type of resolver without needing any hardware modification and by changing only one parameter embedded in the FPGA code.

Several estimator filters are analyzed in both simulation environment and in real-time. The real-time analysis is performed on a DSP board which has necessary components to realize the aforesaid signal conditioner and FPGA-based phase sensitive demodulator. The analyzed estimator filters are;

- Nonlinear observer proposed in [21]

- Tracking differentiator adapted to resolver conversion process
- Linear Kalman filter adapted to resolver conversion process
- Extended Kalman filter adapted to resolver conversion process
- Unscented Kalman filter adapted to resolver conversion process

Since the algorithms are implemented in real-time, not only the estimation performances but also algorithmic complexities of the algorithms are of great importance. Less complexity with higher performance is always the point where we would like to reach for a real-time system. In the implemented algorithms, although the complexity increases severely from nonlinear observer to unscented kalman filter, the estimation accuracy does not increase in a parallel manner to the increasing complexity. At the end of the performed performance analyses, it is concluded that the most practicable filter for resolver conversion is the Linear Kalman filter.

Stability and sensitivity analyses are also performed for the proposed system. The system is proved to be stable according to Liapunov's stability criterion and robust against the most effective disturbances of the system which can be specified as demodulator output errors and delays in filtering circuits. The sensitivity analysis also shows that it is possible to improve the performance of the proposed system by increasing the sampling frequency of the analog-to-digital converters since increased sampling frequency will decrease the level of the aforesaid disturbances.

The replacebility of the ready-to-use RDC IC's with the proposed software-based RDC is proved by the performed analyses. The effects of the position and speed estimation errors on system torque, system speed and system position are analyzed and it is observed that the performance of the servo system equipped with the proposed system is highly satisfactory.

5.2 Future Work

Torque produced by the servo motor fluctuates due to several reasons in a servo system. Torque ripples can be classified according to their frequency spectrum; high-frequency ripple components and low frequency ripple components. Absorbed by the inertia, high-frequency ripple components generally do not result in disturbing effects on the system performance. On the other hand, low-frequency ripple components have dramatic effects on the system performance. Low-frequency ripple components spread into the system speed and turn into real motions which deflect the system performance from the demanded behavior. Moreover, these ripples prevent designers from increasing speed loop gains sufficiently because they are amplified more by higher controller gains. On the other hand, decreasing the gains, a more serious problem is observed. Lower speed loop gains result in unsatisfactory system performance and deteriorates tracking abilities of the servo system. That is to say, the torque ripple problem which may be seen as a simple problem turns into a serious one.

During the thesis study, it is observed that low bandwidth of torque loop results in torque ripples in the servo system. This is due to the fact that torque loop cannot compensate for disturbing effects coming from gears of the system. Since these disturbing effects' frequency spectrum exceeds the bandwidth of the torque loop, the loop can not respond fast enough and oscillations are observed on the torque signal. Uncompensated back-EMF and nonlinear characteristics of drive electronics and motor decreases the torque loop's bandwidth and amplifies the torque ripples.

PWM inverter, connected series to motor resistance and inductance, enables transferring electrical power from a DC bus to the servo motor using sinusoidal modulated PWM signals. The servo motor converts electrical energy into mechanical energy and it produces torque on the rotating shaft. This energy transfer is realized with three phase balanced AC currents. An AC servo motor produces a ripple-free torque signal when current waveforms are pure sinusoidals and do not show harmonic distortions. However, nonlinearities and imperfections of PWM inverter, servo motor and drive electronics result in harmonic distortions in the current waveforms. As a result, torque shows fluctuations which eventually corrupt the speed loop and deteriorate its performance.

In summary, torque fluctuations will always exist in a servo system with a wide frequency spectrum. Low frequency components may result from nonlinear motor characteristics, PWM dead band, nonlinear resistance and inductance of motor windings, nonlinear effects of the bus, snubber circuits, PWM inverter, gain and offset errors in current sensing and voltage drop across the switching elements. High-frequency ripple components may stem from position sensor inaccuracies, low bandwidth current sensors, PWM modulation technique, inadequate bus capacity, low sampling-time and low frequency PWM signals. High-frequency fluctuations in a heavy system may be absorbed by the inertia. However, if low frequency torque ripples are present in torque, then speed of the system will also fluctuate. Needless to say that this will occur if the frequency of the fluctuations is within the system bandwidth. Consequently, low frequency torque fluctuations are not welcome in a servo drive system and should be minimized possibly. Hence, the future work will cover an analysis of this problem and propose a method for removal of the problem with compensation of back-EMF and nonlinear effects. The method may make use of neural networks such as Echo State Network for identification of back-EMF and nonlinear effects.

REFERENCES

[1] “Sensorless Control with Kalman Filter on TMS320 Fixed-Point DSP”, Texas Instruments Europe, July 1997.

[2] L. Harnefors, “Speed Estimation from Noisy Resolver Signals”, Royal Institute of Technology, Stockholm, Sweden, 1996.

[3] Wikipedia Organization, “Servomechanism”, “en.wikipedia.org”, November 2009.

[4] Wally Rippel, “Induction Versus DC Brushless Motors”, “www.teslamotors.com”, January 2007.

[5] “Field Orientated Control of 3-Phase AC Motors”, Texas Instruments Europe, February 1998.

[6] Grenier, D., L.-A. Dessaint, O. Akhrif, Y. Bonnassieux and B. LePioufle, "Experimental Nonlinear Torque Control of a Permanent Magnet Synchronous Motor Using Saliency," IEEE Transactions on Industrial Electronics, Vol. 44, No. 5, October 1997, pp. 680-687.

[7] Ong, Chee-Mun., “Dynamic Simulation of Electric Machinery”, Prentice Hall, 1998.

[8] A. Ometto, “Modulation Techniques”, Università degli Studi di L’Aquila.

[9] Zhenyu Yu, “Space-Vector PWM with TMS320C24x/F24x Using Hardware and Software Determined Switching Patterns”, Texas Instruments, March 1999.

[10] Robert H. Stewart, “Ocean Wave Spectra”, Department of Oceanography, Texas A&M University, 2005.

[11] Katsuhiko Ogata, “Discrete-Time Control Systems”, Prentice Hall Inc, New Jersey, pp. 90-121, 327-336, 1995.

[12] Dan Simon, “Optimal State Estimation”, John Wiley and Sons Inc, New Jersey, pp. 53-58, 123-145, 433-457, 2006.

[13] Sebestian Thrun, Wolfram Burgard and Dieter Fox, “Probabilistic Robotics”, MIT Press, London, England, 2005, pp. 67-71.

[14] Geoffrey S. Boyes, “Synchro and Resolver Conversion”, Memory Devices Ltd., London, Great Britain, 1980, pp. 7-45.

[15] Santanu Sarma, V.K. Agrawal and Subramanya Udupa, “Software-Based Resolver-to-Digital Conversion Using a DSP”, IEEE Transactions on Industrial Electronics, Vol. 55, No. 1, pp. 371-379, January 2008.

[16] Mohieddine Benammar, Lazhar Ben-Brahim, Mohd A. Alhamadi, “A Novel Resolver-to-360° Linearized Converter”, IEEE Sensors Journal, Vol. 4, No. 1, pp. 96-101, February 2004.

[17] Mohieddine Benammar, Lazhar Ben-Brahim, Mohd A. Alhamadi, “A High Precision Resolver-to-DC Converter”, IEEE Transactions on Instrumentation and Measurement, Vol. 54, No. 6, pp. 2289-2296, December 2005.

[18] Mohieddine Benammar, Mohd A. Alhamadi, Nasser Al-Emadi, Mohammed Al-Hitmi, “A New Angle Determination Method for Resolvers”, Electrical Engineering Department, College of Engineering, Qatar University, 2008 IEEE.

[19] Armondo Bellini, Stefano Bifaretti and Stefano Constantini, “A PLL-Based Filter for Speed Noise Reduction in Drives using a Resolver Transducer”, Department of Electronic Engineering, University of Rome, IEEE 2002.

[20] Weera Kaewjinda and Mongkol Konghirun, “A DSP-based Vector Control of PMSM Servo Drive Using Resolver Sensor”, King Mongkut’s University of Technology, Department of Electrical Engineering, Bangkok, IEEE 2006.

[21] Lennart Harnefors and Hans-Peter Nee, “A General Algorithm for Speed and Position Estimation of AC Motors”, IEEE Transactions on Industrial Electronics, Vol. 47, No. 1, February 2000.

[22] B. A. Murray and W.D. Li, “A Digital Tracking R/D Converter with Hardware Error Calculation Using a TMS320C14”, Department of Electronic Engineering, Dublin City University, Ireland, 1993.

[23] Zhiqiang Gao, “From linear to nonlinear control means: a practical progression”, Department of Electrical and Computer Enginnering, Cleveland State University, USA, 2001.

[24] A. Levant,“Robust exact differentiation via sliding mode technique”, Automatica, 34 (3), pp. 379-384, 1998.

[25] Y. X. Su, Dong Sun, B.Y. Duan, “Design of an enhanced nonlinear PID controller”, Mechatronics 15 (2005), pp. 1005-1024.

[26] Guohui Qiao, Minglei Sun, Rong Zhang, Guanghua Zong and Shouzhong Li, “An Improved Self-Adaptive Tracking Differentiator”, Proc. 2009 IEEE International Conference on Information and Automation, pp. 980-984.

[27] Adrian Davies and Phil Fennessy, “Digital Imaging for Photographers”, Focal Press, p. 30, 2001.

[28] Mark Owen, “Practical Signal Processing”, Cambridge University Press, pp.81-82, 2007.

[29] Antolin Agatep, “Xilinx Spartan II FIR Filter Solution”, 2000 Xilinx Inc.

[30] Michael Francis, “Infinite Impulse Response Filter Structures in Xilinx FPGAs”, 2008 Xilinx Inc.

[31] Ma Zhonghua, “Tracking Differentiator in the Application of Signal Processing and Theory Research”, 2008 International Seminar on Future BioMedical Information Engineering.

[32] Yoichi Hori, “Position and Mechanical Impedance Control Method of Robot Actuators based on the Acceleration Control”, Department of Electrical Enginnering, Faculty of Engineering, The University of Tokyo, IEEE 1989.

[33] Yoichi Hori, “Disturbance Suppression on an Acceleration Control Type DC Servo System”, Department of Electrical Enginnering, Faculty of Engineering, The University of Tokyo, IEEE 1988.

[34] Peter B. Schmidt and Robert D. Lorenz, “Design Principles and Implementation of Acceleration Feedback to Improve Performance of dc Drives”, IEEE Transactions on Industry Applications, Vol. 28, No. 3, May/June 1992.

APPENDIX A

HARDWARE AND SOFTWARE

A DSP board is used to realize the software-based RDC. The DSP board has a Digital Signal Processor with proper peripherals and Analog-to-Digital converters for data acquisition. It also includes a Field-Programmable Gate Array (FPGA). A motor drive board and a servo motor are also used in the experimental set-up.

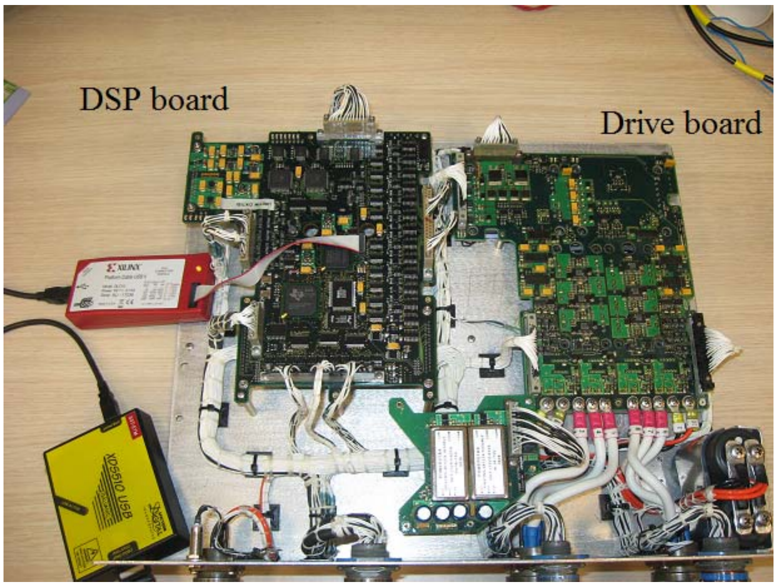

Figure A-1 Experimental set-up

Digital Signal Processor

Texas Instrument's C6000 series Digital Signal Processor is used in digital signal processing. C6000 is a high performance floating-point Digital Signal Processor.

DSP chip is connected to external memory elements through a parallel data bus. It has a 32-bit External Memory Interface Unit (EMIF) and Enhanced Direct Memory Access (EDMA) controller that enables fast data transfer between the CPU and the external memory interfaces without interrupting the CPU. The internal structure of the DSP is shown in Figure A-2.

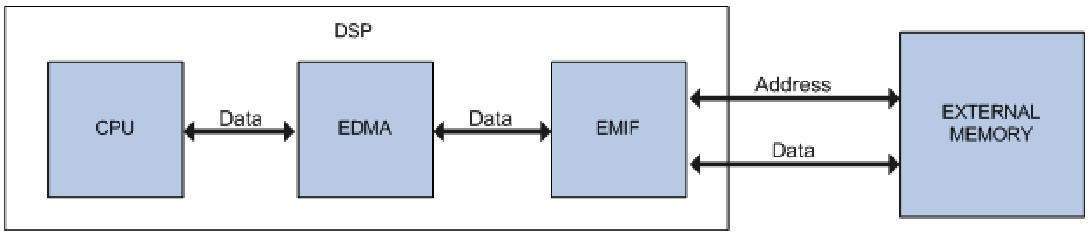

Figure A-2 DSP CPU, EMIF, EDMA and external memory

Analog-to-Digital Converters and Anti-Aliasing Filters

The first remarkable point in selection of a suitable ADC for RDC process is the required sampling frequency. Resolver signals in the experimental system have a bandwidth of 5 kHz. According to Nyquist criterion, a sampler used for RDC should have a sampling frequency of 10 kHz at a minimum. The ADC chips on the DSP board have a maximum sampling frequency of 15.4 kHz. Therefore, they satisfy the Nyquist criterion.

The Signal-to-Noise Ratio (SNR) is another important criterion for the selection of a suitable ADC for RDC. ADC chips used on the DSP board have an SNR of 80 dB. Hence, the Effective Number of Bits (ENB) can be calculated from the equation given below:

$$ENB = \frac{80dB}{6.02} \approx 15bits$$

Effective resolution of the chips is approximately 15 bits. Compared to RDC chips, this value of effective resolution is satisfactory.

Before the conversion, anti-aliasing filters are used to prevent from aliasing. A second order analog Butterworth filter whose -3dB cut-off frequency is at 6 kHz is used for this purpose. The data transfer from ADC chips is realized by the FPGA through the serial interface (SPI).

Field-Programmable Gate Array

FPGA is a programmable logic processor that can be programmed in VHSIC Hardware Description Language (VHDL) to resolve hardware functions. The DSP board used in the thesis study has a Xilinx's Spartan Family FPGA chip. FPGA is used to realize not only some hardware functions but also some signal processing on resolver signals. For instance, up sampling, interpolation and demodulation are performed in FPGA by coding in VHDL. The block diagram in Figure A-3 summarizes FPGA's role in DSP board.

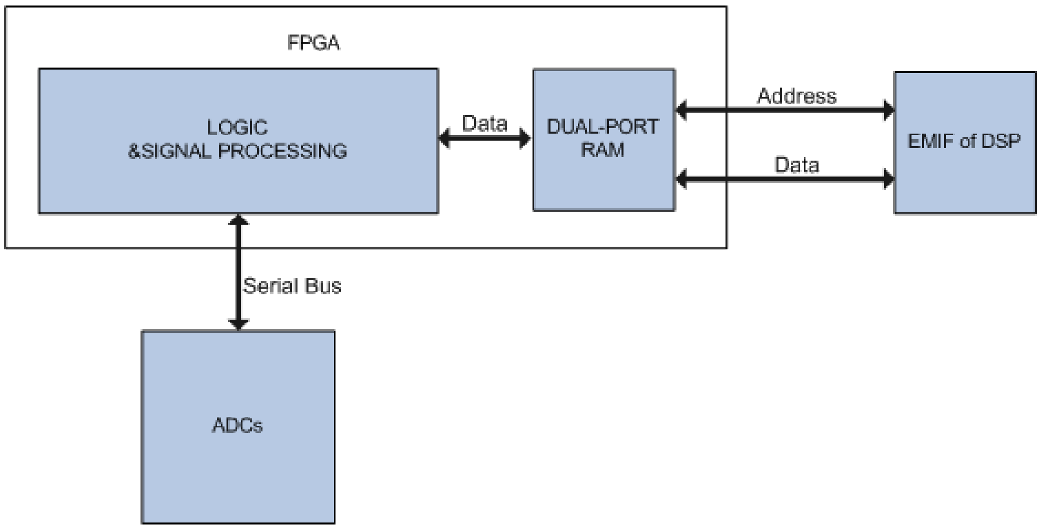

Figure A-3 FPGA's role in the hardware

Resolver and Reference Signal Generator

A 5 kHz resolver and a 5 kHz reference signal generator are used in the experimental set-up.

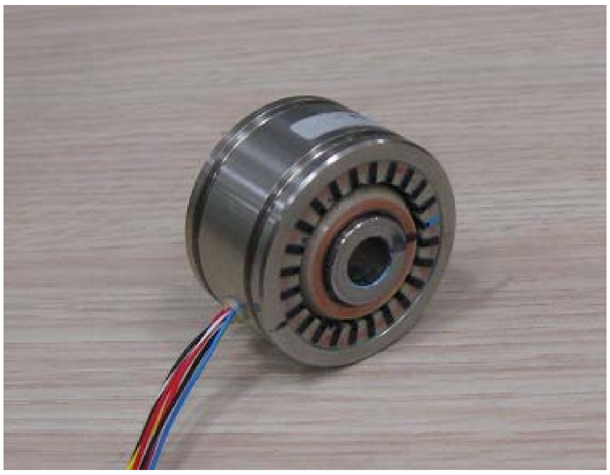

Figure A-4 5 kHz resolver used in experimental set-up

AC Servo Motor and Motor Drive Unit

The experimental set-up has a servo motor and a motor drive board.

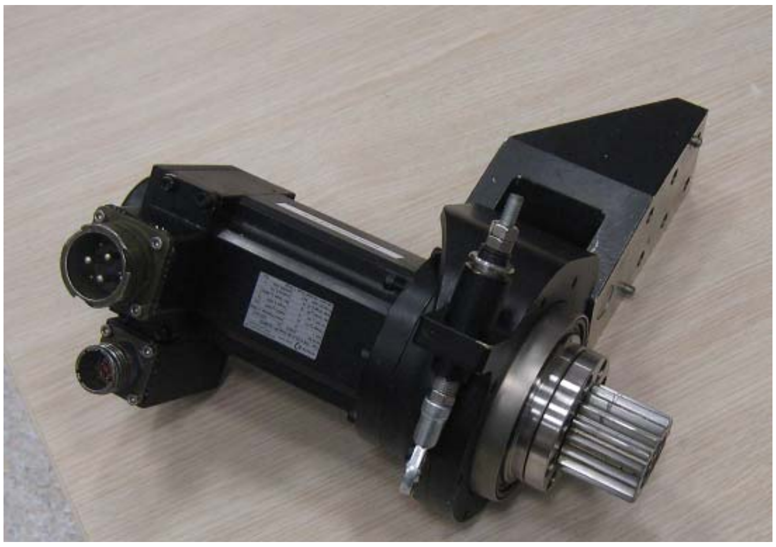

Figure A-5 AC servo motor used in the experimental set-up

Position and Speed Measurement

Measurements of motor speed and position are performed using Analog Devices' AD2S83 Resolver-to-Digital IC.

Software Tools Used for Simulation

Matlab and Simulink are used in simulations. Filter Design and Analysis Toolbox of Matlab is very helpful in designing FIR and IIR filters. The ready to use functions of Matlab and tools of Simulink facilitated the study considerably.

Software Tools used for Programming DSP Board

FPGA code is composed in VHDL and compiled in ISE, a software tool of Xilinx Inc. Using the Xilinx's IMPACT interface, FPGA's boot EEPROM is programmed via a JTAG connection. Debugging of FPGA code is made with Chipscope which is an embedded debugger making use of internal RAMs of the chip to monitor the states of FPGA's internal signals. The Chipscope first stores the internal signals into available RAMs and carry them onto the computer monitor using the JTAG connection.

DSP algorithm is composed in Matlab Simulink using Embedded Target for TI C6000 DSP and compiled in CCS software of Texas Instruments. DSPC6000 is programmed using CCS via a JTAG emulator.

Issues Related to Implementing FIR Filter in FPGA

FIR filters in FPGA can be designed using MAC FIR core generator. MAC FIR core makes use of the conventional tapped-delay line FIR structure. It uses internal multipliers, adders and RAMs of FPGA to achieve multiply-accumulate and delay operations.

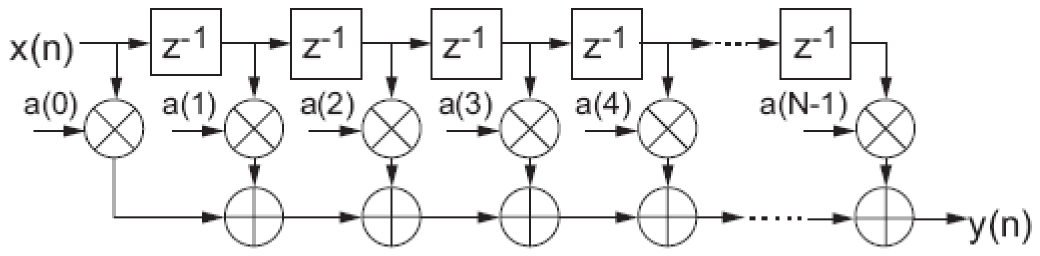

Figure A-6 Tapped-delay line FIR structure

The following figure shows the interface for designing MAC FIR filter in ISE program. Details related to usage of the core are given in the data sheet of the core.

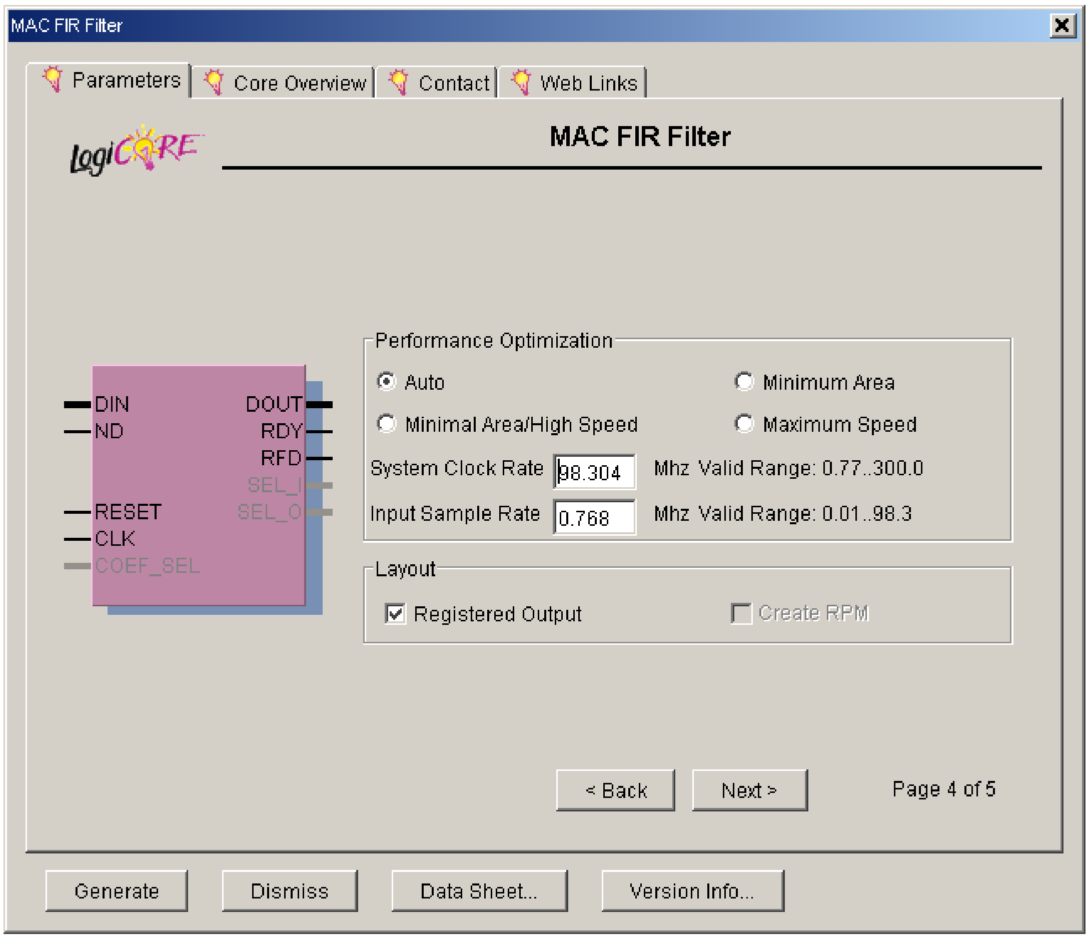
MAC FIR Filter

Parameters | Core Overview | Contact | Web Links

LogiCORE

MAC FIR Filter

Performance Optimization

[✓ Auto] Minimum Area

Minimal Area/High Speed Maximum Speed

System Clock Rate 98.304 Mhz Valid Range: 0.77..300.0

Input Sample Rate 0.768 Mhz Valid Range: 0.01..98.3

Layout

[✓ Registered Output] Create RPM

< Back | Next > | Page 4 of 5

Generate | Dismiss | Data Sheet... | Version Info...

Figure A-7 MAC FIR filter design interface in ISE program